STUDY OF STRATOSPHERIC OZONE USING MILLIMETER-WAVE RADIOSPECTROMETRY

THESIS

Submitted in partial fulfilment of the
requirements for the degree of
DOCTOR OF PHILOSOPHY

By

Vivek C. Nagar

Under the Supervision of

Dr. R. S. Arora

BIRLA INSTITUTE OF TECHNOLOGY AND SCIENCE
PILANI (RAJASTHAN) INDIA
1994

PREFACE

THE WORK REPORTED IN THIS THESIS WAS CARRIED OUT AT THE NATIONAL PHYSICAL LABORATORY, NEW DELHI, IN CONNECTION WITH THE PROJECT, "A GROUND-BASED MILLIMETER-WAVE TECHNIQUE FOR OZONE OBSERVATIONS AT ANTARCTICA", SPONSORED BY THE DEPARTMENT OF OCEAN DEVELOPMENT, GOVT. OF INDIA.

BIRLA INSTITUTE OF TECHNOLOGY AND SCIENCE

PILANI (RAJASTHAN)

CERTIFICATE

This is to certify that the thesis entitled "STUDY OF STRATOSPHERIC OZONE USING MILLIMETER-WAVE RADIOSPECTROMETRY" submited by Mr. Vivek C. Nagar, I.D. No. 90PZYF002 for award of Ph.D. degree of the institute, embodies original work done by him under my supervision.

Signature in full of the supervisor _____

Name in capital block letters (R.S. ARORA)

Date: 12-9-94

Designation SCIENTIST
Radio Science Division
National Physical Laboratory
NEW DELHI-110012

ACKNOWLEDGEMENTS

I record my deep sense of gratitude to Dr. R.S. Arora and Dr. G.S. Uppal for very valuable guidance and constant encouragement throughout the course of this work.

I would like to thank the Director, NPL for providing me the infrastructure facilities to work at NPL and the Council of Scientific and Industrial Research (CSIR) for financial help. I gratefully acknowledge the Deptt. of Ocean Development (DOD) for providing me the opportunity to carry out Ozone observations at Antarctica during the 13th Indian Scientific Expedition.

Thanks are due to Dr. K.K. Mahajan, Chairman, Academic Committee NPL for encouragement and support.

I am also thankful to Dr. M. Vivekanand of TIFR, GMRT project, Pune and Dr. Patrick Dierich of Observatoire-de-Paris, Meudon for help in AOS design.

I thank Dr. V.N. Ojha, Mr. V.N. Moorthy and Mr. R.P. Bhatnagar of NPL for helping me in various ways during the course of this work.

And finally, I would like to thank all my friends, colleagues and family members for providing me encouragement, support and high spirit of work.

Vivek C. Nagar

(Vivek C. Nagar)

Contents

List of Figures

List of Tables

Chapter 1

Introduction

1.1 Introduction

The minor constituents of the atmosphere such as water vapor, CO_2 and Ozone play an important role in the dynamical processes in the atmosphere and chemistry of the surface of earth. The Ozone in the atmosphere at levels above 20 km acts as a filter that absorbs the lethal part of ultraviolet (uv) radiation from the sun and makes life, as we know it, possible on the surface of the earth. In the stratosphere ozone is formed when the solar ultraviolet radiations are absorbed by molecular oxygen, breaking the molecular bond and yielding two free oxygen atoms. A free oxygen atom then combines with the oxygen molecule to form ozone molecule (O_3). Ozone itself undergoes photodissociation and other loss processes yielding a net balance between it's formation and destruction. This balance leads to a quasi steady state concentration of atmospheric ozone which is greatest in the lower stratosphere in 20-30 km height range. The absorption of solar radiation in both the production and destruction of ozone heats up the atmosphere so that it has a positive temperature gradient in the stratosphere. The atmospheric ozone layer is quite sparse and has a maximum fractional concentration of ~10 parts per million by volume (ppmv) in stratosphere. The total column content of ozone if compressed at STP gives a layer of about 3 millimeters in thickness (300 Dobson units). However, disproportionate to it's abundance, this trace atmospheric constituent plays a key role in various chemical and dynamical processes in the atmosphere. Because of its particular absorption characteristics in the ultraviolet and the infrared region, Ozone is a dominant factor in establishing the balance between the radiation reaching to earth's surface from the outside and the radiation from the earth associated with its

surface temperature. It is for these and many other reasons that ozone has been and continues to be a subject of study in atmospheric physics. The research in this field gained additional impetus when it was realized in early seventies that continued uncontrolled release of chlorofluorocarbons (CFCs) in atmosphere could possibly modify the stratospheric ozone layer. The CFCs are stable gases in troposphere but photodissociate in stratosphere to give free chlorine (Cl) which in turn catalyses a chemical ozone destruction cycle. Through the seventies and eighties the estimates of total ozone column density varied greatly with the growing understanding of stratospheric chemistry and with the revision of rate constants of different reactions involving ozone (Allen et. al. 1984 & 1991). The phenomenon of stratospheric ozone depletion took a dangerous shape when there was an almost complete Ozone wipe out in the lower stratosphere observed at some places over Antarctica (Farman et. al. 1985). This phenomenon is widely known as the Antarctic Ozone Hole (Levi 1988). Considerable amount of ozone data has been collected since then by a number of ground based and satellite observations. However, the exact mechanism for ozone depletion is still not fully understood.

Ozone has been regularly monitored for the past several decades by a global network of Dobson-Spectrophotometers which measure total ozone content of the atmosphere by monitoring the absorption of solar ultraviolet radiations at selected wavelengths in the 280-320 nm band. In-situ measurements of ozone have also been carried out by ozone-sondes placed on rockets and balloons. More recently, ozone has been monitored on a global basis by means of total ozone mapping spectrometers (TOMS) as well as solar back-scatter ultra-violet spectrometers (SBUV) carried on satellites. Most of

these methods, however, require sun as the background source of radiation and consequently are limited to only day time observations in good weather conditions. It is in this context that the millimeter-wave technique of ozone measurement offers several unique advantages.

The technique of ozone measurement by millimeter-wave radiospectrometers is comparatively a recent one and makes use of isolated rotational transitions of ozone in the millimeter-wave region. This requires observation of strong mm-wave lines of atmospheric ozone and inversion of the observed line spectrum to obtain ozone height distribution. Millimeter wave lines are predominantly pressure broadened in the middle atmosphere upto an altitude which is dependent on frequency of observation and is approximately equal to 80 km for lines near 30 GHz (λ = 10 mm) down to about 55 km for lines at 300 GHz (λ = 1 mm). Hence the measured line shape can be deconvolved to provide information concerning constituent abundance as a function of pressure or height. The calibration standards used in this technique are black body sources at known temperatures which can be made as highly reproducible because the temperature is an easily maintained physical parameter. For this purpose the two commonly used temperature sources are room temperature load (300 K) and liquid nitrogen load (77 K). Since this experiment is based on emission measurements, and does not require a background source, ozone can be observed during both day and night times. This can, for example, facilitate intercomparison of the data with the data from a satellite passing over the observing site. Another unique advantage of mm wave technique is that the observations are least affected by smoke, dust and aerosols in the atmosphere which can make the results of scattered ultraviolet measurement techniques such as Dobson/UMKEHR uncertain.

Hence the mm-wave technique can be used on a round the clock basis and observations need only be curtailed under thick cloud cover conditions and during active rain episodes. The ozone altitude distribution is obtained from the spectral line profile by an inversion procedure that makes use of pressure broadened nature of the spectral line. The pressure broadening coefficient has been well measured in the laboratory (Connor 1985). The altitude coverage of this technique is approximately 15 to 60 km. In this region, pressure broadening is dominant over all other broadening mechanisms and hence this property is exploited to obtain ozone concentration as a function of height. This altitude coverage, however, depends on the total frequency bandwidth and the frequency resolution of the system back-end. A typical 500 MHz receiver system having 1 MHz frequency resolution will cover 15-55 Km height range. The altitudes near 40 km where ozone depletion is first expected to manifest itself, are those at which this technique works best (Brillet 1989). Also these observations can be carried out at a variety of sites and full latitude coverage can be obtained. Species observed in this way to date include O_3 (Caton et. al. 1968, Shimabukuro et. al.,1973 & 1975, Wilson & Schwartz 1981, Lobsiger 1984, Connor et. al. 1987, Zommerfelds et. al. 1989, Parrish et. al. 1992), H_2O (Radford et. al.,1977; Bevilacqua et. al.,1983; Bevilacqua et. al. 1985), CO (Kunzi & Carlson, 1982; Bevilacqua et. al., 1985), ClO (Parrish et. al. 1981; Solomon et. al., (1983), ClO (Parrish et. al.,1981; Solomon et. al., 1984) and HO_2 (DeZafra et. al., 1984).

1.2 Previous Studies

The first experimental detection of atmospheric ozone in absorption

spectrum of the Sun at 36.025 GHz was obtained by Mouw and Silver (1960). In 1966, Caton, Welch and Silver detected 37.836 GHz transition in absorption and 30.056 GHz transition in emission. The line intensities associated with each of these observations were so weak in comparison to receiver sensitivity that it was necessary to integrate several hours, and in one case, days of data in order to confirm detection. At higher frequencies, in the window region between the two strong oxygen absorption lines at 60 GHz and 118 GHz, ozone was detected by Caton et. al. in 1968 both in emission and absorption modes. This line at 101.737 GHz is relatively stronger (Gora 1959) than all the previously detected lines between 30 to 40 GHz and hence a shorter integration time was needed. The receiver used here was a double conversion superheterodyne front end and five 10 MHz wide filter banks at the back end giving a total receiver bandwidth of 50 MHz. The measured sensitivity of this instrument was 2.7 K (rms) in 20 seconds. In 1973, Shimabukuro and Wilson detected the 110.836 GHz transition of ozone from the National Radio Astronomy Observatory's 36 feet radio telescope located at Kitt Peak, Arizona. This system had a single side band noise temperature of 3600 K and unlike Caton (1968) a frequency switched mode was used. The same transition at 110.836 GHz was observed by Penfield et. al. (1976) in emission mode to estimate day to night variation of the mesospheric ozone. The radiometer used was a radio telescope located at the McDonald Millimeter-Wave Observatory, Texas. In 1979, Wilson and Schwartz used Aerospace Corporation's Millimeter Wave Spectral Line Receiver System located in California to observe 101.737 GHz line of ozone. Similarly, Vivekanand and Arora (1988) used a mm-wave superheterodyne receiver built for radio astronomy to obtain spectral line observations of atmospheric ozone at

110.836 GHz. At still higher frequencies, beyond the 118 GHz strong oxygen absorption line, Lobsiger (1984) operated a dedicated millimeterwave ozone radiometer for one year at Bern (switzerland) to measure the rotational transition of ozone at 142.2 GHz. The scheme of observation was essentially the same as that of Caton (1968) but this instrument had a much better sensitivity and frequency resolution. The single side band noise temperature of this instrument was about 1800 K. The instrument used 31 filter channels with bandwidths ranging from 0.2 MHz near line peak to 30 MHz in the far wings covering a total frequency span of 170 MHz. This radiometer measured ozone density in the stratosphere and mesosphere from 25 to 75 km. Connor et. al. (1985) made ozone observations in the stratosphere using a superheterodyne receiver at 101.737 GHz with single side band noise temperature of 1000 K. Another instrument, developed by De la Noe et. al. (1987) has obtained measurements of the ozone distribution with reported random errors of 1-5% at 40 km. A much more sensitive measuring instrument to observe several atmospheric trace constituents was developed by Parrish et. al. (1988). The front end of this instrument has a cooled (20K) heterodyne mixer and IF amplifier using a closed cycle helium refrigerator. The single side band equivalent noise temperature of this instrument was determined to be 600 K. The operational frequency range is 260-280 GHz with 1 MHz frequency resolution. This instrument can measure stratospheric constituents having peak mixing ratio $<10^{-9}$, which is more than three orders of magnitude less than typical ozone mixing ratios in the stratosphere. Ozone was observed by Connor et. al. (1987) at McMurdo Station, Antarctica in spring 1986 using this instrument. An error analysis carried out on Antarctic data showed measurement accuracies of 15-19% (depending on altitude). This

was supported by intercomparisons with other observations. A detailed theoretical study performed by Bevilacqua and Olivero (1988) showed that the best vertical resolution attainable with ground based millimeter wave measurements is 8-10 km whereas the height discrimination ability of this technique is limited to 5-7 km.

1.3 Present Work

The work presented in this thesis describes the ground-based millimeter wave measurements of stratospheric ozone using a 101.7 GHz radiospectrometer. The millimeter-wave ozone instrument was designed and developed indigenously at the National Physical Laboratory, New Delhi. To the author's knowledge, this is the first dedicated instrument of it's kind to be developed in the country. Using this instrument, stratospheric ozone has been studied over Delhi (28°N) as well as over Maitri Station (70°S) in Antarctica. Though there have been a number of ozone studies at low and mid latitudes, the Antarctic ozone observations, using mm-wave technique, have been carried out only once before (Connor et. al. 1987).

Besides the instrument development, comparison of Delhi and Antarctic ozone distributions and the Antarctic ozone variations during our observational period constitute the major outcome of this work.

1.4 Organization of the Thesis

The work presented in this thesis is divided into following seven chapters.

In chapter 2 the theoretical background for atmospheric ozone observation using mm-waves is presented. It describes fundamentals of the origin of radiative transfer equation (RTE) in the atmosphere and it's Rayleigh-Jean approximation for micro-wave and millimeter-wave frequencies. Expressions for resonant and non resonant absorption by different atmospheric gases are developed. Two different line broadening mechanisms viz., Pressure and Doppler broadenings, which are dominant in the atmosphere upto 90 km are discussed and the corresponding line width parameters are calculated. A detailed description of ozone molecule is presented together with the calculation of ozone absorption coefficient. This chapter also describes methods of retrieving ozone height profile from millimeter-wave spectral line data. The two methods described here are:

(i) Iterative inversion method and

(ii) Spectral comparison method.

Both these methods are later applied for data analysis work depending on quality of the signal observed.

Design and development of a state-of-the-art millimeter-wave ozone radiospectrometer is described in Chapter 3. It first discusses some basic radiometric principles and then describes design of the 101.7 GHz radiospectrometer in some detail. The characteristics and functioning of the individual components such as, the antenna, the front-end radiometer and the back-end spectrometer is given. The data acquisition and controls systems developed for the purpose of automated stand-alone acquisition are also described. Various system tests carried out to find the actual performance of the system are also presented.

Chapter 4 describes ozone observations carried out with the present

radiometer at National Physical Laboratory, New Delhi. It also describes initial setting up and calibration of the instrument in the lab. The calibration standards used are the liquid nitrogen and room temperature reference loads. The method of extracting ozone signal from the observed noisy data is described, which includes data integration, smoothing and baseline removal processes. The observed ozone spectra and the corresponding retrieved ozone profiles are presented graphically in this chapter.

Chapter 5 describes working of the system at the Indian Station Maitri (70 South latitude) in Antarctica. The ozone spectra obtained during the period January-February 1994 and their corresponding retrieved ozone height profiles are presented.

In chapter 6 main contributory outcomes of this study are summarized. An overall analysis of the results obtained is carried out and the scientific implications of these results, namely, the latitudinal variability of ozone as found over two observing sites viz. Delhi(28°N) and Antarctica(70°S) and the ozone trend over Antarctica (70°S) during Jan.-Feb. '94 by the mm-wave technique are discussed.

Some remarke on capabilities of ground-based millimeter-wave technique to make continuous observation of atmospheric ozone and the suggestions for further research are outlined in chapter 7.

Chapter 2

Microwave Radiative Transfer of Ozone in the Terrestrial Atmosphere

2.1 Introduction

At millimeter wavelengths, absorption and emission by constituent atmospheric gases affect the electromagnetic radiation passing through it (Yates 1970). In the frequency region 1 to 300 GHz which is considered here, absorption by atmospheric gases is dominated by water vapor and oxygen (Meeks 1976). These two molecules have rotational transition lines at 22 and 183 GHz (H_2O) and near 60 GHz and at 118 GHz (O_2). Also there are relatively weak and narrow ozone lines above 100 GHz (figure 2.1). Other atmospheric molecules also have spectral lines in the millimeterwave region, but the expected strength of these lines is too small to cause any significant absorption. For detection of these trace atmospheric constituents present in the stratosphere or beyond only those frequency bands are useful where the tropospheric opacity is low. These low absorption regions are called 'atmospheric windows' for observations. These 'windows' in the millimeter-wave region are shown in table 2.1.

The atmospheric absorption and emission by all its constituents is governed by the Radiative Transfer Equation (RTE) (Chandrasekhar 1960). In the following sections we shall first formulate the radiative transfer expressions appropriate for calculating absorption and emission by atmospheric gases. Then the general expression for the spectral line absorption coefficient will be given, followed by specific expressions for calculating absorption by ozone.

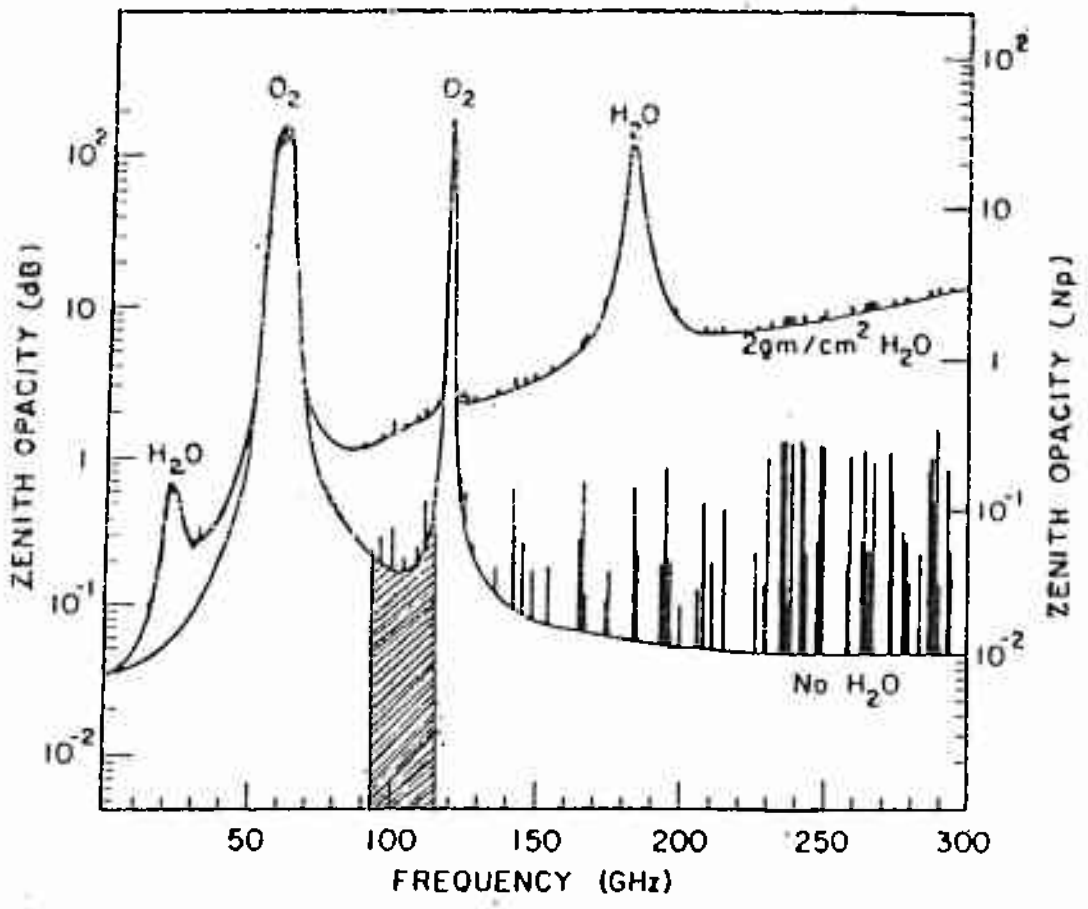

Fig. 2.1 Atmospheric zenith opacity in 0-300 GHz frequency range. The hatched part shows the window region between strong oxygen transitions at 60 and 118 GHz. The curve for 2gm/cm^2 water vapor assumes a water vapor density of 10 gm/m^3 at the surface.

Table 2.1 : Main atmospheric absorption features due to oxygen and water vapor in the troposphere and the 'window regions' in frequency.

Absorption Feature	Frequency Window
22 GHz H_2O line	24 to 48 GHz
60 GHz O_2 line cluster	70 to 115 GHz
118 GHz O_2 line	125 to 165 GHz
183 GHz H_2O line	200 to 310 GHz

2.2 Radiative Transfer

When a monochromatic radiation of wave length λ and intensity I_λ passes through a thin layer 'ds' of a gas, a small increment dI_λ of it is absorbed (figure 2.2). By the definition of the fractional absorption (Gordy 1953)

$$dI_\lambda = -a_\lambda I_\lambda \qquad (2.1)$$

First we will consider that the gas is cool and it's emission at the given wavelength is negligible, later we shall take this emission into consideration. The measurement of radiation entering and leaving such a layer pertains only to the absorption (a_λ) which is proportional to the density of the gas and the thickness 'ds' of the volume

$$a_\lambda = k_\lambda . \rho . ds \qquad (2.2)$$

k_λ is constant of proportionality and is called absorption coefficient of the gas. This k_λ may also vary with pressure and temperature of the gas despite varying with wavelength of the propagating radiation. So we take the density term inside 'k' and define it as the absorption coefficient of a gas at a given temperature and density ($k_\lambda = k_\lambda . \rho$) From equation (2.1)

$$dI_\lambda / I_\lambda = -k_\lambda . ds \qquad (2.3)$$

This is fractional decrease in intensity of the incident radiation on passing through a small thickness 'ds' of the gas of absorption coefficient 'k'. When we integrate equation (2.2) over a finite length 's' we have

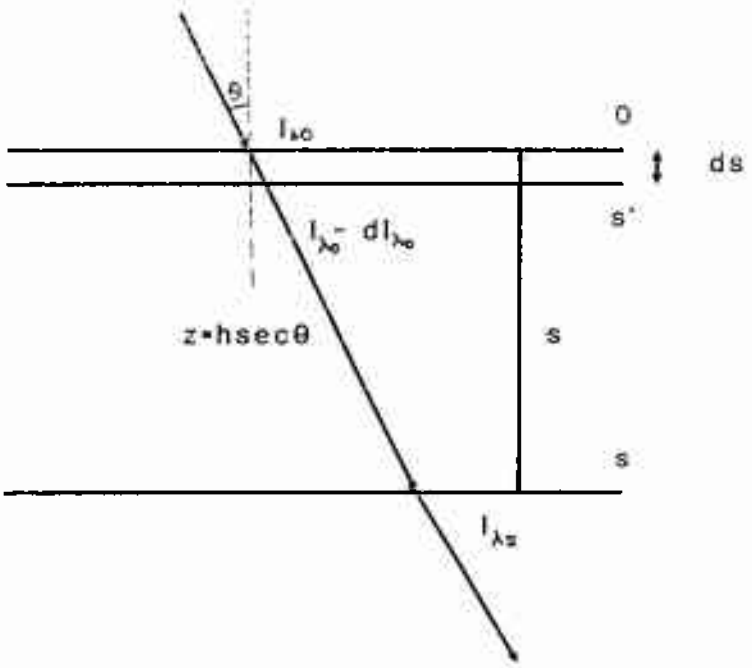

Fig. 2.2 Geometry for the Radiative Transfer Equation

$$\int_{I_{\lambda 0}}^{I_{\lambda s}} dI_\lambda / I_\lambda = -\int_0^s k_\lambda . ds \qquad (2.4)$$

or

$$I_{\lambda s} = I_{\lambda 0} \exp(-\int_0^s k_\lambda . ds) \qquad (2.5)$$

where

$I_{\lambda 0}$ = incident intensity (at wavelength λ)

$I_{\lambda s}$ = intensity after penetration to distances 's'

The integrand on the right hand side in equation. (2.5) is written as

$$k_\lambda . ds = d\tau_\lambda \qquad (2.6)$$

where τ = optical depth or opacity of the medium. Thus equation (2.3) becomes

$$I_{\lambda s} = I_{\lambda 0} . e^{-\tau_\lambda} \qquad (2.7)$$

When τ = 1, the intensity of radiation reduces to 1/e of its original incident value on passing through the medium. When the radiometer is looking at an angle θ from the zenith (elevation angle = (90-θ), (see figure 2.2) then the above equation (2.5) becomes

$$I_{\lambda s} = I_{\lambda 0} \exp[-\int_0^s k_\lambda \sec\theta dz] \qquad (2.8)$$

In the above development we have assumed that the re-emission from the atmosphere is zero/negligible compared to the incident radiation. This assumption is valid only for high frequency radiations viz. visible light passing

through the atmosphere. However, in case of millimeter waves, re-emission is no longer negligible. Air does emit significantly in the millimeter wave region. The amount of this re-emission could be found out by using the Kirchoff's law for the black body radiation emission. The intensity of this radiation is give by

$$I_\lambda = a_\lambda . B(\lambda, T) \tag{2.9}$$

Where B(λ,T)is Planck's black body emission rate. Thus when a monochromatic radiation enters a layer of gas there is a loss of intensity by gaseous absorption and a gain in intensity by the re-emission from the gas at that wavelength. The amount of this re-emitted radiation depends on the temperature of the gas and could be calculated as follows. If the radiation emerging out only due to re-emission at level s' in figure 2.2 be $dI_{\lambda s}$ then the radiation reaching at point 's' due to the layer 'ds' is

$$dI_{\lambda s} = [B(\lambda, T).K_\lambda . ds].e^{-\tau_\lambda (s', s)} \tag{2.10}$$

If we consider the horizontally stratified atmosphere with layers of thickness 'ds' then the total re-emission radiation is the integral of equation (2.10) over thickness 0 to s

$$I_{\lambda s} = \int_o^s B(\lambda, T).k_\lambda (s').\exp(-\tau(s', s)).ds' \tag{2.11}$$

and the complete equation including both the absorption and re-emission terms becomes

$$I_{\lambda,s} = I_{\lambda,0}.\exp[-\tau_\lambda(0,s)] + \int_0^s B(\lambda,T(s')).k_\lambda(s').\exp[-\tau(s',s)].ds'$$

(2.12)

This is the Radiative Transfer Equation in it's simplest form. For the frequency region considered here and for the real atmospheric temperatures, the intensity of radiation is proportional to the brightness temperature (T_B). This brightness temperature is the temperature of a blackbody radiator having the equivalent intensity of radiation as expressed by equation (2.12) above and is defined by

$$T_B(s') = \frac{c^2.I_\lambda(s')}{2K\nu^2} \qquad (2.13)$$

Equation (2.12) is then re-written in terms of brightness temperature as

$$T_B(s) = T_B(0).\exp[-\tau_\lambda(0,s)] + \int_0^s T(s).k_\lambda(s').\exp[-\tau_\lambda(s',s)].ds'$$

(2.14)

If the temperature of the whole absorbing medium is constant then the above equation (2.14) becomes

$$T_B(s) = T_B(0).\exp[-\tau_\lambda(0,s)] + T(1-\exp[-\tau_\lambda(0,s)])$$

(2.15)

from this equation we can see that for totally opaque atmospheric conditions ($\tau = \infty$) the first term on R.H.S. becomes zero and $T_B(s) = T$ (temperature of the medium). Similarly for completely transparent atmosphere ($\tau = 0$) and $T_B(s)$

$= T_B(0)$ which is the background temperature. Also if the medium temperature is equal to the background temperature ($T = T_B(0)$) the received temperature will be equal to the background temperature or $T_B(s) = T_B(0) = T$.

2.3 Absorption by Gases

There are two types of absorption characteristics shown by the atmospheric gases. These are resonant and non resonant absorptions as described below

2.3.1 Resonant Absorption

Resonant absorption is exhibited by gaseous molecules having electric or magnetic dipole moments which can couple to the electromagnetic fields passing through the medium. The frequencies at which the electromagnetic field couples to the molecules is determined by the differences between the energy levels (mostly rotational energy levels in case of millimeter-wave transitions) of the molecule. In absence of any line broadening mechanism transitions can occur only at frequencies (υ) given by $\upsilon = (E_1 - E_2)/h$ where symbols have their usual meanings. These energy levels are not sharp but have width determined largely by electric or magnetic field which originate externally or due to the intermolecular interactions.

The general quantum mechanical expression for the absorption coefficient for a single microwave transition was given by Van Vleck (1947). This is

$$k_{\nu_{lm}} = \frac{8\pi^3 N_i \nu \mu^2}{3hcQ} . \exp[-\Delta E_{lm}/kT] . \phi^2_{lm} f(\nu, \nu_{lm}) \qquad (2.16)$$

where:

c = velocity of light

k = Boltzmann constant

T = excitation temperature describing energy level population (it is assumed here that excitation temperature is the atmospheric kinetic temperature, i.e. the levels are populated by collision.)

N_i = number of molecules (of species 'i') per unit volume

g_l = statistical weight of lower state of transition

ΔE_{lm} = $\exp(-E_l/kT) - \exp(-E_m/kT)$, l & m represent two different levels

ϕ_{lm} = transition matrix element

ν = frequency of measurement

ν_{lm} = transition frequency of the molecule

Q = partition function

= square of interaction energy matrix between the states <l> and <m> of transition. For the temperature encountered in the atmosphere the partition function is given by following expressions

(a) for linear molecules

$$Q = \frac{kTg}{\sigma hB} \qquad (2.17)$$

(b) for non linear molecules

A, B and C are the rotational constant of the molecule and σ is the

$$q = \frac{G}{\sigma}\left[\frac{\pi}{ABC}\left(\frac{kT}{h}\right)^3\right]^{1/2} \qquad (2.18)$$

molecular symmetry number.

$f(\nu,\nu_{lm},\Delta\nu)$ = line shape function, where $\Delta\nu$ is a line width parameter, this shape function is normalized such that

$$\int f(\nu,\nu_{lm})d\nu = 1 \qquad (2.19)$$

For pressure broadened lines this shape function is described by the following formula and is called Van Vleck Weisskoff shape

$$f(\nu,\nu_{lm}) = \left[\frac{\nu}{\pi\nu_{lm}}\right]\left[\frac{\Delta\nu}{(\nu-\nu_{lm})^2+\Delta\nu^2} + \frac{\Delta\nu}{(\nu+\nu_{lm})^2+\Delta\nu^2}\right] \qquad (2.20)$$

Where

ν_{lm} = actual transition frequency between levels <l> and <m>

ν = frequency of observation

$\Delta\nu$ = pressure broadening

2.3.2 Non Resonant Absorption

The atmospheric absorption away from the resonant absorption lines is caused by the far wing effect of the lines which extends in the window regions of atmosphere. This absorption is mainly caused by the presence of oxygen and water vapor in the troposphere. The contribution due to oxygen remains essentially constant but absorption due to water vapor changes with the change in it's density in the troposphere. We consider the following two

cases;

(a) When $\nu << \nu_{lm}$ or when the observational frequency is on the left wing of the line

$$f(\nu,\nu_{lm}) = \frac{\nu\Delta\nu}{\pi\nu_{lm}^{3}} \tag{2.21}$$

(b) When $\nu >> \nu_{lm}$ or when the observational frequency is on the right wing of the line

$$f(\nu,\nu_{lm}) = \frac{\Delta\nu}{\pi\nu\nu_{lm}} \tag{2.22}$$

These line shapes are then multiplied by an appropriate quantity as given in equation 2.16 to give the additive terms of non resonant absorptions to the resonant absorption. The total absorption coefficient then becomes

$$k_{total} = k_{resonant} + k_{nonresonant} \tag{2.23}$$

These non resonant absorptions cause base line effects in the observed spectrum. The total absorption coefficient k_ν at frequency ν can also be written as the summation of the absorption coefficients for the individual transitions at that frequency

$$k_\nu = \sum_{all\ transitions} k_{\nu_{l-m}} \tag{2.24}$$

2.4 Line Broadenings

In the earth's atmosphere there are mainly two types of dominant broadening mechanisms responsible for spectral line broadening. These are collisional or pressure broadening and thermal or Doppler broadening. These two are described in some detail in the following section

2.4.1 Pressure Broadening

This broadening arises due to collision excitation of the molecules. In a gas the molecules undergo collisions with the surrounding molecules of the volume. After every collision the energy and the momentum of the colliding pair are redistributed leaving a net effect on the frequency of emitted radiation. This pressure broadening is described in terms of parameters γ and x defined such that the half width at half maximum of the Lorentzian line shape for a given pressure 'p' and temperature 'T' is

$$\Delta\nu = \gamma_0 . p . \left(\frac{300}{T}\right)^x \qquad (2.25)$$

A parameter γ defined as $\gamma = \Delta\nu/p$ is used for convenience reducing the equation 2.25 to the following form

$$\gamma = \gamma_0 \left(\frac{300}{T}\right)^x \qquad (2.26)$$

γ_0 has units of MHz/millibar. The value of γ_0 was calculated theoretically (Tejwani et. al. 1975, Gamache and Devies, 1985) and obtained experimentally (Connor 1985) for a wide range of transitions and

over a sufficiently large temperature range. These values were obtained for pure O_3-N_2 and O_3-O_2 broadenings. The air broadened line widths were then calculated by using the following formula

$$\gamma = 0.79\gamma_{O_3\text{-}N_2} + 0.21\gamma_{O_3\text{-}O_2} \qquad (2.27)$$

The value of x is crucial here and depends upon the type of interaction present between the molecules. If molecules are considered as hard spheres and the collision cross section is independent of molecular velocities then according to kinetic theory x = 0.5. But this is not found to be true for millimeter wave lines where the collision cross sections are several times larger then the hard cross sections of molecules calculated by kinetic theory. This is a reasonable assumption as energy involved in millimeter wave transitions are much smaller than kT ($h\nu << kT$) and therefore molecules have much larger effective cross sections. The collision cross section is dependent on molecular velocities also. A slow molecule spends more time near the radiating molecule and causes more disturbance compared with the one which passes quickly. Hence the collision line broadening is dependent on temperature of the gas as well as on the intermolecular forces. For the force which varies with separation r as r^n, the value of 'x' is given by

$$x = \frac{(n+1)}{2(n-1)} \qquad (2.28)$$

Typical intermolecular forces have n = 3 to n = 6 which gives $\Delta\upsilon_C$ proportional to $T^{-1.0}$ to $T^{0.7}$. This is in agreement with the results obtained experimentally (Connor 1985). The collision linewidth is proportional to pressure so long as the collisions involving more than two molecules are

negligible which holds true in case of stratospheric ozone (Tejwani & Yeung 1975, Gamache & Davies 1985)). The collision line shape function is described by Lorentzian function given below (Townes and Schawlow 1955)

$$f(\nu,\nu_{lm},\Delta\nu_C) = \frac{1}{\pi}\left[\frac{\Delta\nu_C}{\Delta\nu_C^2+(\nu-\nu_{lm})^2}\right] \qquad (2.29)$$

This equation is derived from equation 2.20 by putting the second term inside the bracket equal to zero as $(\nu+\nu_{lm})^2 >> \Delta\nu^2$ and equating ν with ν_{lm} outside bracket as $\nu \approx \nu_{lm}$.

2.4.2 Doppler Broadening

This broadening is a consequence of the motion of radiating molecules relative to the detector. If the velocity of a radiating molecule in the direction of observation be V then the actual frequency of radiation ν_0 appears to the observer (detector) as

$$\nu = \nu_0\left(1+\frac{v}{c}\right) \qquad (2.30)$$

where c is the velocity of light. Considering a Maxwellian distribution of velocities of gas molecules we get an expression for Doppler broadening as

$$\Delta\nu_D = \frac{\nu_0}{c}\left(2kt.\frac{ln2}{M}\right)^{1/2} \qquad (2.31\ A)$$

or

$$\Delta \nu_D = 3.85\times10^{-7}\ \nu_0\left(\frac{T}{M}\right)^{1/2}\ Hz \qquad (2.32\ B)$$

where

ν_o = resonance (transition) frequency

T = Temperature

M = Molecular wt. of the gas

Doppler line shape function is given by (Townes and Schawlow 1955)

$$f_D(\nu,\nu_{im},\Delta\nu_D) = \left(\frac{ln2}{\pi}\right)^{1/2}\left(\frac{1}{\Delta\nu_D}\right)\exp\left[-ln2\left(\frac{\nu-\nu_o}{\Delta\nu_D}\right)^{1/2}\right]$$

(2.32)

Natural line broadening resulting from the finite lifetime of molecular states because of spontaneous transition is of the order of 10^{-9} to 10^{-4} Hz for millimeter-wave electric dipole transitions and is completely negligible in comparison to the above two broadenings.

These two line broadenings (Pressure & Doppler) are calculated upto height Z = 90 km and are shown in figure 2.3. It is clear from these curves that in the region of troposphere and stratosphere pressure broadening is much larger than the Doppler broadening (calculated for ν_o = 100 GHz) and hence the latter can be safely ignored upto 60 km altitude for all practical purposes. Doppler broadening becomes important only at altitudes above 60 km where the molecular collision frequency is comparable to or smaller than the doppler line width.

When both Doppler and pressure broadenings are important the resulting line shape ($f_{C\,D}$) is given by the convolution of the individual line shapes

(2.34)

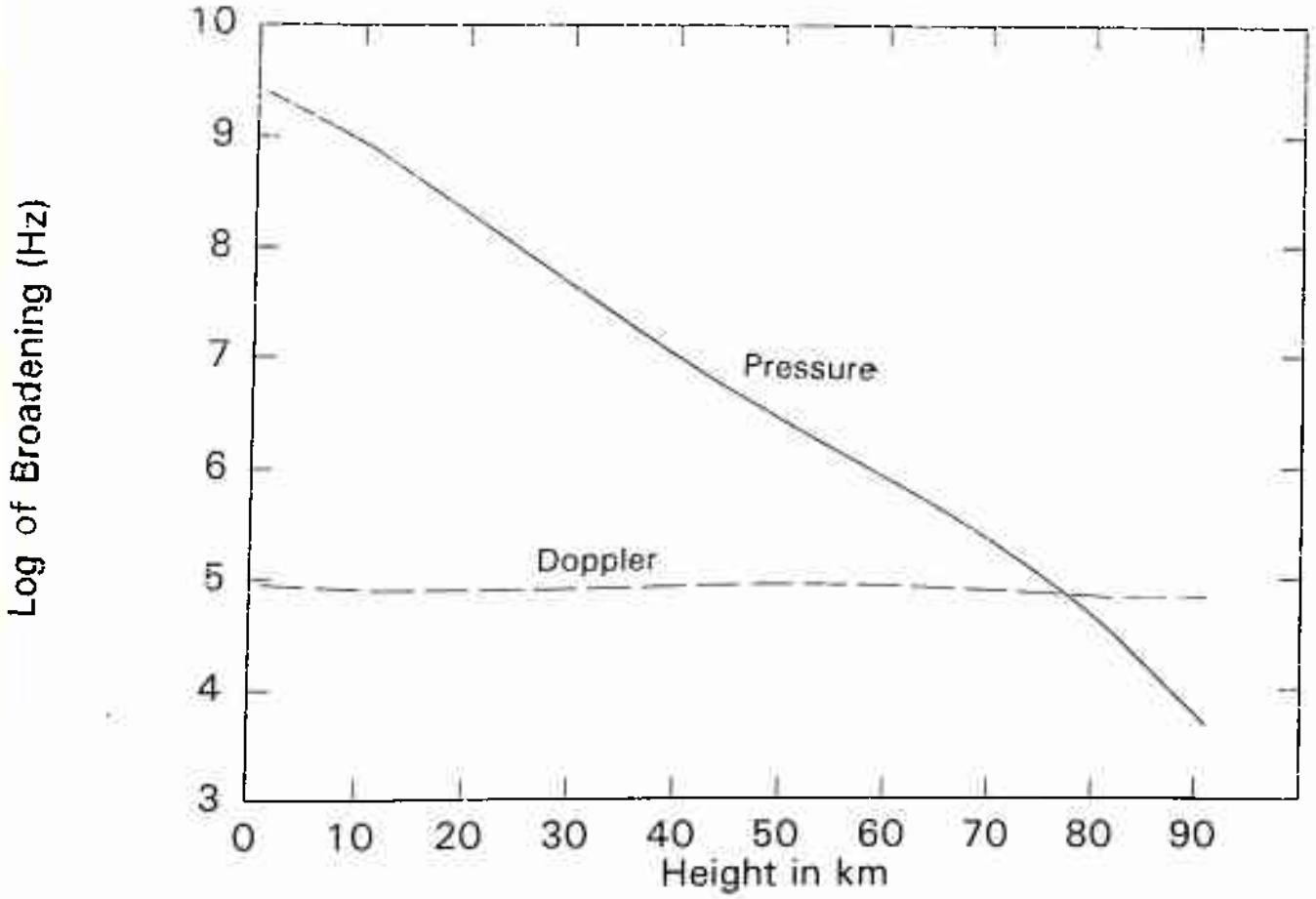

Fig. 2.3 Pressure and Doppler broadenings in the earth's atmosphere upto 90 km from the surface.

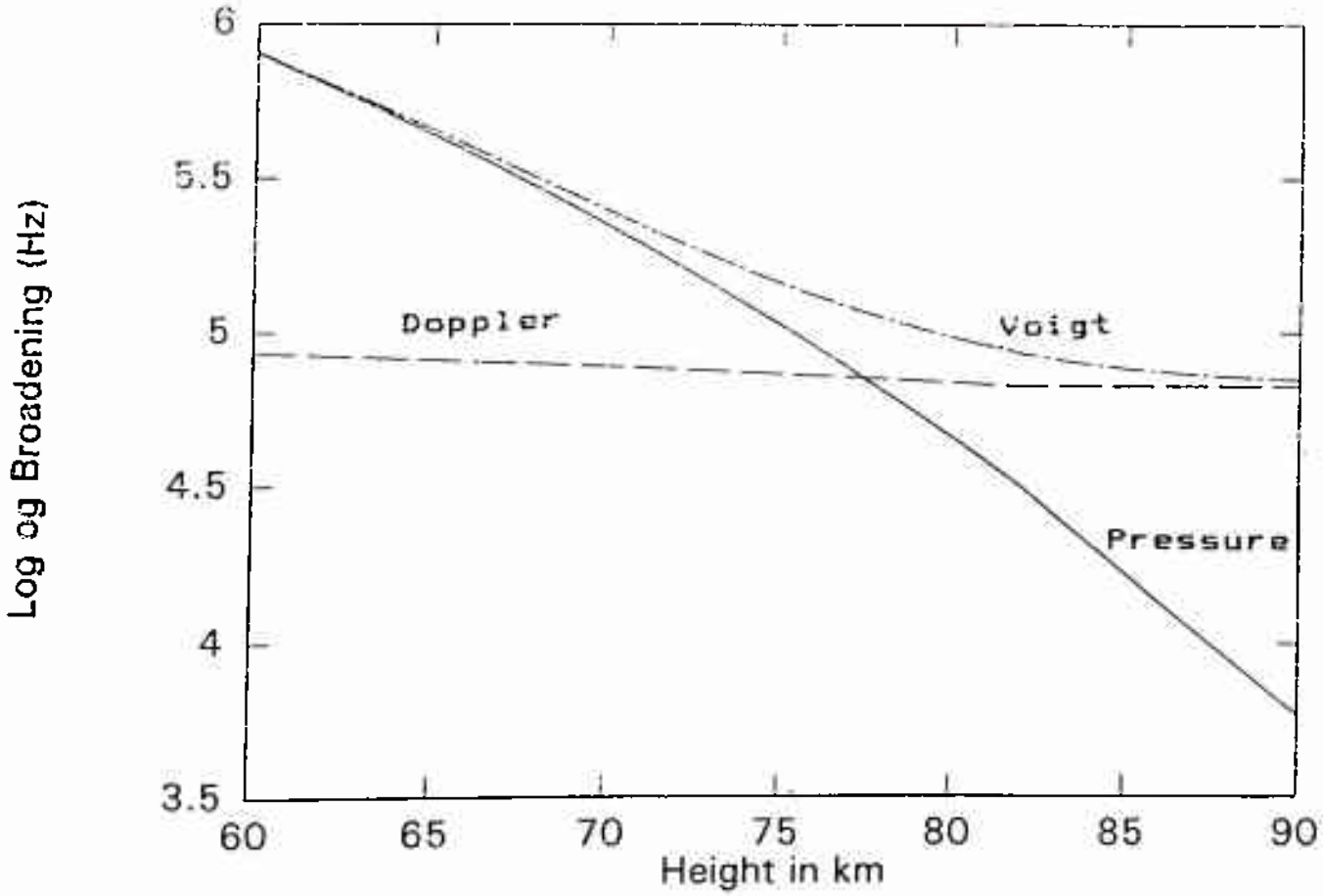

Fig. 2.4 Convolution of pressure and Doppler broadenings (Voigt profile) in 60-90 km region.

$$f_{CD}(\nu,\nu_{lm},\Delta\nu_C,\Delta\nu_D) = \int_{\Omega} f_C(\nu,\Omega,\Delta\nu_C) * f_D(\Omega,\nu_{lm},\Delta\nu_D) d\Omega$$

(2.34)

where * represents convolution. This line shape is called the Voigt shape. The above convolution function is rather complicated and hence the empirical fits to the Voigt line widths (Olivero and Longbothum, 1977) can be used for the economy in computation time. Here the function used for calculating the Voigt line shape is

$$\Delta\nu_\nu = \frac{1}{2}(C_1\nu_P + \sqrt{(C_2\nu_P^2 + 4c_3\nu_D^2)}) \qquad (2.34)$$

Where C_1, C_2 and C_3 are the constants and are given the following values

$C_1 = 1.0692$

$C_2 = 0.86639$ and

$C_3 = 1.00$

This Voigt shape is plotted in figure 2.4 in the height range 60-90 km.

2.5 The Ozone Molecule

The microwave spectrum investigations (Hughes 1953, Trambarulo 1953) have determined ozone to be a slightly asymmetric molecule. It's three principal moments of inertia are all different. In spectroscopy molecules are categorized as

(i) symmetric rotors (symmetric top) having at least two out of three principal moments of inertia equal and

(ii) asymmetric rotors having all the three principal moments of inertia unequal.

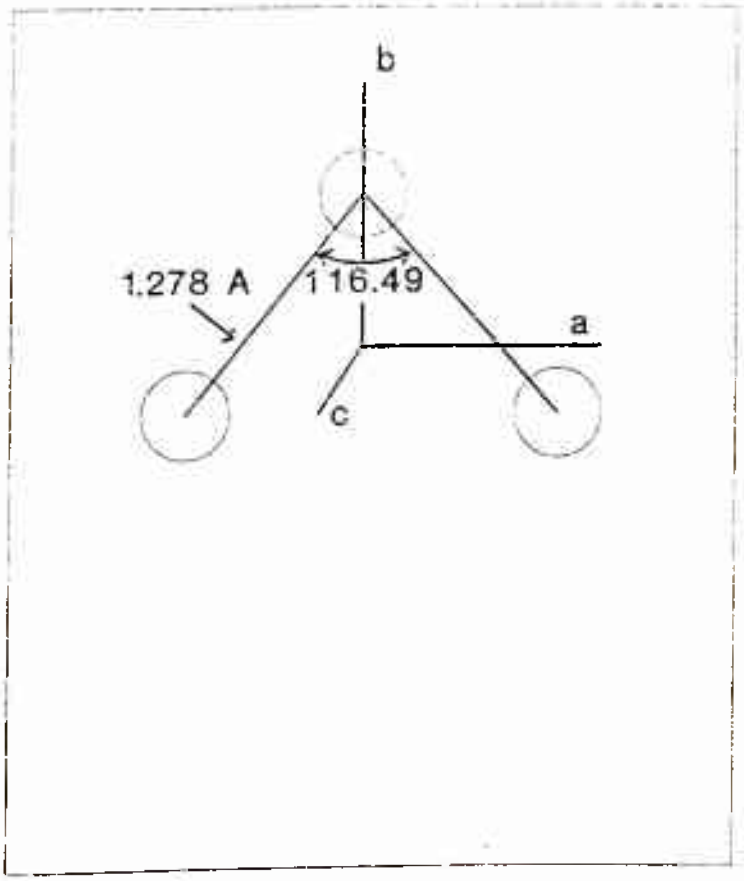

Fig 2.5 The Ozone Molecule

Ozone is a slightly asymmetric rotor. A measure of molecular asymmetry (k) is given by the following formula

$$k = \frac{2B-A-C}{A-C} \qquad (2.35)$$

Where A, B and C are the rotational constants of the molecule about three independent axes. If B = C the molecule has prolate symmetry and if B = A it is has oblate symmetry. These prolate and oblate shapes are the shape of the molecular moment of inertia surface around it's center of mass. For prolate symmetry rotor k = -1 and for oblate symmetry rotor k = +1. In case of ozone ($^{16}O_3$) k = -0.97 being a nearly prolate symmetric rotor. These k's are the values of quantum number (k) describing the projection of angular momentum (J) on an axis fixed in space (molecular symmetry axis). These J and k are the good quantum numbers to specify the state of the rotor. However, in the rotating asymmetric molecule the component of J along any fixed axis is not constant and hence k is not a good enough quantum number to specify the molecular rotational state. In fact there is no one set of good quantum numbers and hence for asymmetric top molecules the energy levels are specified by giving the value of J, and the value of K_{-1} for the limiting prolate and K_1 for the limiting oblate symmetry top. The value of the molecular rotational constants for ozone are

$$A = 106530.0 \pm 1.1 \text{ MHz}$$

$$B = 13349.0 \pm 0.06 \text{ MHz}$$

$$C = 11834.0 \pm 1.1 \text{ MHz}$$

The O-O bond length is 1.278×10^{-8} cm and an angle of 116°49′ between the central and the outer atoms figure 2.5. The value of the electric dipole moment (μ) is

$$\mu = 0.53\times10^{-18}\ csu\ cm$$

Ozone has zero nuclear spin so the partition function expression (2.18) becomes

$$Q = \frac{1}{2}\left[\frac{1}{ABC}\left(\frac{kT}{h}\right)^{3}\right]^{1/2} \qquad (2.36)$$

The calculation of absorption coefficient equation (2.16) requires the value of energy levels between which the transition is taking place. The energy of level 'I' for a slightly asymmetric prolate rotor (ozone) is given by

$$E_I = E_{j,k_{-1}} = h\left[\frac{B+C}{2}J(J+1) + \frac{2A-B-C}{2}(k_{-1})^2\right] \qquad (2.37)$$

Where J is the total angular momentum quantum number and K_{-1} is the quantum number denoting the projection of angular momentum along the symmetry axis of corresponding prolate symmetry rotor.

2.6 Absorption by Ozone Molecule at 101.7 GHz

The key quantity in the calculation of transmission coefficient of the atmosphere and the emission or the effective brightness temperature of the atmosphere due to ozone is the absorption coefficient as a function of frequency and altitude. The absorption coefficient of O_3 at a given frequency is in principle the sum of the contributions from all the spectral lines. If, however, the lines are very narrow such that the wings of the other lines do not expand appreciably into the region under consideration then the contribution due to these lines can be neglected. In the region of atmosphere

where the Ozone is present the pressure is quite low and although there is pressure broadening it is not of such an extent as to put appreciable intensity into the overlapping wings. In order to calculate the absorption coefficient of Ozone we used the following formula (Gora 1989)

$$k_i^0(\nu,z) = \frac{8\pi^2 N\mu^2\nu^2 XY}{3KTcQ\nu}\left[\frac{\Delta\nu}{(\nu-\nu_0)^2+(\Delta\nu)^2} + \frac{\Delta\nu}{(\nu+\nu_0)^2+(\Delta\nu)^2}\right]$$

(2.38)

Where

N = No of ozone molecules per cubic cm

μ = Dipole moment of Ozone molecule

X = $kT/h\upsilon(1-e^{-h\upsilon/kT}) = 1$ (for our case because $h\nu << kT$)

Y = $/ \phi /^2 e^{-Ei/kT}$ is the matrix element of transition giving rise to the line and Ei is the energy value of the lower of two states (This Y is also called the line intensity factor. For 101.737 GHz line Y = 4.11

$\Delta\upsilon$ = line frequency broadening due to pressure and Doppler broadening mechanism. The value of $\Delta\upsilon$ has been calculated using formulae described in section 2.4. The following value of γ when multiplied by the atmospheric pressure (in millibars) will give pressure broadening as a function of altitude (z) $\gamma = 3.20(T/300)^{-0.73} \times 10^6$ Hz/mb. here a value 0.73 is taken for x (Connor 1985).

N = r.N(atm.) , where r is the ozone mixing ratio and N(atm.) is the number of molecule per unit volume in the atmosphere. This is given by

$$N(atm) = \frac{0.966\times10^{19}P(mm)}{T(K)}\,cm^{-1} \qquad (2.39)$$

(From US Standard atmosphere 1976)

Q = rotational partition function given by the following formula

$$Q = \frac{1}{2}\left[\frac{K}{T}\right]^{3/2}\left[\frac{\pi}{A.B.C}\right]^{3/2} \qquad (2.40)$$

A,B,C are rotational constants of Ozone molecule around three independent axes as described in section 2.5

Using these values we get

Q = $0.65\ T^{3/2}$

μ = Dipole moment of Ozone molecule

= 0.53 Debye

= 0.53×10^{-18} esu cm

ν = frequency of observation.

Putting above values in the expression for absorption coefficient we get

$$k_1^0 = \frac{1.28\nu^2}{T^{2.8}}\left[\frac{(\Delta\nu)^2}{(\nu-\nu_0)^2+(\Delta\nu)^2}+\frac{(\Delta\nu)^2}{(\nu+\nu_0)^2+(\Delta\nu^2)}\right] \qquad (2.41)$$

here υ appearing outside the bracket is in GHz and all the terms inside square bracket are in same unit of frequency. The term outside the bracket is max. absorption coefficient (α_{max})

$\alpha_{max} = (1.28 \times 10^5\ \upsilon^2)/T^{2.8}\ km^{-1}$

$\alpha_{max} = (1.28 \times \upsilon^2)/T^{2.8}\ cm^{-1}$ (2.42)

Now for our case $\upsilon^2 = (101.737)^2$ (as we have already used 10^{18} factor) & putting T = 220 K we get $\alpha_{max} = 185 \times 10^{-5}\ cm^{-1}$ (185 Km^{-1}). This α_{max} can directly be taken from Gora (1959). Annexure I gives the general micro-

wave/millimeterwave spectrum of ozone for all strong transitions occurring in this range 90-300 GHz) as calculated by (Gora 1959) and experimentally determined by Lichtenstein & Gallagher (1971) and Connor (1985).

For the Ozone molecule the atmospheric condition considered here only the ground electronic and vibrational states will be appreciably populated as thermal energies are not sufficient to excite a significant number of molecules into the higher states. for example, the fraction of molecules for the ground vibrational state is given by (Townes & Schawlow 1955)

$$f_o = 1 - e^{-\hbar\omega/kT} \qquad (2.43)$$

Where ω is the molecular vibrational constant. The lowest f_o which we shall encounter corresponds to lowest ω ($\omega = 2.1 \times 10^{13}$/sec) and highest temperature ($T = 300$ °K) is $f_o = 0.965$. It is clear from here that only the distribution of the molecules among the various rotational levels need to be considered.

2.7 Inversion Procedures for Retrieval of Ozone Height Profile from Ground Based Spectral-Line Data

Numerous methods of interpreting radiometric measurements in terms of meteorological parameters have been developed and presented in the literature (Wark & Fleming 1966, Rodgers 1976, Twomey 1977 etc). They all require the inverse solution of the radiative transfer equation (RTE). It is well known that the inverse solution of radiative transfer equation is non unique; that is, there are many temperatures and absorbing gas profiles which will satisfy a set of observed radiances within practical experimental errors (smith 1970). Therefore the physical validity of the solution becomes inherently

dependent on the particular algorithm used to solve the radiative transfer equation. The most successful interpreting algorithms generally fall in one of the two different classes of solutions: (1) the statistical matrix inversion class and (2) the iterative inversion class. (Direct matrix inverse solutions which do not use statistical functions or some other form of conditioning agent produce highly unstable results in case of near singular matrices which is mostly the case for any ground based limited frequency band observation). Statistical solutions are advantageous for retrieving atmospheric characteristics in regions where current or historical empirical observations are available for generating representative statistical functions (Rodgers 1976). For remote regions iterative methods which do not depend significantly on other empirical observations are useful. In the following sections two inversion techniques which are used to retrieve the ozone profile in this study, are presented.

2.7.1 Iterative Method of Inversion

In this method the ozone Volume Mixing Ratio (VMR) is determined from the observed line spectrum with an iterative inversion technique. We start from an arbitrary initial guess of ozone profile of 1ppm VMR to calculate a brightness temperature spectrum by integrating the radiative transfer equation. The observed brightness temperature differences of the neighboring channels are then compared with the equivalent brightness temperature differences obtained from the calculated spectrum in order to correct the initial guess of ozone profile. This process is repeated until the difference between the calculated and observed data is smaller than the experimental error level. The iterative algorithm then modifies the profile at the iteration points using the

relaxation formula derived by Chahine (1972) and interpolates the profile linearly for the integration of radiative transfer equation.

Here in the following sections the generic RTE is first simplified for the mm-wave frequency region using Rayleigh-Jeans approximation to it. Only after this the iterative inversion scheme is developed.

2.7.1.1 Solving RTE

In the millimeterwave region the radiative transfer equation can be written as (Randegger 1980)

$$I(\nu) = I^0(\nu)\exp[-k(z_1z_2)] + \int_{z_1}^{z_2} B(\nu T(z))k(z_1z)\exp[-\int_{z_1}^{z} k(z_1z')dz']dz \qquad (2.44)$$

where ($z_1 = s$, $z_2 = 0$ & $z' = s'$ in fig. 2.2)

$I^0(\nu)$ = background radiance

$\exp[-K(z_1,z_2)]$ = The transmittance between z_1 and z_2

$B(\nu,T(z))$ = $2\pi h\nu^3/c^2$ [exp($h\nu$/kt)-1] - Planck's Law and

$K(z_1,z)$ = $K(\nu,T(z),q_1(z),q_2(z)\ ...)$ is the length absorption coefficient, where the q's are the mixing ratios of the absorbing atmospheric constituents, T(z) is the temperature of the atmosphere and other symbols have their usual meanings.

For well isolated lines we can assume that the absorption mechanism of participating atmospheric constituents are independent of each other so we write

$$k(\nu,T(z),q_1(z),q_2(z)...) = \sum_i q_i(z)k_i^0(\nu,T(z)) \qquad (2.45)$$

where $K^{o}_{l}(\nu, T(z))$ is individual lth component's absorption coefficient per unit mixing ratio and $q_l(z)$ is mixing ratio of this constituent. Since in the millimeter wave region $h\nu/kt << 1$, the Rayleigh-Jeans approximation for $B(\nu,T(z))$ is valid. Hence substituting the intensity $I(\nu)$ by an equivalent blackbody brightness temperature $T_B(\nu)$ and neglecting the background term in equation (2.44) we get

$$T_B(\nu) = \int_{z_1}^{z_2} k(\nu, T(z), q_1(z) q_2(z) \ldots) \exp\left[-\int_{z_1}^{z} k((\nu), T(z'), q_1(z') q_2(z') \right.$$

$$\left. \ldots) dz' \right] T(z) dz \quad (2.46)$$

This is the integral equation we have to solve to get the mixing ratio of lth absorbing constituent (ozone in our case). In order to solve this equation for ozone mixing ratio $q_1(z)$ we would have to linearize it with respect to this quantity. Regarding sum of absorptions the integrand part of (2.46) is

$$k_1 \exp\left[-\int_{z_1}^{z} (k_1 + k_2 \ldots)\right] + (k_2 + k_2 \ldots) \exp\left[-\int_{z_1}^{z} (k_1 + k_2 \ldots)\right]$$

Where K_1 is the absorption coefficient of Ozone and K_2, K_3 etc. are the absorption coefficients for other gases. Also we have

$$k(\nu, T(z), q_l(z)) = q_1(z) k_l^0(\nu, T(z)) \quad (2.47)$$

where $K_l^o[\nu, T(z)]$ is the absorption coefficient per unit mixing ratio of the lth absorbing constituent. Now to linearize the integrand on the right hand side of equation 2.46 we divide it into two limit zones

(1) In the stratosphere (altitude > x ~ 12 km)

$K_1 >> (K_2 + K_3 + \ldots)$

(2) In troposphere (altitude $< x \sim 12$ km)

$K_1 << (K_2 + K_3 + ...)$

Consequently expression of absorption coefficient reduces to

$$k_1 \exp[-\int(k_1 dz)]\exp[-\int_{z_1}(k_2+k_3...)dz'] + (k_2+k_3...)\exp[-\int_{z_1}^{z}(k_2+k_3...)\ dz']$$

This is valid as the ozone line at 101.737 GHz is an isolated weak line and is situated in a tropospheric transmission window. The exponential for ozone absorption coefficient ($\exp[-\int k_1 dz]$) in second term is taken to be equal to unity. In this expression the absorption (k) is the sum of two terms:

(i) Highly frequency dependent contribution due to the pressure broadened ozone absorption. This term contains the ozone profile to be retrieved.

(ii) Only slightly frequency dependent contribution due to tropospheric gases mainly oxygen and water vapor's far wing effect and the dielectric losses in cloud water droplets.

In the first term we assume the Ozone opacity $k_1 dz' << 1$ so the transmittance becomes equal to 1 ($\exp[-\int K_1 dz'] \sim 1$). Therefore, we can replace $q_1(z)$ in the opacity approximation by a standard ozone profile $\tilde{q}_1(z)$. The expression for absorption coefficient now becomes

$$q_1(z)k_1^0[\nu, T(z)]\exp[-\int_{z_1}^{z}\tilde{q}_1(z')k_1(\nu, T(z'))dz']\exp[-\int_{z_1}^{z}(k_2+k_3...)dz'\ ] +$$

$$(k_2+k_3...)\exp[-\int_{z_1}^{z}(k_2+k_3...)dz']$$

This function gives the desired linearization with respect to the ozone mixing ratio profile ($q_1(z)$)

$$T_B(\nu) = \int_{z_1}^{z_2} q_1(z) k_1^0(\nu, T(z)) \exp[-\int_{z_1}^{z} \tilde{q}_1(\hat{z}) k_1^0(\nu, T(\hat{z}))dz'] D(\nu) T(z) dz + A(\nu)$$

(2.48)

where

$$D(\nu) = \exp[-\int_{z_1}^{z} (k_2 + k_3 \ldots) dz'] \qquad (2.49)$$

$$A(\nu) = \int_{z_1}^{z_2} (k_2 + k_3 \ldots) \exp[-\int_{z_1}^{z} (k_2 + k_3 \ldots) dz'] T(z) dz \qquad (2.50)$$

and z_1 and z_2 are lower and upper limits of atmosphere between which the integration of equation (2.48) is to be performed. This Equation (2.48) is a linear integral equation which can be inverted for obtaining ozone mixing ratios as a function of altitude $q_1(z)$. It's weighting function is

$$W(\nu, z) = k_1^0(\nu, T(z)) \exp[-\int_{z_1}^{z} \tilde{q}_1(z') k_1^0(\nu, T(z') dz'] D(\nu) T(z)$$

(2.51)

And using this the radiative transfer equation can be written in a linearized form of $q_1(z)$ as

$$T_B(\nu) = \int_{z_1}^{z_2} q_1(z) W_1(\nu, z) dz + A(\nu) \qquad (2.52)$$

In our case, we have channels of discrete frequency values so the integration in equation (2.52) could be replaced by a summation as follows

$$T_B(\nu) = \sum_i q_i W_i(\nu) \Delta z + A(\nu) \qquad (2.53)$$

2.7.1.2 Character of Weighting Functions

Inspection of the weighting function W (ν,z) in the above equation (2.51) shows that it is basically the product of temperature profile T(z) and the Ozone length absorption coefficient $K_1(\nu, T(z))$. Upto 60 km altitude, pressure broadening prevails over all other line broadening effects. Hence lower stratospheric layers, where the pressure is high, contribute most to the wings of the broadened line. Mesospheric ozone, on the other hand, contributes only to the brightness temperatures in the central channels around the peak (figure 2.6). The upper limit Z_2 of integration should be such that the atmosphere beyond it does not contribute significantly to $T_B(\nu)$. In case of ozone it is approximately 90 km. The above equation (2.52) is then discretised for 1 km atmospheric layer widths and the summation in the equation runs from z = 0 km (ground) to z = 90 km.

The key quantity in the entire inversion scheme is the Weighting Functions (WFs) which link the observed brightness temperature to the ozone content at a certain height. These WFs do not have any sharp maxima in our region of interest (stratosphere & lower mesosphere) hence we adopt the suggestion of Waters (1974) for orthogonalization by subtracting neighboring frequencies' weighting functions & obtain difference Weighting Functions (DWF) given by

$$\Delta W(\nu,z) = W(\nu,z) - W(\nu',z) \qquad (2.54)$$

This orthogonalization can always be done for two frequencies ν and ν'

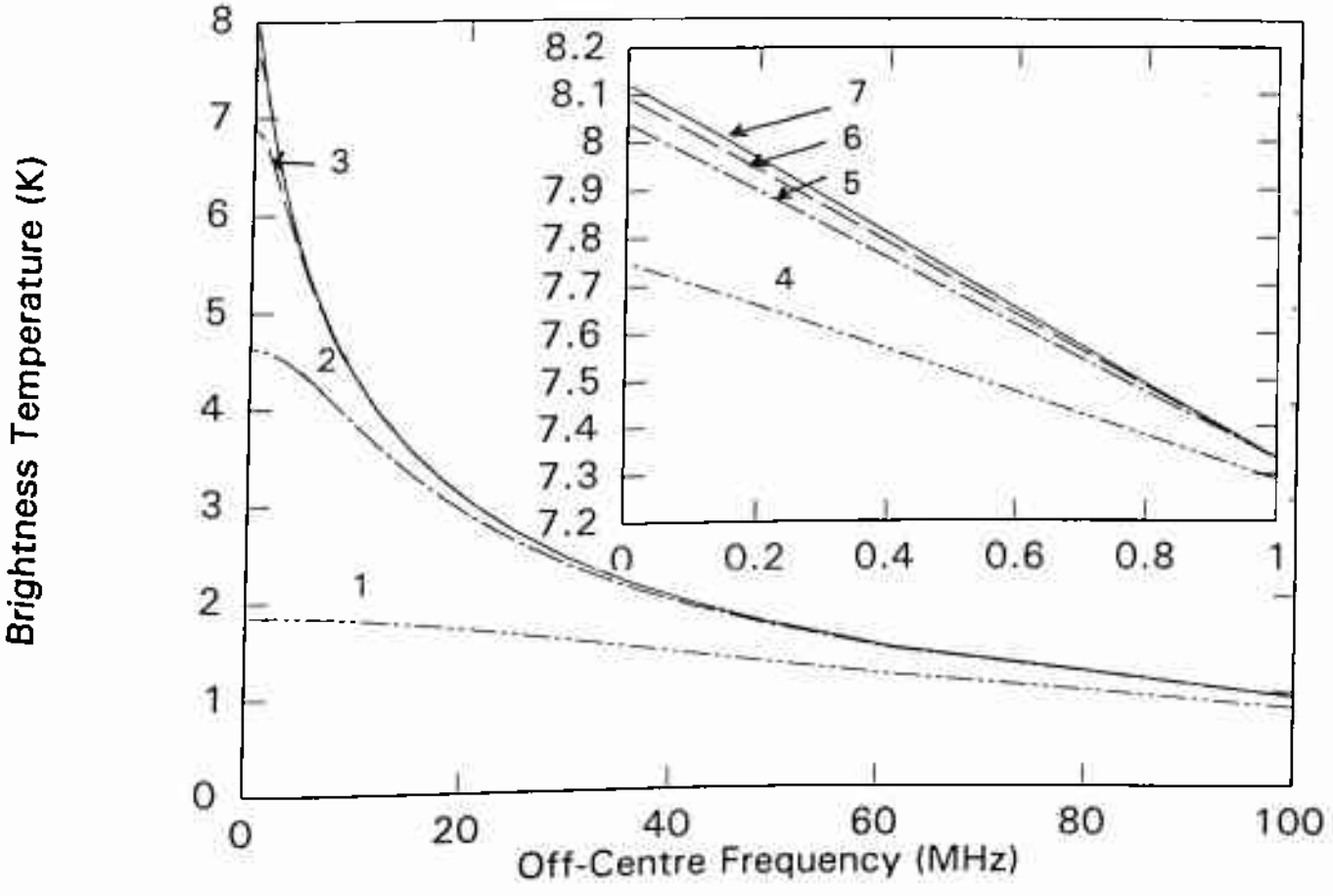

Fig 2.6 Synthetic spectra calculated for a mid lattitude ozone model upto Z = Z_{max} assuming $N(O_3) = 0$ for $Z > Z_{max}$. The values of Z_{max} for different curves are

(1) Z_{max} = 30 km (2) Z_{max} = 40 km (3) Z_{max} = 50 km

(4) Z_{max} = 60 km (5) Z_{max} = 70 km (6) Z_{max} = 80 km

(7) Z_{max} = 90 km

because q in (2.52) is independent of frequency (ν). The difference in brightness temperatures is given by the following formula

$$\Delta T_B(\nu) = \int_{z_1}^{z_2} q_1(z)\Delta W(\nu,z)dz + \Delta A(\nu) \qquad (2.55)$$

These DWFs show peaks in our region of interest, however, their shape is not narrow enough to establish one to one correspondence between the frequencies and the altitude points. The ideal situation would have been if they had shown delta function like behavior. In such a situation weighting function matrix gets diagonalized itself. Then we could assign different frequencies to the different heights in atmosphere. But this is not the case and the shape of weighting functions are not in our hands in this inversion scheme. The height resolution obtained by this method is about 8-10 km (Smith 1970, Waters 1970, Conrath 1972), which is essentially half power width of the difference weighting functions. However, if the true profile is assumed to be a single very thin layer, the formal resolution is 6 km; that is, the minimum separation between two thin layers which can be resolved in the retrieved profile is 5-7 km (Bevilacqua & Olivero). A few of these difference weighting functions normalized to unity are plotted in figure 2.7. They show a typical half power width of about 10 km. This half power width is a little less (about 8 km) in the lower stratosphere compared to mesosphere. This is a consequence of the fact that pressure decreases exponentially as one moves away from the surface of the earth and hence in the lower stratosphere there is relatively smaller height range where the line broadening is comparable to the υ-υ_0 giving a smaller height range where DWF has significant amplitude. As we have already neglected presence of Ozone in troposphere, the shape of weighting function

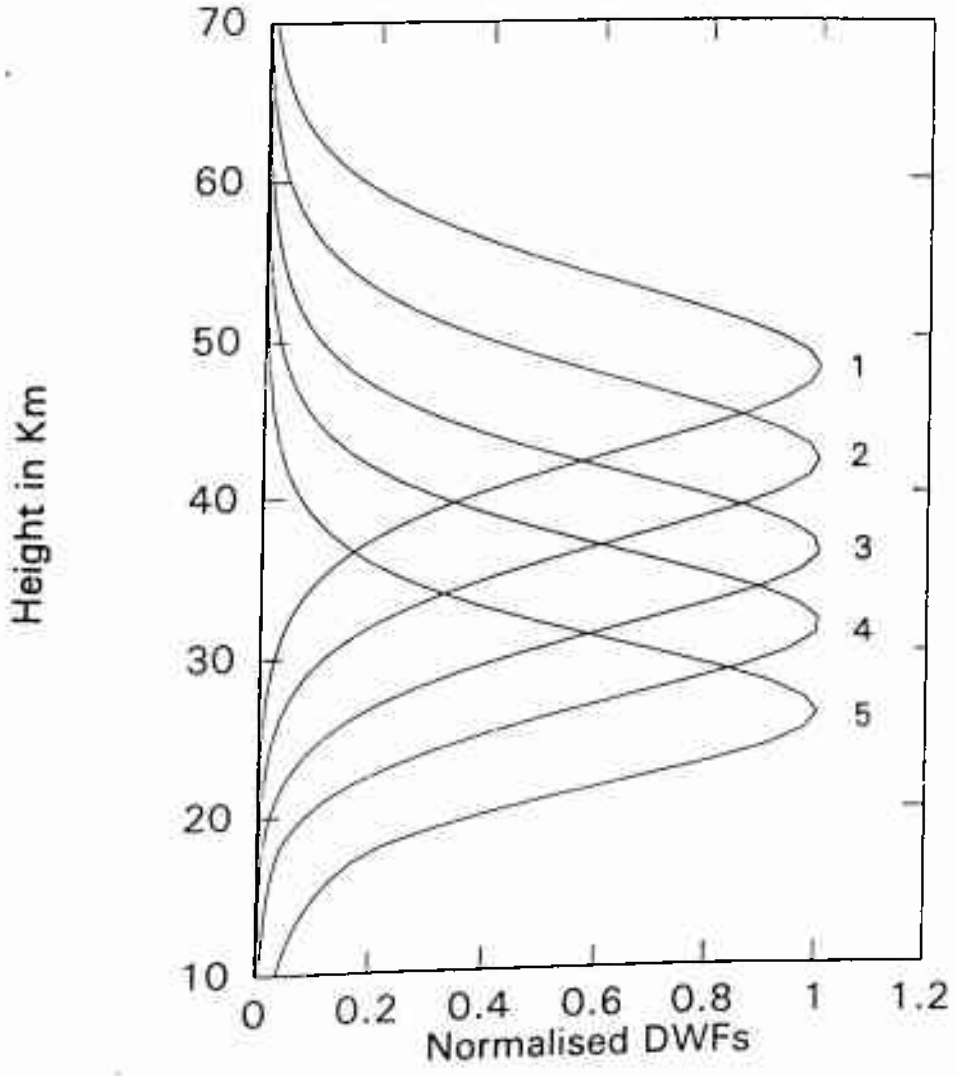

Fig. 2.7 Difference Weighting Functions (DWF) as defined by eqn 2.54. Each DWF has been normalised so that it's maximum value is 1. The frequency pairs used are

(1) 101.733 & 101.734 GHz (2) 101.729 & 101.730 GHz

(3) 101.719 & 101.722 GHz (4) 101.701 & 101.707 GHz

(5) 101.636 & 101.676 GHz

here has no real information. An important fact here is that the weighting function matrix W, whose elements are $W(\nu_i, z_j)$ is a square matrix (i = j). This may seem surprising in view of the fact that the no. of pressure levels used in the numerical integration are usually not equal to the sampling frequencies. Nevertheless the squareness of W is an intrinsic feature of this method and implies that q(z) is obtained at the altitude points determined by the number of frequency channels in the receiver. Thus having selected the N frequencies $\nu_1, \nu_2 \ldots \nu_n$ optimally this method aims at computing the volume mixing ratios at N heights points. At other intermediary levels the mixing ratios are obtained by interpolation. One very legitimate question arises at this stage - why can't we evaluate q by finding the inverse of W matrix. The reason beeing that the matrix W of interest is an ill conditioned matrix. The computation of W^{-1} is a very delicate operation and highly sensitive to measurement noises which can give a totally wrong result. In iterative inversion scheme computation of W^{-1} is avoided. The second advantage of this method is related to the positivity of q.

If W_{ij} is a non negative matrix then

$$W_{ij} > 0 , \quad i, j = 1,2 \ldots\ldots N$$

and

$$T_{Bi} \geq 0, \quad i = 1,2, \ldots\ldots N$$

Then provided $I^{\circ} > 0$ (first guess) the subsequent approximations generated will always be positive.

2.7.1.3 The Iteration Formula

The iteration formula used for running the iterative inversion scheme for our purpose is the following (Chahine 1972)

$$q_1^{n+1}(z_i) = q_1^n(z_i)\frac{T_B(\nu(z_i))}{T_B^n(\nu(z_i))} \qquad (2.56)$$

Where

q^n (z_i) = nth approximation of the ozone mixing ratio value at height z_i,

$\nu(z_i)$ = two frequencies ν_i & ν'_i for which the DWF has it's maximum at height z_i.

$T_B(\nu(z_i))$ = Difference of two measured brightness temperatures at frequencies ν_i and ν_i'

$T_B^n[(z_i)]$ = nth approximation of the calculated difference of the two brightness temperatures at frequencies according to equation (2.55) including the new approximation for the ozone mixing ratio profile $q_1^n(z)$.

Here the term $\Delta A(\nu)$ has been eliminated using the fact that other atmospheric effects such as baseline curvature etc. are already removed from the data by using a proper switching technique.

2.7.2 Inversion Through Spectral Comparison (Model Fitting)

It is well known that inversion of even a high quality spectral line shape generally does not yield an unambiguous choice for the shape of vertical profile (Barcilon 1975, Twomey 1977). However, a given profile of such nature does unambiguously produce a specific spectral line shape. Hence a comparison between calculated line shapes and observed data can provide a basis for judging the validity of the model vertical profile. Any discrepancy between the two, till it is more than the instrument noise level, is removed by

modifying the input parameters of the assumed model. This method has two considerable advantages. First, the direct problem of equation (2.48) has an explicit and unambiguous solution and second, useful comparison may be made with data having low signal to noise ratio (S/N). An outline of this method is given here :

We assume that the ozone exist, from the surface of the earth upto a maximum height of 90 km. A parametric model for ozone density distribution in the atmosphere D(h) is assumed which is similar to the one proposed by Green(1964) and used by Shimabukuro et. al. (1975). Green has shown that this model fits in the measured ozone distribution above 7 km very well. The mismatch below 7 km is not significant because the pressure broadening is so large at the lower altitudes that good estimation of density could not be obtained anyway. Mathematically, this model of ozone density distribution can be described as

$$D(h)=4D_{max}\frac{\exp(r(h-h_{max}))}{[1+\exp(r(h-h_{max})]^2} \qquad (2.57)$$

where D_{max} is the peak ozone density in molecules per cubic centimeter, h_{max} is the altitude of the peak density in kilometers and r is shape factor in units of $(\text{kilometer})^{-1}$.

With this models we calculate the ozone absorption coefficient $k(\upsilon,z)$ using the following formula

$$k(\nu,z)=\frac{1.7\times1.0^{-24}D(h)\nu^2 f(\nu,z)\exp[-25.3/T(h)]_{km^{-1}}}{T(h)^{5/2}} \qquad (2.58)$$

here T(s) is the temperature profile and $f(\upsilon,z)$ is the line shape function of ozone at various heights. Using this absorption coefficient (k) of ozone the

opacity (τ) is calculated at all atmospheric height. Now to solve the equation of radiative transfer we need the temperature and pressure of the atmosphere as a function of height. For our calculations we used the values of International atmosphere at our observational latitudes. These quantities are then fed to the general radiative transfer equation to obtain the brightness temperatures generated by our model ozone distribution. These brightness temperatures are then compared with the observed values. A least square curve is fitted to the observed data by selecting all the combinations of the input parameters in a given range. For our observations the absorption coefficient is calculated for a set of frequencies at 1 MHz resolution. In this technique, choice of a proper model is very important and hence this inversion method could only be used at those places where a good a priori information about ozone distribution already exists.

In our work we have used an empirical approach to the interpretation of data, using both spectral comparison and iterative inversion in a complementary way.

For the calculation of total ozone content (TOC) the above equation (2.56) for D(h) was integrated from 0 to infinity (90 km)

$$TOC = \int_0^\infty D(h)dh \tag{2.59}$$

This solves out to be

$$TOC = \frac{(4D_{max}/r)10^5}{1+\exp(-r.h_{max})} \tag{2.60}$$

This is the total number of ozone molecules in a column having base of 1 cm^2. This when multiplied by 3.73×10^{-20} (a factor obtained by dividing 1 gm ideal gas volume at STP (22,414 cm^3) by Avogadro number ($N_A = 6.02217 \times 10^{23}$) gives the total ozone content in atmosphere centimeters (1 milli-atmosphere centimeter = Dobson Unit).

2.7.3 Inversion Algorithms

In order to implement these inversion schemes for our applications computer programs were developed using the commercial software called "Asyst". For implementing spectral comparison method , Asyst based software programs were found to be very slow on our system computer (PC-386) and hence a bigger computer UNIX 9000/735 was used for running the program. These programs required the value of zenith opacity and the angle of antenna elevation besides the observed brightness temperatures at a defined set of frequencies. These computer programs are given in Annexure II.

Chapter 3

Design and Development of 101.7 GHz Radiospectrometer

3.1 Introduction

In the millimeter wave region the power received from most of the atmospheric and the extra terrestrial sources is quite low and hence a very sensitive and stable receiver system is needed to observe these sources. For spectral line observation from atmospheric trace gases like ozone the power received from a given spectral feature might be of the order of 10^{-20} watts which, depending on the type of the receiver, is about 3 to 6 orders of magnitude lower than the noise power generated in the receiver itself (Dicke 1946). Hence the main problem is that of designing a radiometer which can extract a small useful signal from the ocean of undesired contribution of the receiving system and the atmosphere.

3.2 Radiometer Design Considerations

Since the powers encountered at mm-wavelengths are very low hence it is impossible to detect such a signal without large amplification. Conventional electronic devices which are used to amplify signals can not operate in the millimeter wave region due to their high frequency limitations. Therefore it is necessary to bring down the signal to a convenien lower frequency range where it can be appropriately processed (Penzias & Burrus 1973). The method of bringing down the spectral information to lower frequencies is based on the principle of heterodyning. In this type of receiver the frequency conversion takes place in the non linear mixer by combining the signals received at the antenna with a highly stable local oscillator signal. This mixing shifts the band down to an intermediate frequency (IF). The relation of

this IF to the signal and local oscillator frequencies is as follows

$f(LO) + f(IF) = f(S)$ &

$f(LO) - f(IF) = f(I)$

where S is signal and I is image. A system in which both these frequency bands (S and I) are retained is called a double sideband system. In many cases the image frequency is rejected by a filter resulting in single sideband operation. Double side band systems are most commonly used for continuum observations. Since the continuum signal is broad-band in nature it is accepted in both side bands essentially improving the effective noise temperature of the system. On the other hand when one is interested in observing spectral features where the image band contributes only noise and no signal, single side band mode of operation is preferred.

After the mixer, a suitable band pass filter amplifier is used to pick up the difference signal and to amplify it. The band-pass characteristic of this IF amplifier usually determines the bandwidth of the receiver. Amplified IF signals are then passed to a square law detector for continuum or to a back-end spectrometer for spectral-line receivers. The total power gain of such type of receivers is usually from 80 to 120 dB. If the signal is still buried in the noise the detected output is integrated for a suitable period of time (usually several minutes). Since the random component of the noise goes down as the square root of the number of data samples taken for integration, the output, after integration, shows up the non random signal component. The only requirement for this to happen is that the source should be stable over the entire period of integration.

Also, if the system gain itself is not constant over an observing cycle a switching mechanism is applied at the input end of the receiver (Brillet

Fig. 3.1 Block diagram of 101.7 GHz Radiospectrometer.

1989). The input is alternately switched ON and OFF at a sufficiently fast rate so that gain of the receiver does not change during one observation cycle. The ON and OFF data is then stored, integrated and processed separately. The most commonly switched parameters are frequency and load. Beam switching is also employed in astronomy for observing point sources, but this can not be used for atmospheric work for obvious reasons.

3.3 Quality Factors of a Radiometer

In the absence of systematic effects the theoretical sensitivity of a receiver system would be limited only by statistical fluctuations in the total noise power input to the system. Since temperature has direct physical significance we quantify this power as a temperature 'T_s' (system temperature) which is a time averaged power spectral density of the form (Staelin 1969)

$$T_s = k^{-1} (\Delta p / \Delta B) \qquad (3.1)$$

where (Δp/ΔB) is noise power per unit bandwidth and k is Boltzmann constant. (This relation is obtained using the fact that at millimeter wavelengths the Planck's law of thermal emission could be approximated to Rayleigh-Jeans's law for almost all the temperatures encountered in the atmosphere). The power incident on the antenna from any given direction can be described by an equivalent brightness temperature $T_B(\nu, \theta, \rho)$. The antenna temperature is then an average of the brightness temperature weighted over 4π steradian.

$$T_A = \frac{1}{4\pi} \int_{\Omega} T_B G(\nu, \theta, \rho)\, d\Omega \qquad (3.2)$$

where

υ = frequency of observation

θ = zenith angle

ρ = azimuth angle and

$G(\upsilon,\theta,\rho)$ = antenna gain function

When defined in this way, the antenna temperature (T_A) has the same value as the physical temperature to which an ideal resistor would have to be heated to generate a power spectral density equal to the system noise power. This antenna temperature is in turn related with the angular distribution of the power incident upon antenna. T_B is actually used in the equation of radiative transfer. If the receiver noise power expressed in temperatures is added to the antenna temperature it is equal to a quantity called system temperature (T_{sys}).

$$T_{sys} = T_A + T_R \qquad (3.3)$$

where

$$T_A = T_{source} + T_{background} + T_{atmosphere} + T_{sidelobes} \qquad (3.4)$$

The system temperature is a figure of merit for a radiometer and represents the total output of the system as coming from a resistor at temperature T_{sys} placed across the input terminal of an ideal receiver. The system temperature includes the continuum component from the sky as well as the noise generated within the receiver.

The signal from the sky that is coupled into the receiver via the antenna gives rise to the antenna temperature. This antenna temperature has two components: The first of these is a weak stratospheric spectral line component which is a function of frequency. The second, continuum component, is quasi independent of frequency and has a major component from the thermal

emission from the troposphere, with a small contribution from the cosmic background.

The spectral lines of interest are typically very weak compared to both the continuum and the receiver noise. The spectral line antenna temperature can be compared with the statistical fluctuations in the system noise to determine the integration time required to detect the line. The root mean square of these fluctuations is given by

$$\Delta T_{rms} = \frac{\alpha T_s}{(B\tau)^{1/2}} \qquad (3.5)$$

where B is the band width of each of the spectrometer's filter, τ is the integration time, and α is a constant that depends on system parameters. Here it is assumed that the gain and the bandwidth of the system remain stable during the entire period of observation. But if there is any instability in these, it would further worsen the system sensitivity. The general formula for sensitivity then becomes (Meeks 1977)

$$\Delta T_{rms} = \frac{T_{sys}}{\left[\frac{1}{B\tau} + \frac{\Delta G^2}{G} + \frac{\Delta B^2}{B}\right]^{1/2}} \qquad (3.6)$$

Although the above definition of minimum detectable signal is theoretically correct yet a signal strength of 3-5 times of this level is considered more reliable.

Good amount of literature exist on design & development aspect of radiometers. This includes Gloersen 1977, Harsman & Poe 1981, Njoku 1980 & 1982, Tomiyasu 1974, Ulaby et. al. 1981 and Uppal et. al. 1990.

3.4 System Design for 101.7 GHz Radiometer

The instrument principally consists of a millimeter wave receiver (front end) and a multi-channel back end spectrometer. The receiver converts the millimeter wave signals received through the antenna to lower (intermediate) frequencies by heterodyning them with a locally generated signal. The spectral information at the receiver input is preserved in the process of frequency conversion. The output at intermediate frequency is then conveniently processed by the electronic assembly of the front end. After amplification in the front end the output is fed to the multi-channel back end spectrometer, which produces a voltage at each frequency point which is very nearly proportional to the input power. This output voltage is then digitized and fed to the system computer which accumulates it over a defined time period. A simplified block diagram of the radiospectrometer is shown in figure 3.1. Various parts of the system are described below in some detail:

3.4.1 Antenna

The selection of correct millimeter-wave antenna for use in radiometer is one of the most important choices in specifying a millimeter-wave system. A properly selected and designed antenna pays dividends in improved all round performance. In our radiometer the antenna is a lens corrected corrugated horn. The diameter of the horn is 6" which gives about one degree beamwidth at 101 GHz. This narrow beamwidth helps in reducing pick up of scattered

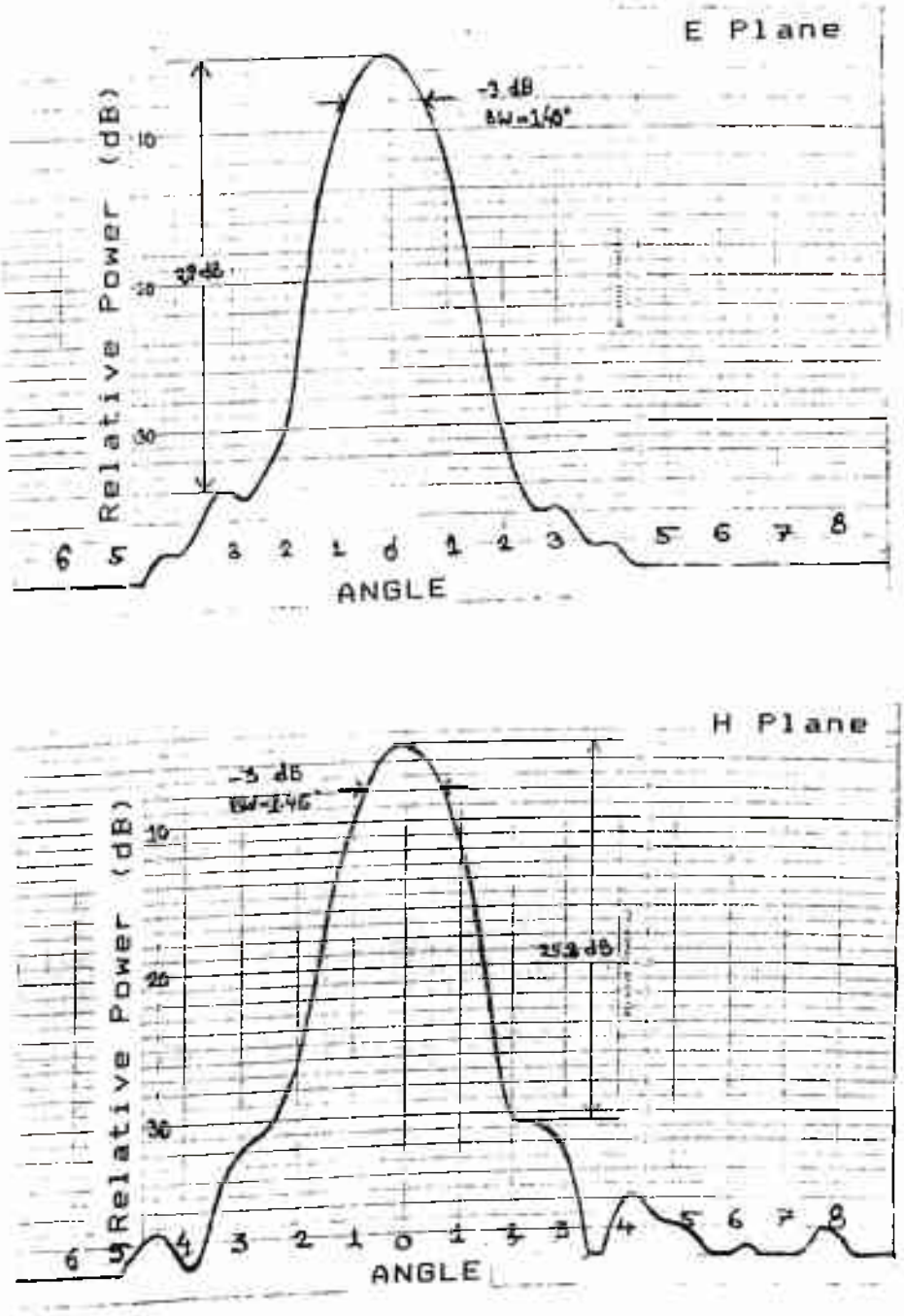

Fig. 3.2 E and *H* plane beam patterns of horn antenna

ground radiation. Another advantage of using corrugated horn is its nearly similar E & H plane radiation patterns. The side lobe pickup of the antenna is also quite low, typically less than 0.25 %. The beam patterns of the antenna are shown in figure 3.2.

3.4.2 MM-Wave Radiometer (Front-End)

A photograph of the front-end part of the system is shown in figure 3.3 along with the 6" lens corrected corrugated horn antenna. This is a superheterodyne receiver system in which a GaAs Shottky-diode mixer is used to convert the incoming mm-wave radiation to an intermediate frequency range of 10-1000 MHz. A mm-wave phase-locked Gunn source at 101.0 GHz is used to pump the mixer diode. The down converted intermediate signal is amplified in a low noise GaAs FET amplifier before being sent to the back-end spectrometer for further processing. A separate unit called mm-wave isolator is used between the mixer and the local oscillator to avoid the energy being reflected back into the local oscillator. The DC power requirement of Gunn oscillator (PLO) is 5 volts while the mixer and amplifier require 15 volts of supply. Two separate highly stabilized power supplies are used for the purpose. These were kept outside the front end box in order to avoid excessive heating of the critical front-end components. The noise figure of the radiometer, measured at the input of the horn antenna was found to be 8 dB (Double Side Band). To make the system suitable for spectral line observations, arrangements were made for frequency switching. The local rf source (phase locked oscillator) is connected to a highly stabilized signal generator at it's reference frequency input. With the change in signal generator

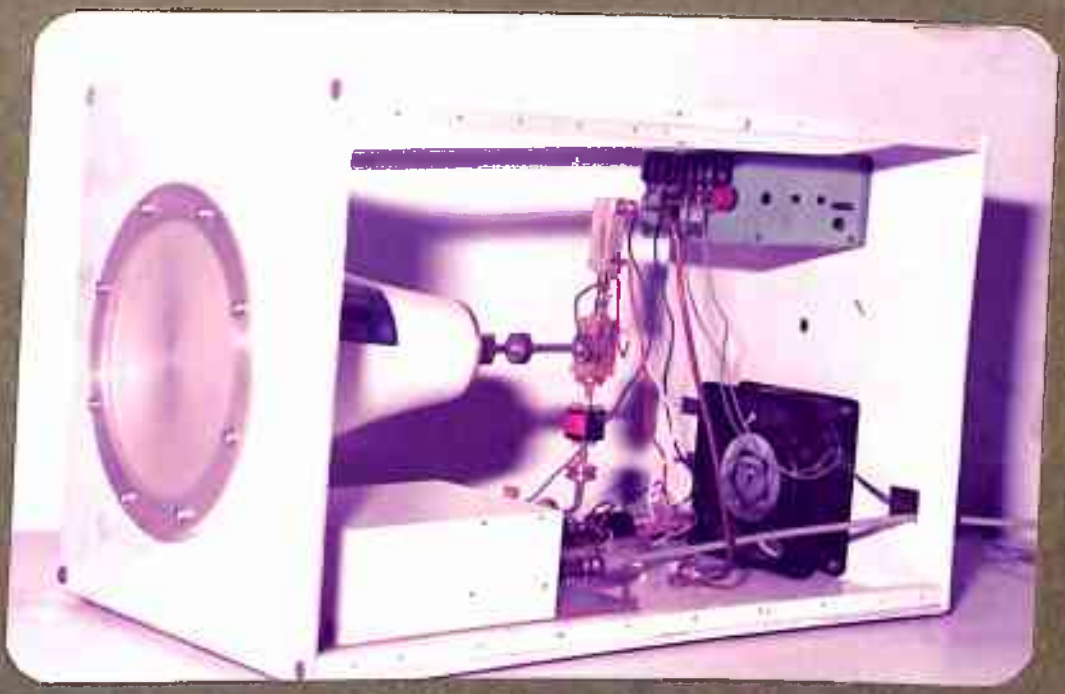

Fig. 3.3 Internal view of the instrument Front-End.

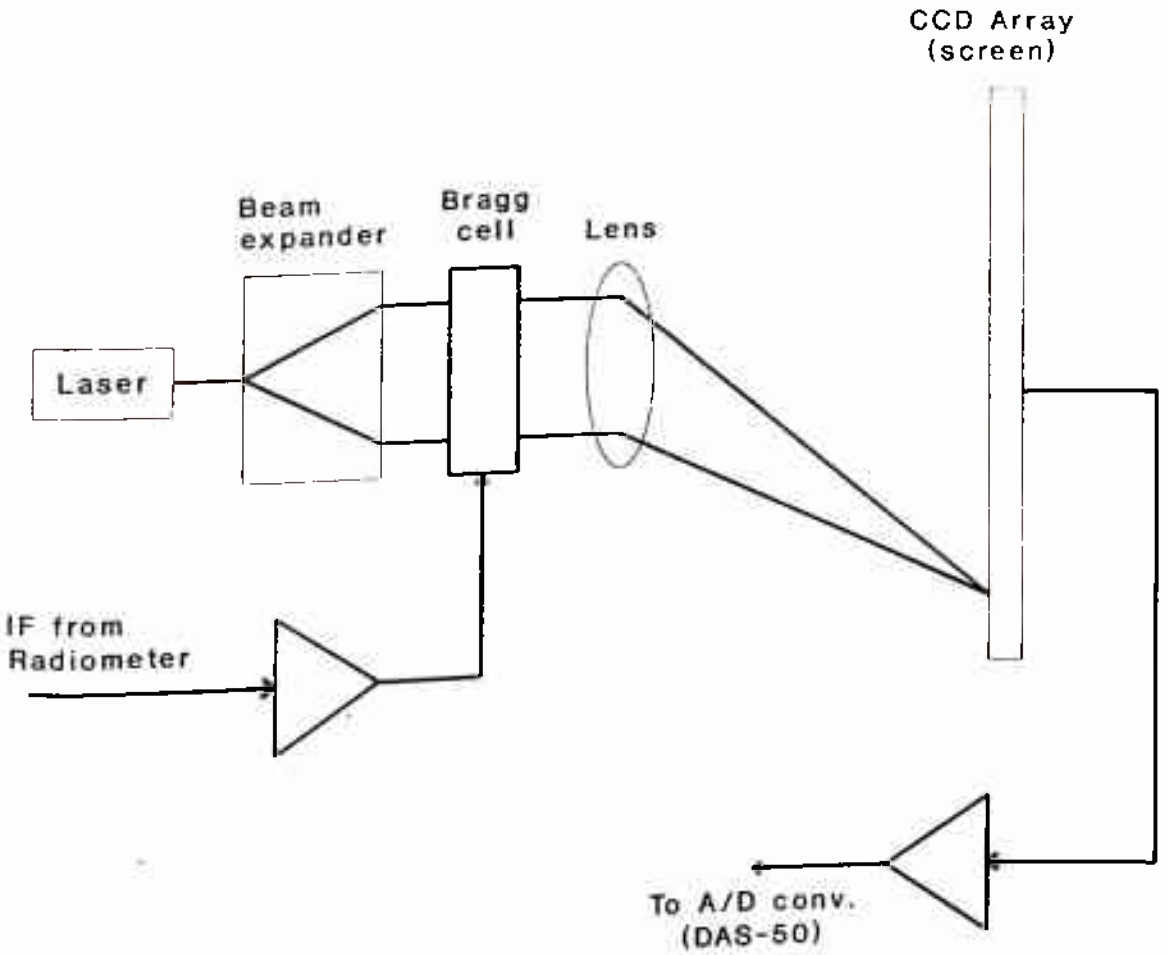

Fig. 3.4 The geometry of AOS optics

aperture dimension of the Bragg cell. When this light is incident on the cell it is diffracted according to the grating principle. A convex lens is used to converge the outgoing beam on a point on the screen. It's intensity is measured by CCD pixel array on the screen and the position of this pixel tells about the frequency of RF signal. If 'θ' be the angle of diffraction and F the focal length of the lens then the distance of individual (ith) pixel from the lens axis is given by

$$d(i) = F.\theta(i) \qquad (3.7)$$

The CCDs are sampled every few milliseconds and the resulting video signal is digitized and stored. The theoretical frequency resolution of the AOS is reciprocal of the transit time of acoustic waves across the body of the Bragg cell. This transit time depends on the density and the elasticity of the cell medium. Hence for a better resolution the cell should have low density and high elasticity. In practice the theoretical resolution is seldom achieved due to many practical constraints like imperfect optics, non uniform illumination of the Bragg cell, attenuation of the acoustics and the cross talk in the photodetector array. The AOS that we have used for our study has a frequency resolution of about 1 MHz.

An important sub-system of the spectrometer is the on-line data acquisition system. For efficient, automated observation, one needs to sample all the 1024 channels in a very short time. In our system this time is 12.5 milliseconds. A trigger pulse is generated by AOS at the beginning of every new cycle and a clock pulse at every CCD readout. The CCD array is sampled by means of a data acquisition system (Keithley DAS-50) card installed in the PC, as described in the next section.

3.4.4 Data Acquisition and Control System (PC)

The computer is basically needed to acquire and store data as well as to implement the inversion algorithm. For data acquisition purpose our computer (PC/AT-386), is interfaced to the back end spectrometer(AOS) through a data acquisition system(DAS-50). DAS-50 card, which has 1 megabyte on-board memory is installed in a spare AT-slot of the computer. This is a 12 bit analog to digital (A/D) converter with 2.44 mV voltage resolution. The signals from AOS are first converted to digital form through this A/D converter of DAS-50 and then stored in the computer. The data tracking was done by the trigger and clock pulses of AOS received at the DAS-50 card's trigger and clock ports respectively. A program was written for frequency switched mode of operation. In the frequency switching mode of operation the acquisition program can automatically acquire the ON-frequency and OFF-frequency data continuously by controlling the signal generator frequency. Data thus acquired are integrated, smoothened and analyzed by a separate algorithm developed for the inversion procedures described in chapter 2. A photograph of the complete system is shown in figure 3.5.

3.5 System Performance

Before actually using the system for atmospheric observation a number of tests were done for checking it's performance. The front end was separately tested using a millimeter wave black body absorber at two fixed temperatures (the liquid nitrogen & the room temperature). The noise figure of front end was found to be about 8 dB as already mentioned. The testing of back-end

Fig. 3.5 Photograph of the complete system setup at NPL, New Delhi.

spectrometer was done by using a signal generator. This signal generator delivered powers at various levels for all the spectrometer channels. The dark current level of the AOS system was found to be about 20-25 mV. However, its effect was removed by subtracting it from total observed output. The system output remained reasonably stable for an ambient temperature range of 24 ± 3 degree celsius. Beyond this range the system showed instabilities in the total power output. The total power detected at the front-end and the local oscillator lock indication voltage were continuously monitored on two separate panel meters for checking the health of the system. By using millimeter-wave absorbers at room temperature and liquid nitrogen temperatures the DSB receiver noise temperature was found to be ~ 1350 K. With 1 MHz per filter frequency width about 47 minutes were needed to make the statistical fluctuations equal to ~ 0.03 K (the maximum noise tolerance for the iterative inversion scheme to work). The total power gain of the system is about 110 dB. Initially, some 15-20 minutes are needed for the system to warm up and attain the stable operating mode. The complete system specifications are summarized in table 3.1.

Table 3.1 System specifications - 101.7 GHz Radiospectrometer

Antenna	6" lens corrected corrugated horn
Type of receiver	Double Side Band (DSB)
Operating Frequency	101.737 GHz
Total Bandwidth	500 MHz
Back-End Spectrometer	750-1250 MHz
AOS frequency span	1024 Channel AOS
Frequency Resolution	1 MHz
Power Gain	110 dB
DSB Receiver Noise Temperature	1350 K

Chapter 4

Observations of Ozone over Delhi (28N)

4.1 Observational Setup at Delhi

The observations reported in this chapter were conducted at the National Physical Laboratory, New Delhi (latitude ~ 28° North) in October-November 1993. The radiometer system was installed in the millimeter-wave lab of the Radio Science Division of NPL on the 2nd floor (about 10 meters height from the ground). For the purpose of observation a window of the room was used. The slant path of antenna beam could reach to a maximum elevation of 30 degrees without hitting the window frame. This observation window was kept covered with a thin thermocol sheet having negligible absorption at millimeter wave frequencies. Since the radiometer antenna is fixed to the front end box the whole front end assembly was mounted on a wooden structure to set the antenna at an appropriate elevation angle. A photograph of the observational set up at Delhi is shown in figure 3.5. To maximize the signal strength we kept the antenna elevation at about 19 degrees. At this low elevation the total air mass encountered by the antenna beam is about three times the air mass of zenith observation. All the sub-systems of the radiometer worked perfectly well in supply voltage range 220-240 volts but tended to show instabilities when the voltage went down below 210 Volts. Hence for the purpose of keeping the supply voltage constant a ferroresonant type voltage stabilizer having an almost constant output of 230 Volts was used. The main supply stabilizer was kept at about 5 feet away from the rest of the instrument boxes to minimize the electromagnetic interference (EMI). The radiometer front end was found to be temperature sensitive and used to show best performance in the temperature range 24 ± 3 degree centigrades. Therefore, a room temperature was maintained in this

range through out the observational period. Although the system design had provided for both the load and frequency switching mode of operations, however, only frequency switching was used for the purpose of actual observations. This mode of operation was favored because of the following reasons:

(1) The frequency switching mode was found more time efficient because the switching overlap time for this mode was significantly less than that of load switching mode.

(2) With our observing window there was not enough margin to vary the antenna elevation angle and to make the sky temperature equal to the load temperatures (the room temperatures were found to be too high and the liquid nitrogen temperature was too low compared to the sky temperatures in the given elevation range).

(3) Frequency switching method proved to be simple and effective in eliminating the continuum background as well as the effect of radiometer gain instabilities.

The observations were carried out at two local oscillator frequencies : one when the output band was centered at the main ozone line (ON-frequency) and the other about 80 MHz away (OFF-frequency). The best switching rate was also empirically found out by having different time periods for data integration. It was found that about 100 scans from the AOS at ON frequency and subsequent 100 scans at OFF frequency could be integrated in a block without any gain variation problem. These 100 scans meant only 1250 milli seconds (1.25 seconds) of data. Hence the frequency was switched at every 1.25 seconds of the actual observation time and the ON and OFF data were separately integrated and stored in the computer. Due to various time

overheads like acquisition speed limit of A/D card, extra time consumed in the system control and the delay introduced for stabilization after switching, program execution time etc., this 1.25 seconds of integrated data was actually acquired in about 9 seconds. Since one scan of AOS took about 12.5 milliseconds and the frequency was switched every 100 scans, a block of 100×100 scans took about 30 minutes. These 30 minutes blocks each having 100×100 ON-frequency and 100×100 OFF-frequency data scans were separately stored in the hard disk of the computer. On subtracting the OFF-frequency data from ON-frequency data in all these blocks a somewhat garbled but definite appearance of the ozone line signature could be viewed. During every observation period the total power output of the system was separately monitored on a panel meter and the data were rejected if the output changed abruptly. This change was mainly caused by erratic receiver performance.

The tropospheric opacity was measured using the so-called "chopper wheel method" (Penzias & Burrus 1973). In this method of opacity measurement the total power sky output of the radiometer is compared against that from a room temperature microwave absorber. If there were no atmospheric absorption the broad-band brightness temperature difference between the sky and the room temperature load should be equal to the room temperature itself (neglecting the 2.7 K cosmic background radiation as it is too small compared to room temperature). Therefore, for any real sky condition the factor obtained by dividing room temperature by the difference of the room and sky temperatures, can be used to correct for atmospheric opacity.

4.2 Calibration

Calibration of the system was done by measuring the response of the system to known thermal noise input signals. This process derives the system noise temperature and also provides a relation between the power received at the input and the corresponding output voltage produced by the system. For the purpose of calibration a millimeter wave blackbody "Eccosorb" (carbon loaded foam) was kept filling the beam of the antenna at two known constant temperatures. These two reference temperatures were chosen to be the room temperature and the liquid Nitrogen boiling point temperature (77 K). The load was made suitably rough to avoid the development of standing waves between the instrument and the load. The output power levels were determined and their ratio was calculated. If this ratio be 'R' then the system temperature can be calculated using the following formula

$$T_{sys} = \frac{T_{amb} - T_{cold}}{R-1} - T_{cold} \qquad (4.1)$$

where

T_{amb} = ambient or room temperature

T_{cold} = liquid nitrogen temperature

4.3 Data Smoothing and Baseline Removal

The stored ON and OFF data was first corrected for the dark current counts of the AOS. For this the AOS output was taken on the computer for a number of times without any input signal. The average shape of the AOS

function was determined from here which was then subtracted from all the ON and OFF data readings. These corrected ON and OFF data were then used to form the quantity (ON-OFF)/OFF: which on multiplication with the system temperature produced the actual signal. This could be understood as follows. Let the power received by the radiometer at ON-line frequency in term of equivalent temperature be T_{ON}. Similarly let T_{OFF} be the power received by radiometer at OFF-line frequency. These two can be written as following (Bevilacqua et. al. 1983)

$$T_{ON} = T_l + T_{sky} + T_R \qquad (4.2)$$

$$T_{OFF} = T_{sky} + T_R \qquad (4.3)$$

Where

T_l = line temperature

T_{sky} = sky temperature excluding line temperature

T_R = receiver noise temperature

The (ON-OFF)/OFF operation leads to the

$$\frac{T_{ON} - T_{OFF}}{T_{OFF}} = \frac{T_l}{T_{sky} + T_R} \qquad (4.4)$$

When this quantity is multiplied by $(T_{sky} + T_R)$ the net output comes out to be T_l. Receiver temperature T_R is derived from the calibration described in section 4.2. T_{sky} was calculated by placing room temperature load in from of antenna and taking down the total power output corresponding to it. This we call $P_{R.T}$. If the power received at sky be P_{sky} then the ratio $P_{sky}/P_{R.T}$ when multiplied with T_{sys} will correspond to $(T_{sky} + T_R)$. Although in equation 4.4 T_{sky} in denominator does not contain T_l whereas P_{sky} used later does, however, the error caused

by this can be neglected as the actual line strength contribution is negligible compared to T_{sky} taken over the entire band.

All these data sets were then integrated for one day's observation. On this type of data integration the signal quality was built up sufficiently good where the spectral comparison inversion scheme could be implemented. The long term integration was also done on the data for about 1 week to 10 days, which produced a good signal to noise ratio. However, for the iterative inversion scheme to work, a Lorentzian function was fitted in the integrated data in least square sense to avoid letting the statistical fluctuations make solution unstable. The result of this analysis yielded the average vertical distribution of the ozone during this period of observation.

The total useable band-width around the line center was about 60 MHz. The baseline obtained after (ON-OFF)/OFF analysis was not linear and hence a second order curve was fitted to extract the real ozone signal (Bevilacqua et. al. 1983). For the purpose of fitting the baseline only those channels which are more than 40 MHz away on both sides from the line center were used. The weight of the actual line spread of 80 MHz around line peak was taken as zero for the baseline fitting process. The reason for fitting the second order baseline is discussed in some detail later in this section.

For the initial smoothing process the spectra were folded about their center points. Any odd baseline functions are removed through it. However, there can be significant amplitude in the higher order even terms which might affect the shape of the spectra and still may elude the removal in spectra folding exercise. Removal of these even power terms is rather difficult and cumbersome exercise. The following method was applied to get rid of these even power baseline structures. Theoretical rationale of the method is

discussed here.

The observed spectrum can be broken into two parts - the signal and the baseline functions

$$T(\nu) = B(\nu)+S(\nu) \tag{4.5}$$

where

T(ν) = Observed spectral data

B(ν) = Baseline function and

S(ν) = Signal

The baseline function can be represented by a power series in frequency

$$B(\nu) = \sum_{N=0}^{\infty} A_N \nu^N \tag{4.6}$$

where A_n are constants. In folding the spectra all odd power terms are removed and only even power terms are left in the data. Hence after folding the data around the center the above equation becomes

$$B(\nu) = \sum_{N=0}^{\infty} A_{2N} \nu^{2N} \tag{4.7}$$

The remaining odd power function should be equal to the difference function generated during subtraction on folding the wings

$$\frac{1}{2}[T(\nu)-T(-\nu)] = \sum_{N=0}^{\infty} A_{2N-1} \nu^{2N-1} \tag{4.8}$$

In order to determine the magnitude of the odd power coefficient the difference function 1/2[T(ν) - T(-ν)] was fitted with a power series. In nearly all cases this analysis revealed that the cubic and all higher order odd power terms had insignificant amplitude. Since there is no reason for energy in the

baseline function to be preferentially distributed in either even or odd power terms, we assumed that the fourth and all higher order even terms can also be safely ignored. Hence, the problem is effectively reduced to estimating the quadratic baseline components. A second order baseline was fitted in the data. A total frequency span of 60 MHz was used. Since a frequency switched mode does not bring a very symmetric spectrum, the same operation of switching was done on load keeping it in front of the antenna. This had become necessary as the baseline shape left in the (ON-OFF)/OFF exercise had a baseline feature close to the line peak leaving a very small number of clean frequency channels on the line wing using which the actual inversion could be performed. These features are actually generated by the frequency dependent characteristics of the receiver which shows up during frequency switching process. The load data processed by the same operation when subtracted from the sky data helped greatly in removing the baseline features. Out of 60 MHz used for model fitting only 20 MHz was used the right side of the peak and the rest 40 MHz was taken from the left wing of the line. This was necessary as only one peak in subtracted sky data was covered in our back-end spectrometer. The total range of this 500 MHz device was from 750 MHz to 1250 MHz. On subtraction of data only one (positive) peak appeared at about 815 MHz frequency point. The other (negative) peak should accordingly appear at 735 MHz frequency point for a 80 MHz frequency switching operation. Since this value falls outside our range it is not visible in the data. Also, for the purpose of getting full line amplitude it is necessary to put the two switching frequencies as distant from each other as possible. The maximum flexibility of phase locked oscillator in shifting the frequencies was utilized. This value was empirically determined to be 80 MHz, maintaining the

stability of operation.

After baseline removal the spectra were corrected for tropospheric opacity which were measured using the "Chopper Wheel Method" as described earlier in this chapter. Finally, the spectra were scaled for zenith observation using the zenith angle and the secant law of stratified atmosphere (Waters 1976).

Since a day's observation integration did not produce adequate S/N, only spectral comparison method of data analysis was used for analyzing daily ozone spectra. The following three parameter model as described in chapter (2) was used (Shimabukuro et. al. 1975).

$$D(h) = \frac{4D_{max}\exp(r(h-h_{max}))}{[1+\exp(r(h-h_{max}))]^2} \qquad (4.9)$$

Various combinations of the three parameters viz. D_{max}, h_{max} & r were taken in a given range and the corresponding theoretical ozone line shapes were calculated. Table 4.1 gives the ranges and the increments used in the programme for calculation of theoretical line shape. In principle, as the wings of the ozone line extend to infinite distance on either sides of the line center, our baseline fit procedure would introduce an extra curvature into the observed ozone profile. To correct for this, the same analysis of baseline removal was carried out on the theoretically computed ozone profiles. After this the two profiles were compared in a least square sense for all the combinations of input parameters. The values of D_{max}, h_{max} & r were found out corresponding to the best least square fit in the data. These values were then used in equation (4.9) above to give the actual ozone number density corresponding to 0 to 90 km altitudes. The spectral line of ozone obtained by this process and their corresponding retrieved ozone profiles are shown in

figures 4.1 to 4.6 for three days in November.

Table 4.1 Ranges and increments of D_{max}, h_{max} and r used in spectral comparison method

Parameter	Range	Increment
D_{max}	3.0 to 9.9×10^{12} /cc	0.1×10^{12}
h_{max}	15.0 to 30 km	1.0
r	0.15 to 0.4 /km	0.01

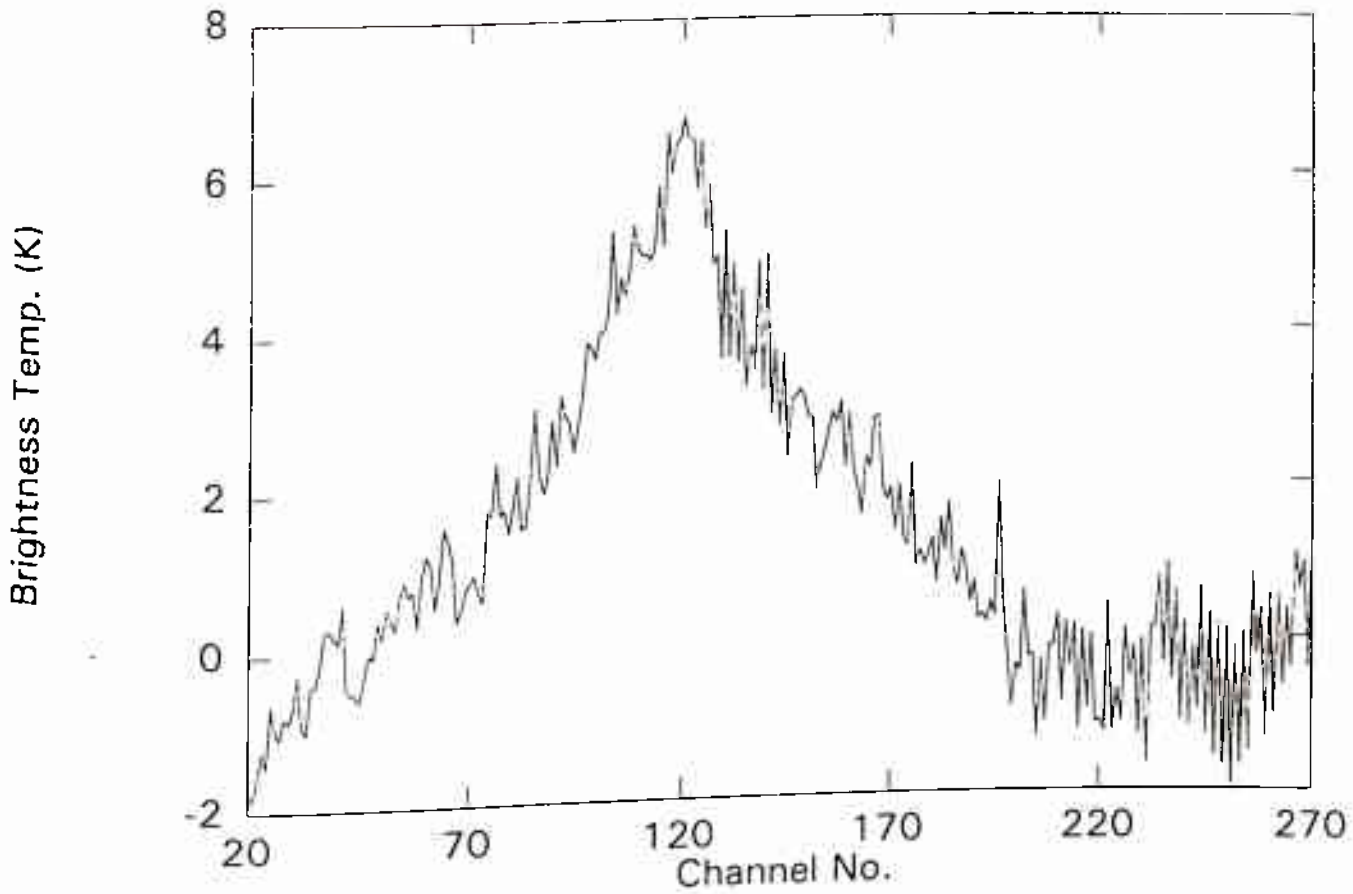

Fig. 4.1 Ozone spectrum obtained on 7/11/93 at Delhi. Each channel represents about 0.5 MHz frequency span.

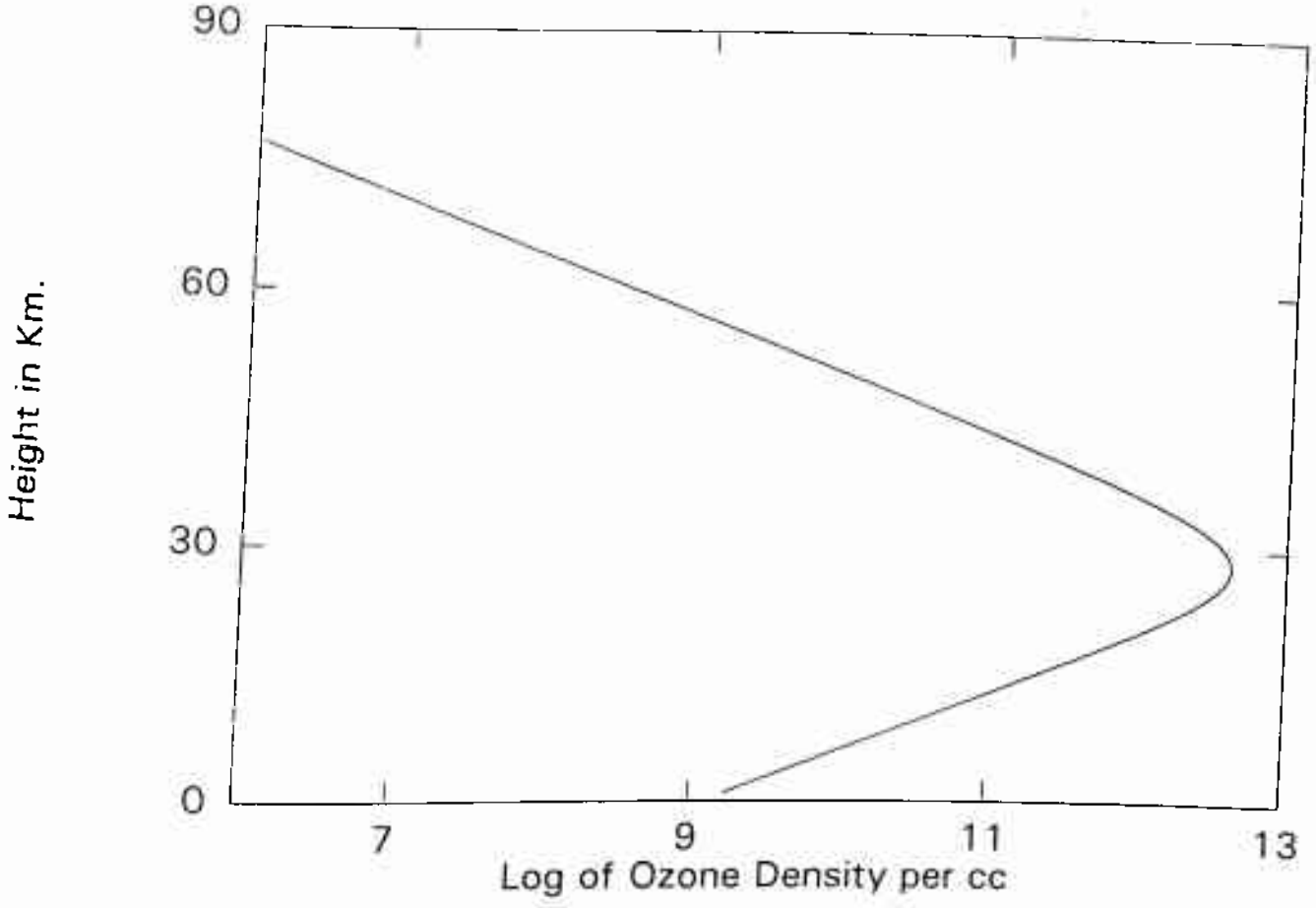

Fig. 4.2 Retrieved ozone profile for 7/11/93.

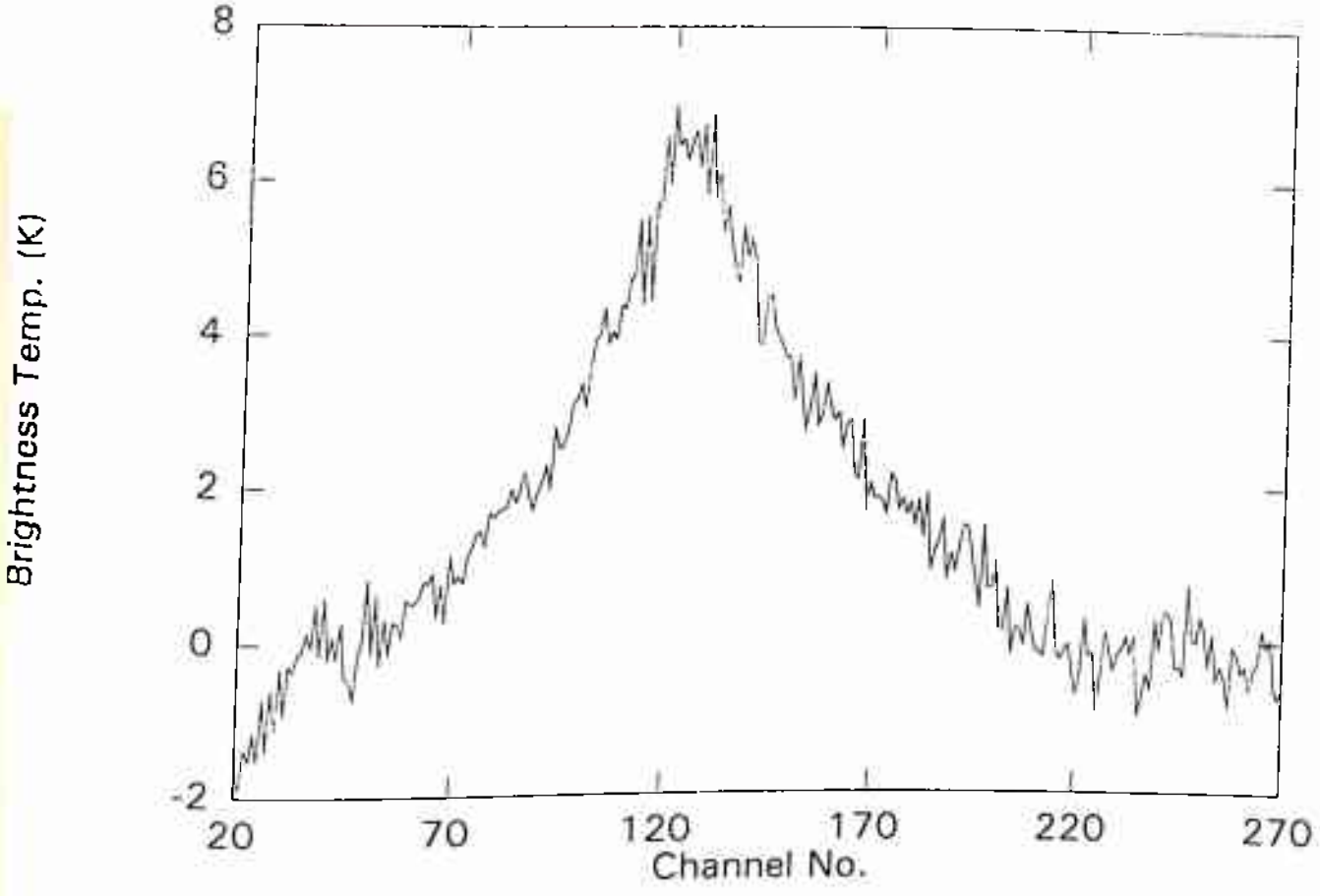

Fig. 4.3 Ozone spectrum obtained on 11/11/93 at Delhi.

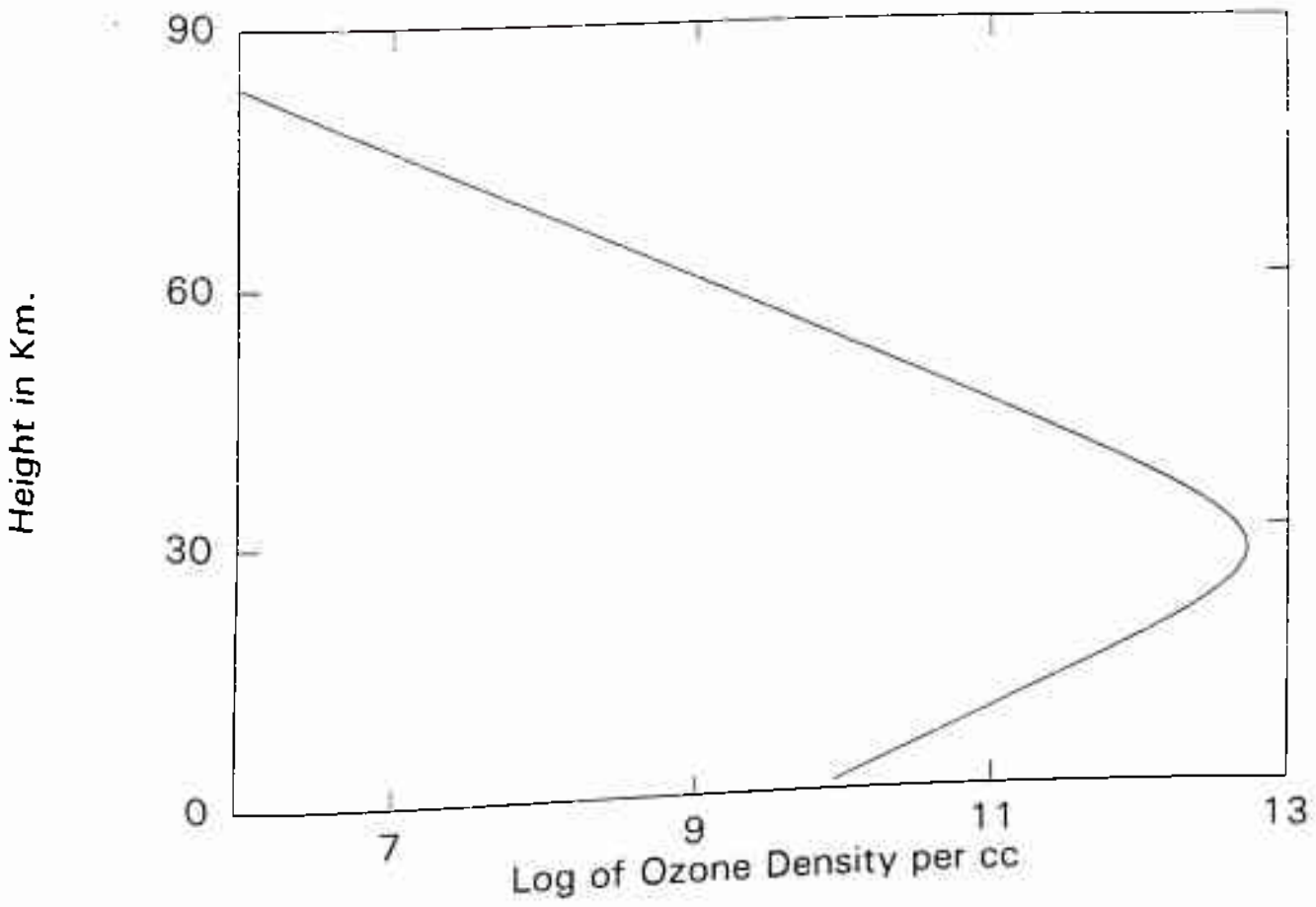

Fig. 4.4 Retrieved ozone profile for 11/11/93

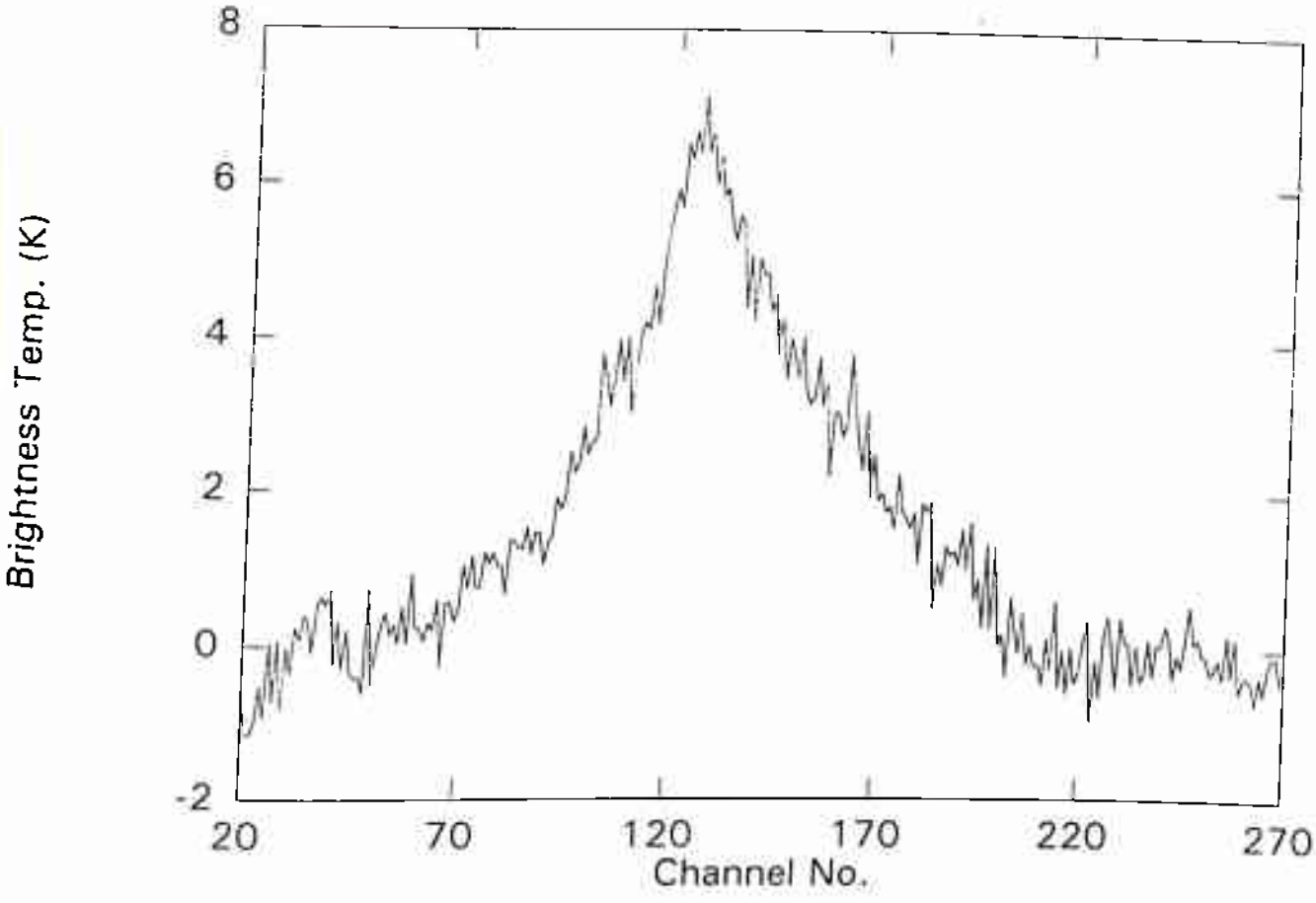

Fig 4.5 Ozone spectrum obtained on 12/11/93.

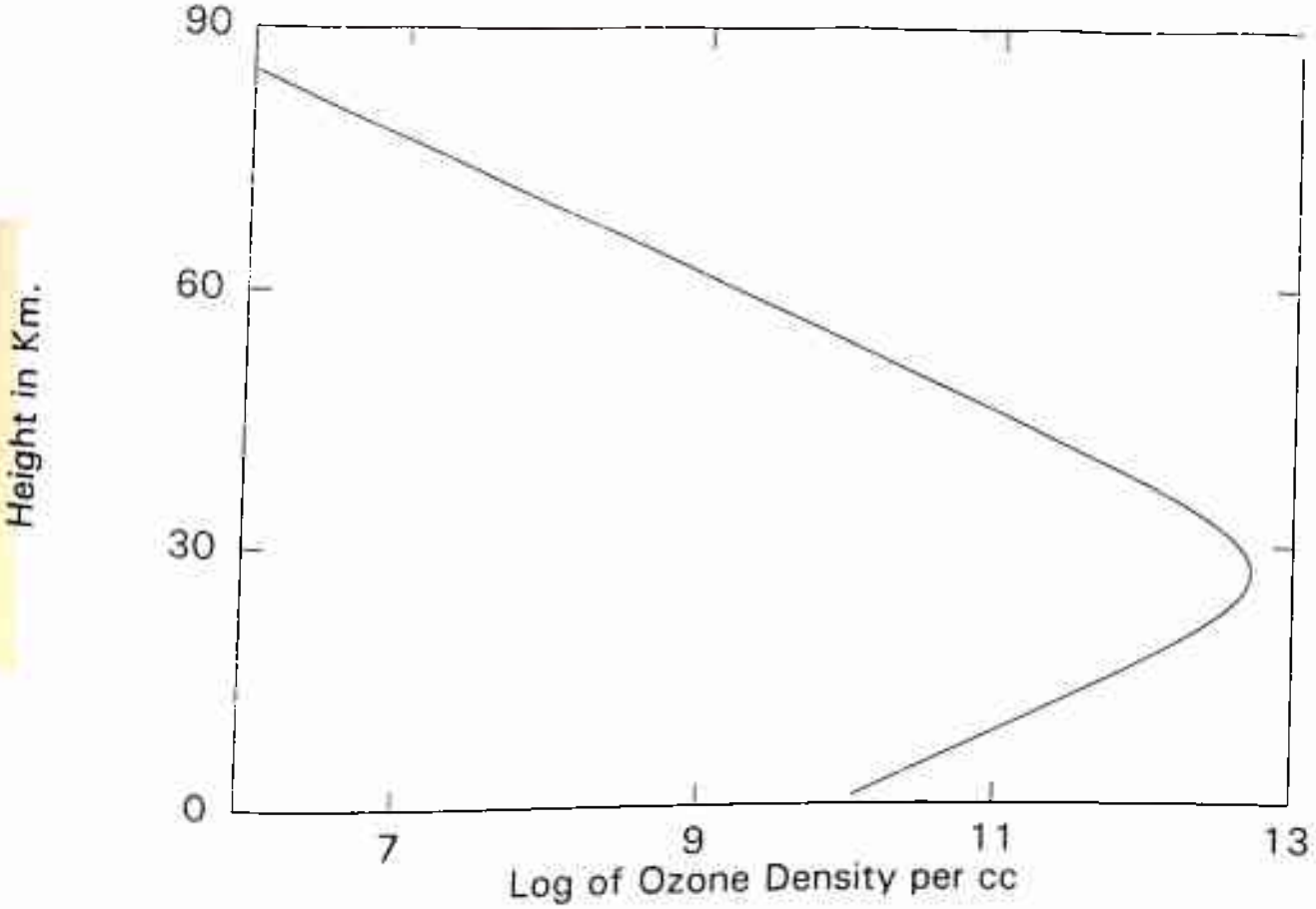

Fig 4.6 Retrieved ozone profile for 12/11/93

Chapter 5

Observations of Ozone over Antarctica (70S)

5.1 Instrumental Setup and Observations

Observations reported in this chapter were carried out at Maitri (70 South latitude), the permanent Indian Station at Antarctica. The complete system described in chapter 4 was dismantled in our lab at Delhi and taken to Antarctica in the 13th Indian Scientific Expedition during December 1993 to March 1994. The actual observations were made there for about a month during January-February 1994. The atmospheric temperatures over Antarctica are quite low (most of the time below freezing point) and hence the water vapor content in the troposphere is very small. This condition makes Antarctica an excellent site for observing stratosphere and other celestial sources. The observation of Antarctic ozone is important for it's implications on global ozone content (Atkinson et. al. 1989). The dramatic decrease of ozone over antarctica during austral spring was reported first time by Farman et. al. in 1985. The phenomenon widely known as the Antarctic ozone hole has been observed to be continent wide and continues to occur every year (Lemonick 1992). It is therefore important to know the implications of the Antarctic ozone depletion for Arctic (Levi 1992) and global stratospheric ozone. The weather over Antarctica is not always clear and the clouds do cover the sky rapidly after a short span of clear days usually not more than 2 or 3 in number (these are not the stratospheric clouds as discussed by Hamil & Toon 1991). Most of the tropospheric clouds appearing in the sky do not significantly affect the millimeter wave signals. However, some very low dark clouds (at about .5 to 1 km height from the ground) on 14th and 28th January '94 reduced the ozone signal by about 50%.

The instrument was installed in the science hut (Nandadevi) at Maitri.

One small 2×2 feet size window of the hut was used for the purpose of observation. The window was covered with a thin sheet of teflon material which gave very little absorption at our frequencies. The ambient temperature was maintained in the range 24±3 degree celsius by two hot air blowers inside the hut. A separate temperature monitor was available in the hut and the blowers were manually switched on/off to keep the temperature in the desired range. The whole instrument setup was on the ground floor only and hence an elevation angle of > 25 degrees was found suitable for observations. This was necessary for antenna beam to clear the surrounding structures and also the polar ice sheet in the direction of observation. The angle of elevation was set to be 29.5 degrees. Various beam elevation and dipping exercises were done before setting the angle of observation. The secant law was found to be applicable only in the elevation range 25 to 45 degrees. Below 25 degrees elevation the ground structures started contributing and for angles > 45° the main beam of the antenna started looking in the window frame itself. Since it was not practical to take the instrument outside the hut due to freezing cold weather the only observational elevation range left was 25 to 45 degrees. For the purpose of signal maximization we chose the elevation angle at 29.5 degrees. A photograph of instrumental setup at Maitri is shown in figure 5.1.

The EMI disturbances generated by the nearby HF transmitters were avoided by properly shielding the front end box. Though this shielding minimized the radiative interferences, the huge power line fluctuations sometimes managed to pass through our voltage stabilizer and disrupted the acquisition process. These fluctuations were mainly caused by the high power transmitters working on the same phase. This problem was later alleviated

Fig. 5.1 Photograph of the system setup at Maitri (Antarctica).

somewhat by shifting the instrument power supply to a different phase.

The tropospheric opacity was determined after every half an hour of observation by the method described in chapter 4. The calibration procedures adopted were also exactly the same as described in the previous chapter. The system temperature measured after reassembling the radiometer at Maitri was found to be 1650 K, the same as measured at Delhi earlier . This includes the 300 K room temperature load. The receiver temperature was 1350 K. The radiometer was operated throughout in the frequency switched mode. The two frequencies ON & OFF were about 80 MHz away from each other. The data storing, smoothing and scaling processes have already been described in the previous chapter, however, only sky readings for frequency switching were taken. This was done to maximize the sky observation time. A second order baseline was removed after performing (ON-OF)/OFF exercise on sky data. Since the line shape thus obtained was not very symmetric it was not folded around the peak and only the right wing of the spectrum was used for analysis work. Table 5.1 gives the dates, total time of observation and the effective integration time. The profiles presented here were retrieved using the inversion techniques described in chapter 2. Ozone spectra observed at Antarctica along with their retrieved height profiles are shown in figures 5.2 to 5.20. Some extra features seen in the spectra over and above the system noise are due to the electromagnetic interference (EMI) caused by the high power HF transmitters at Maitri. The correlation coefficients (R) calculated for goodness of fit determination of the theoretical fits are shown in table 5.2.

Table 5.1 Date, duration and effective integration time for Antarctic observations.

Date of Observation	Observation Period (GMT)	Effective Integration Time (Minutes)
13/1/94	1220 to 0005 (n.d)	16.7
14/1/94	1445 to 0110 (n.d)	16.7
16/1/94	1300 to 2000	25.0
17/1/94	1215 to 2040	18.7
18/1/94	0950 to 1250	8.3
19/1/94	1030 to 2100	20.8
20/1/94	1300 to 2015	12.5
21/1/94	1045 to 0015 (n.d)	35.4
22/1/94	1325 to 1700	8.3
24/1/94	1655 to 1920	10.4
25/1/94	1450 to mid night	10.4
28/1/94	1815 to 2030	8.3
29/1/94	1705 to 1852	4.2
30/1/94	1125 to 2335	18.7
31/1/94	1135 to 2000	20.8
3/2/94	1545 to 1813	8.3
4/2/94	1235 to 1510	4.1
5/2/94	1455 to 1825	14.6
6/2/94	1236 to 1605	10.4

n.d = next day

Table 5.2 Correlation coefficients (R) Calculated for fits in Antarctic data. R^2 gives the goodness of fit.

Date	R^2	Date	R^2
January:		February:	
13	0.9124	3	0.7899
14	0.8757	4	0.9054
16	0.8822	5	0.8146
17	0.7366	6	0.8178
18	0.9242		
19	0.9084	January 13-20	0.9397
20	0.8798	January 21-29	0.9306
21	0.8997	Jan.30 - Feb.6	0.9454
22	0.8988		
24	0.9164	January (Total)	0.9473
25	0.7966		
28	0.8865		
29	0.7870		
30	0.9216		
31	0.9401		

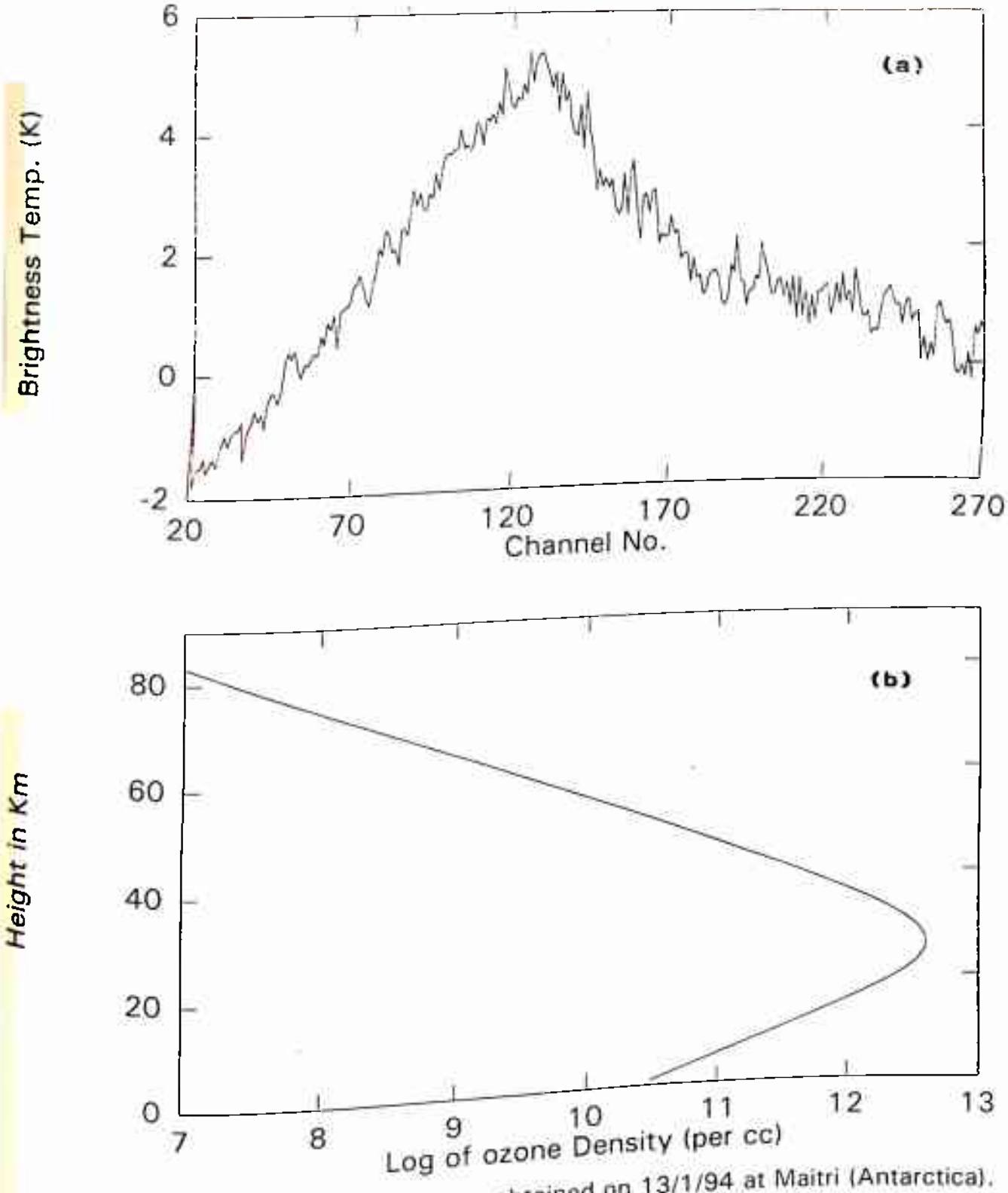

Fig. 5.2 ***(a)*** Ozone spectrum obtained on 13/1/94 at Maitri (Antarctica). Each channel represents about 0.5 MHz frequency span.

(b) Retrieved ozone profile.

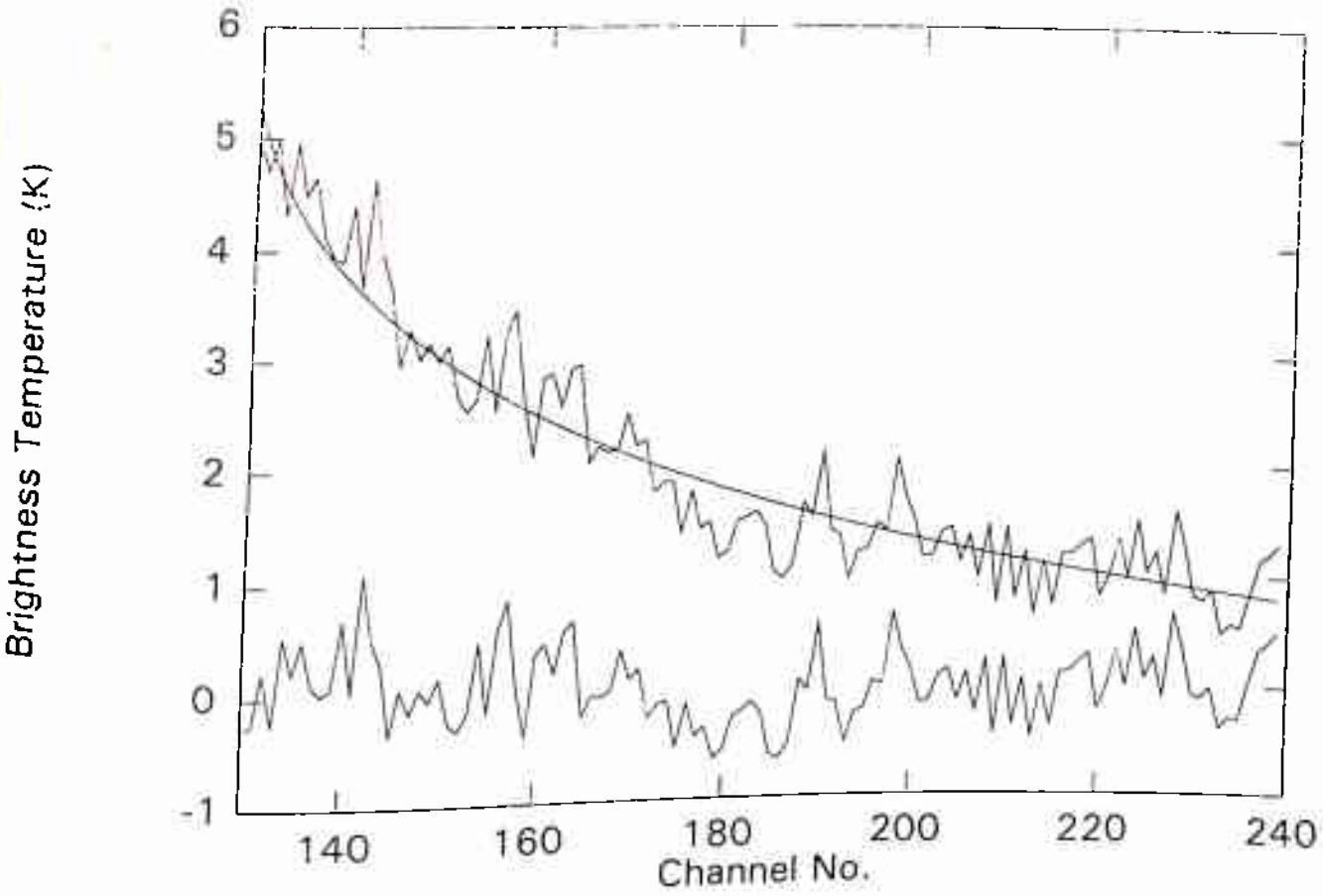

Fig. 5.2 ***(c)*** Theoretical curve fit in the right wing of the spectrum using spectral comparison method. The difference of these two is also shown in the figure.

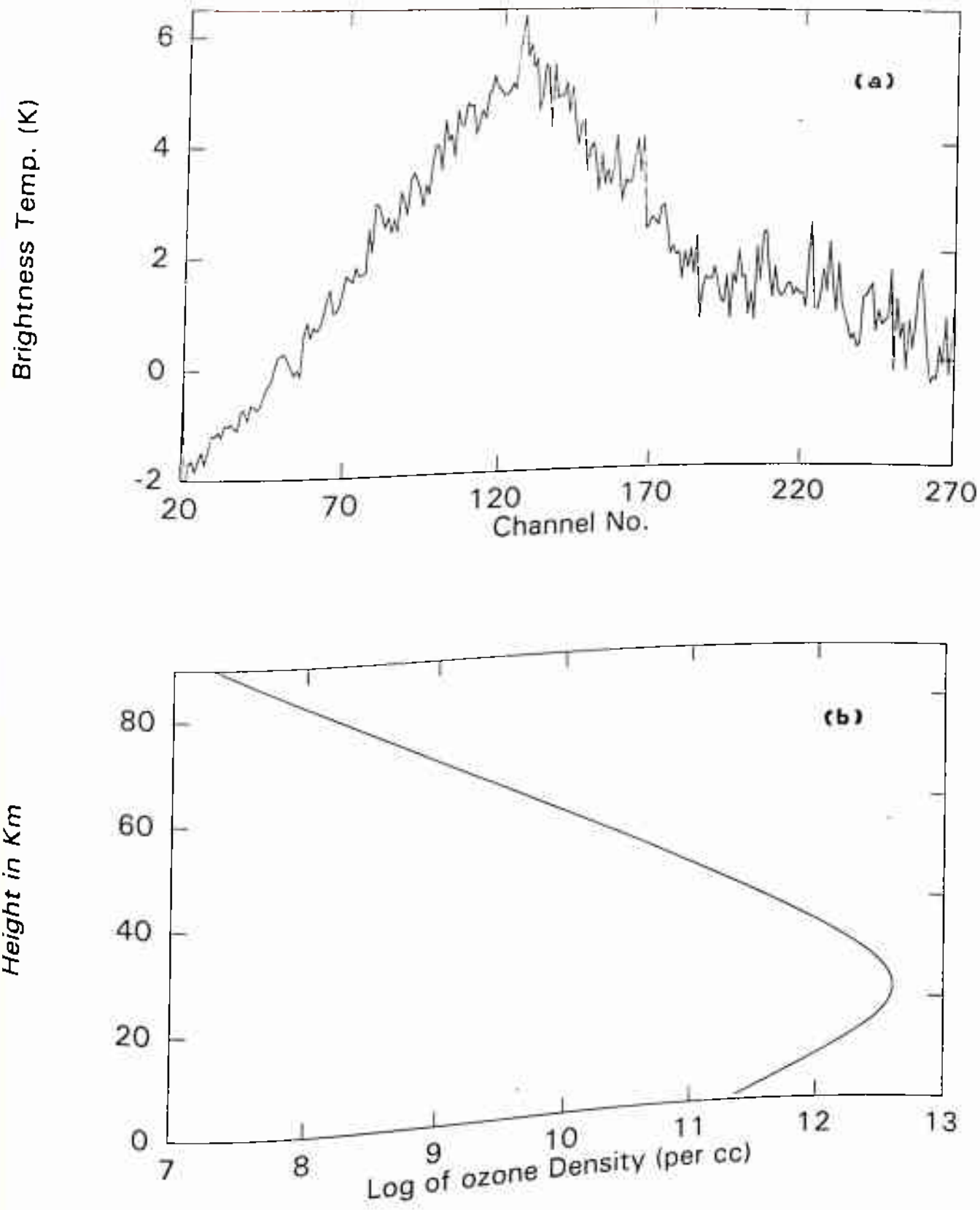

Fig. 5.3 *(a)* Ozone spectrum obtained on 14/1/94 at Maitri (Antarctica).

(b) Retrieved ozone profile.

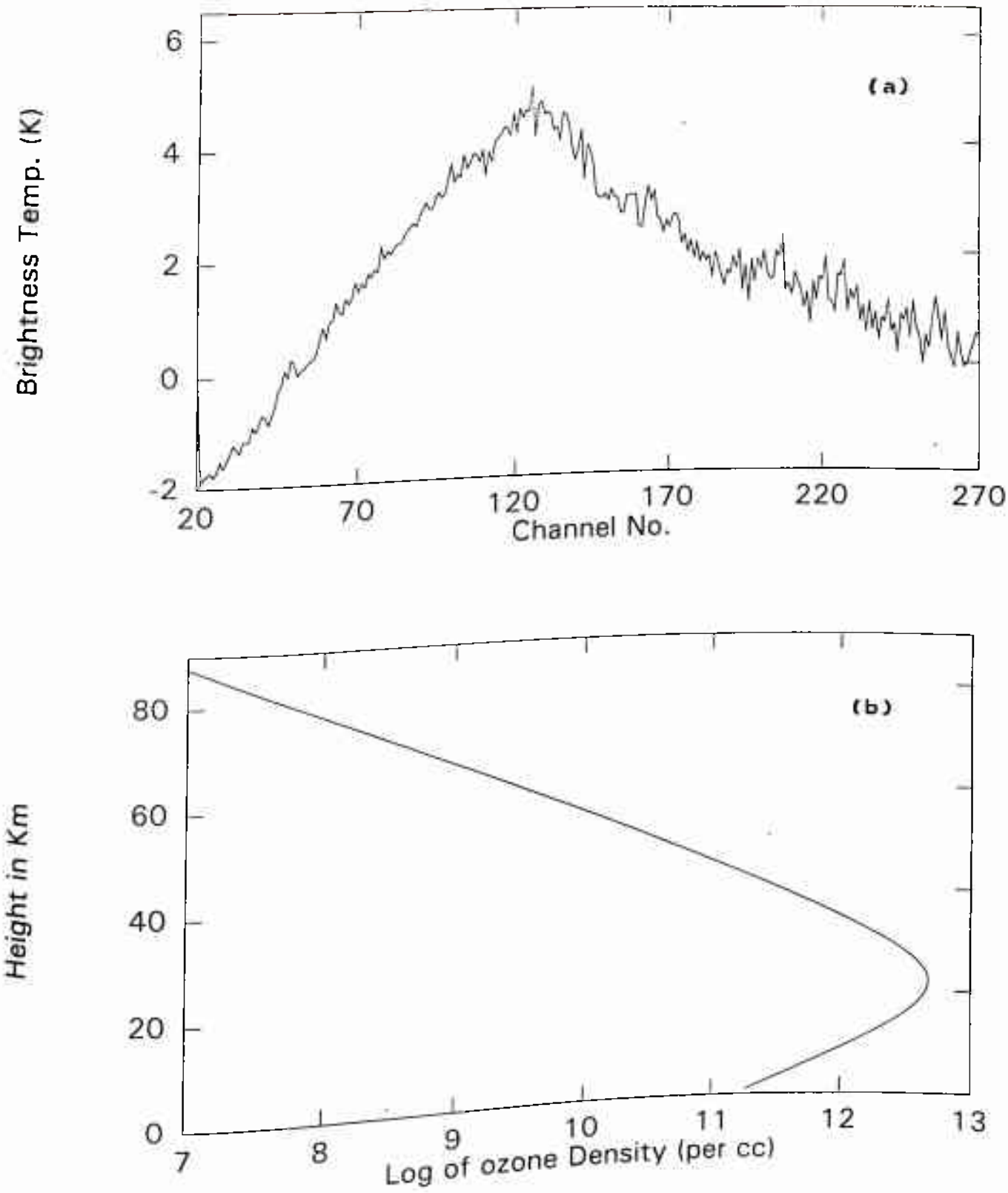

Fig. 5.4 ***(a)*** Ozone spectrum obtained on 16/1/94 at Maitri (Antarctica).

(b) Retrieved ozone profile.

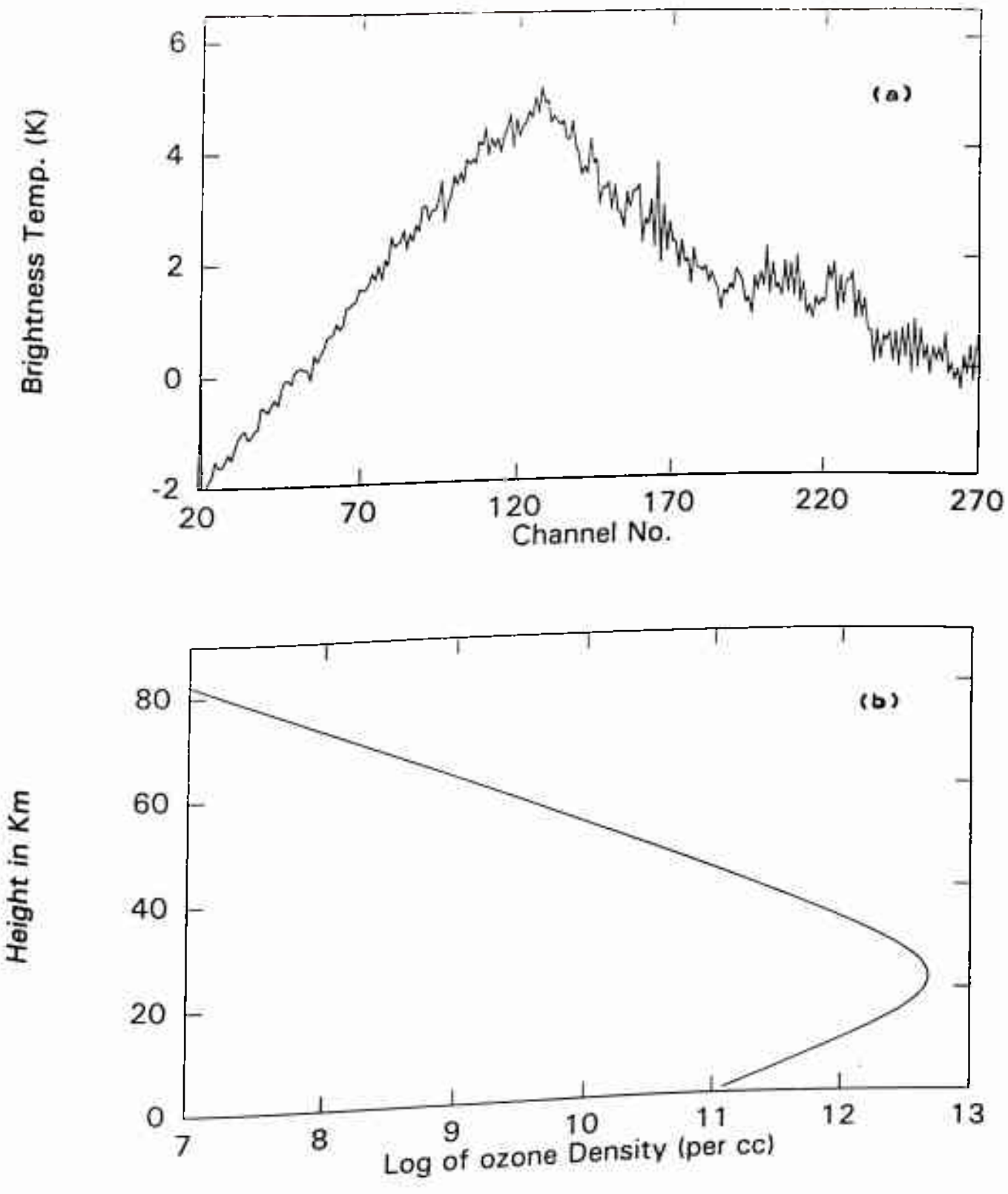

Fig. 5.5 ***(a)*** Ozone spectrum obtained on 17/1/94 at Maitri (Antarctica).

(b) Retrieved ozone profile.

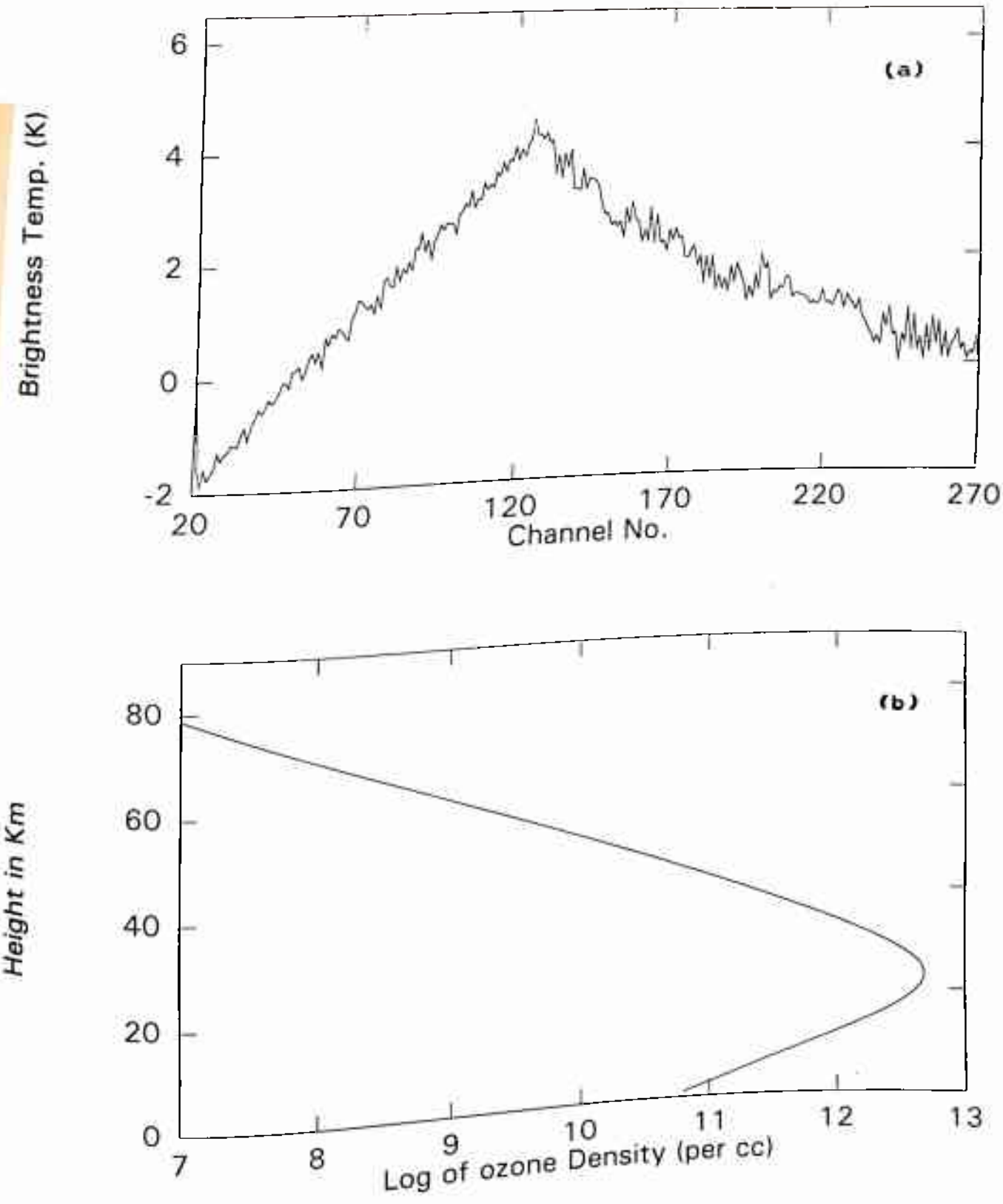

Fig. 5.6 *(a)* Ozone spectrum obtained on 18/1/94 at Maitri (Antarctica).

(b) Retrieved ozone profile.

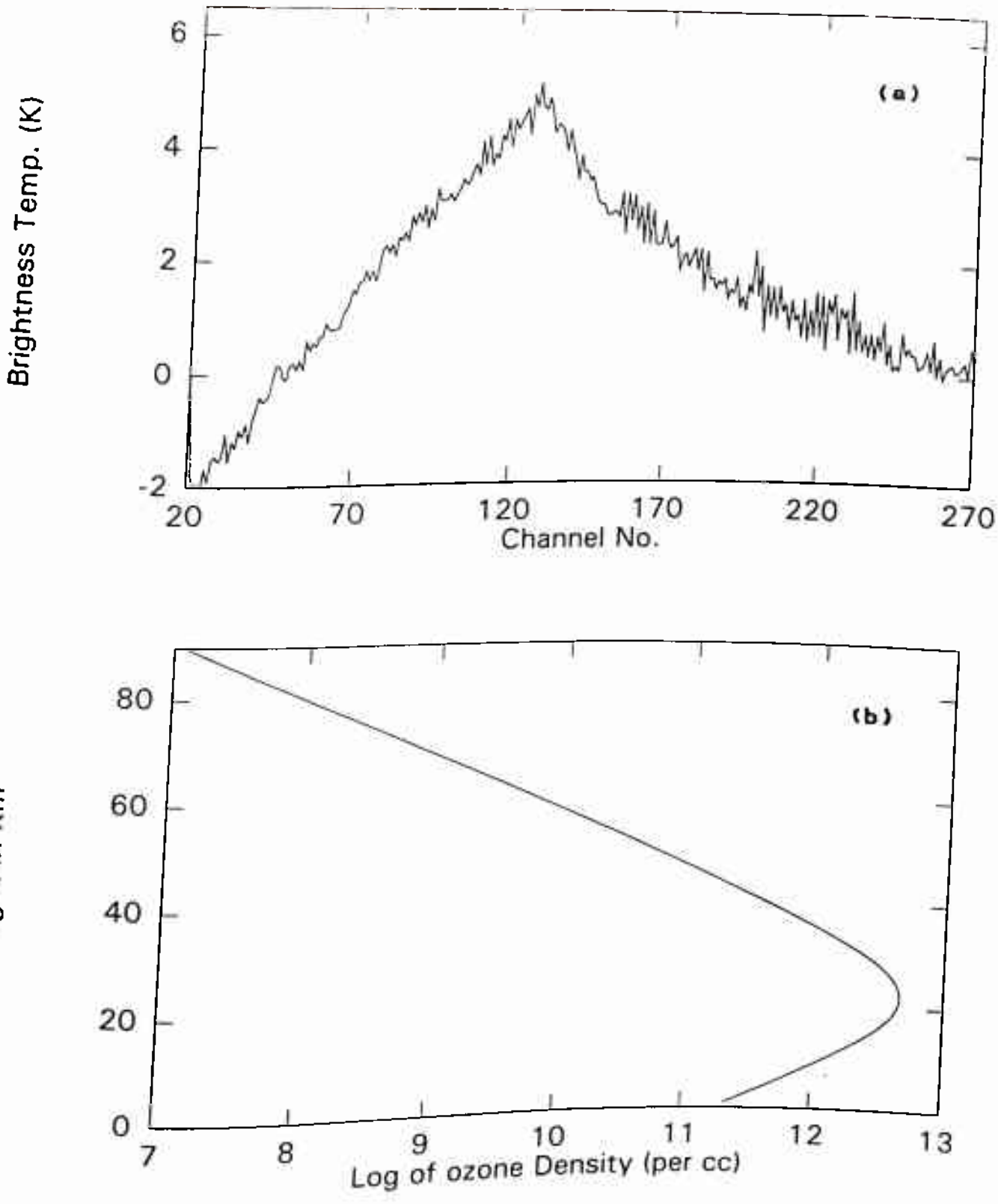

Fig. 5.7 ***(a)*** Ozone spectrum obtained on 19/1/94 at Maitri (Antarctica).

(b) Retrieved ozone profile.

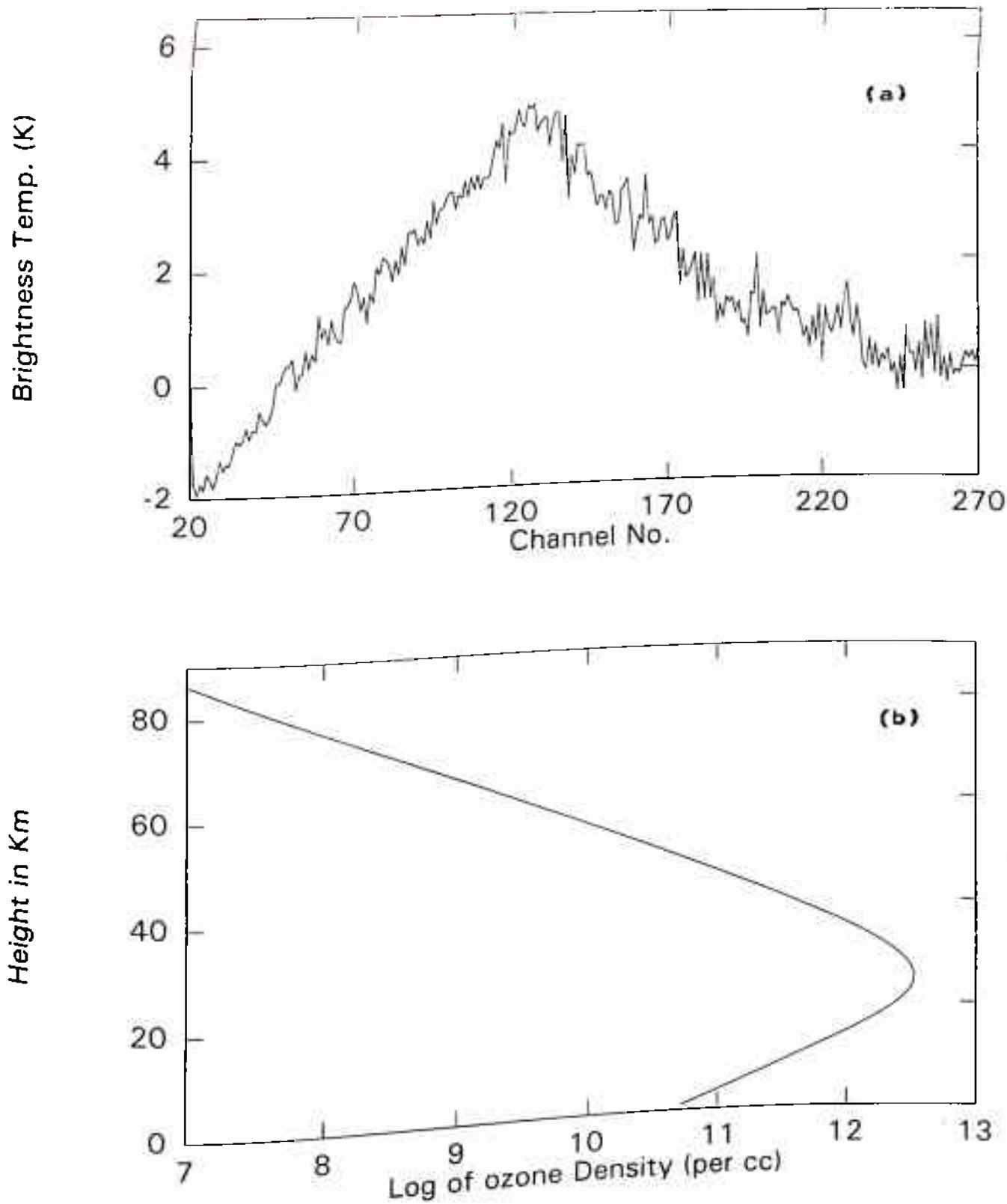

Fig. 5.8 ***(a)*** Ozone spectrum obtained on 20/1/94 at Maitri (Antarctica).

(b) Retrieved ozone profile.

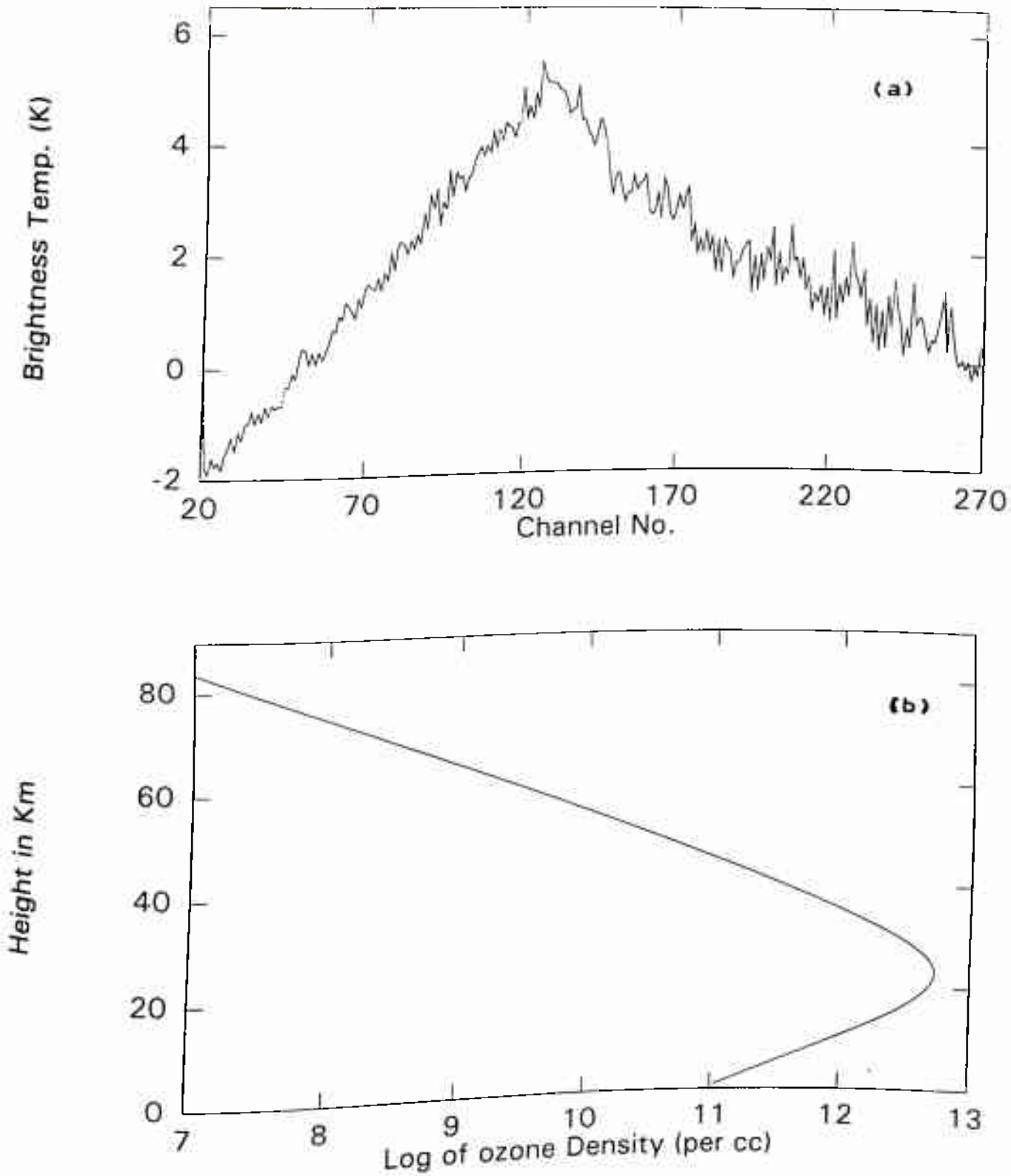

Fig. 5.9 ***(a)*** Ozone spectrum obtained on 21/1/94 at Maitri (Antarctica).

(b) Retrieved ozone profile.

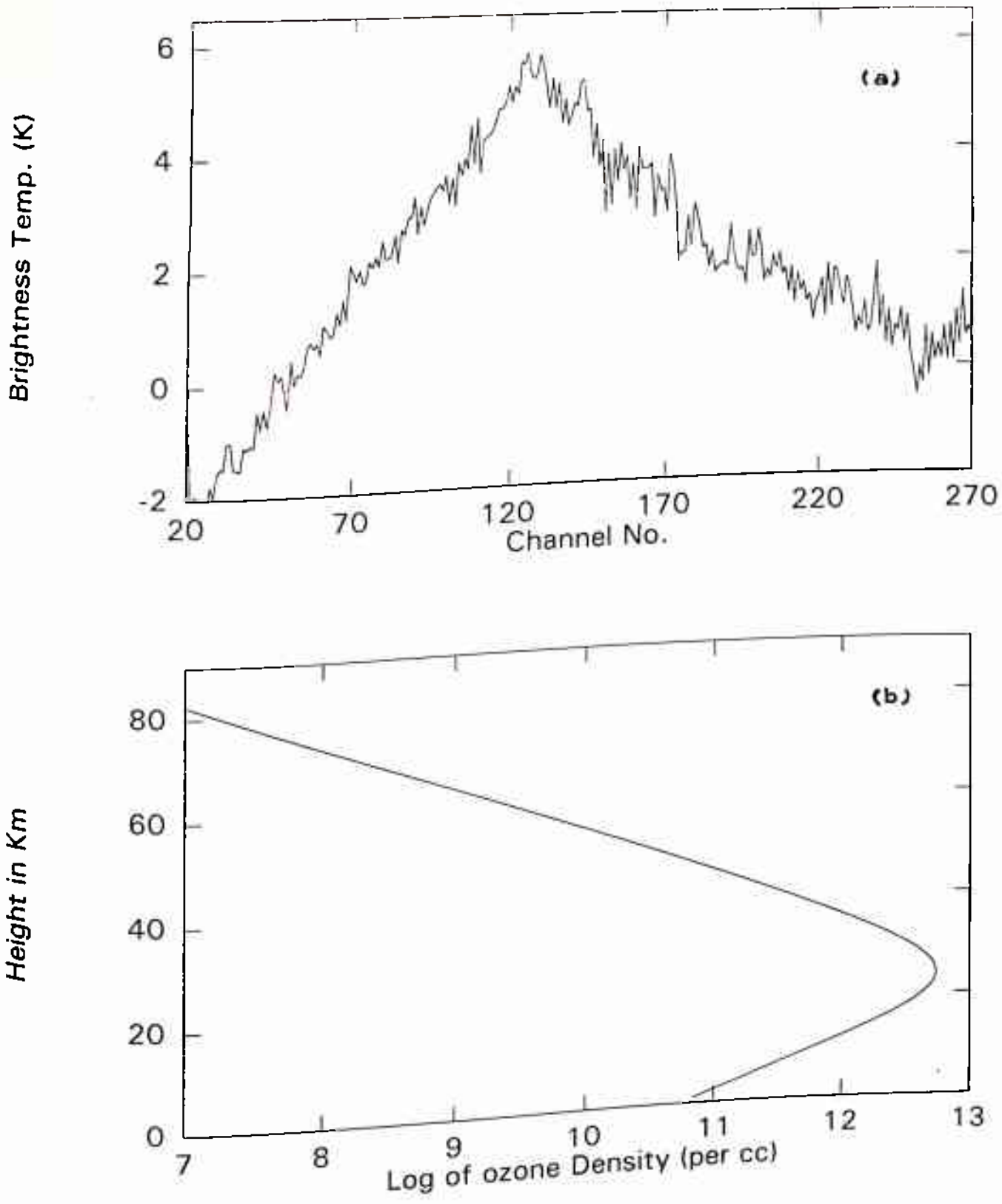

Fig. 5.10 ***(a)*** Ozone spectrum obtained on 22/1/94 at Maitri (Antarctica).

(b) Retrieved ozone profile.

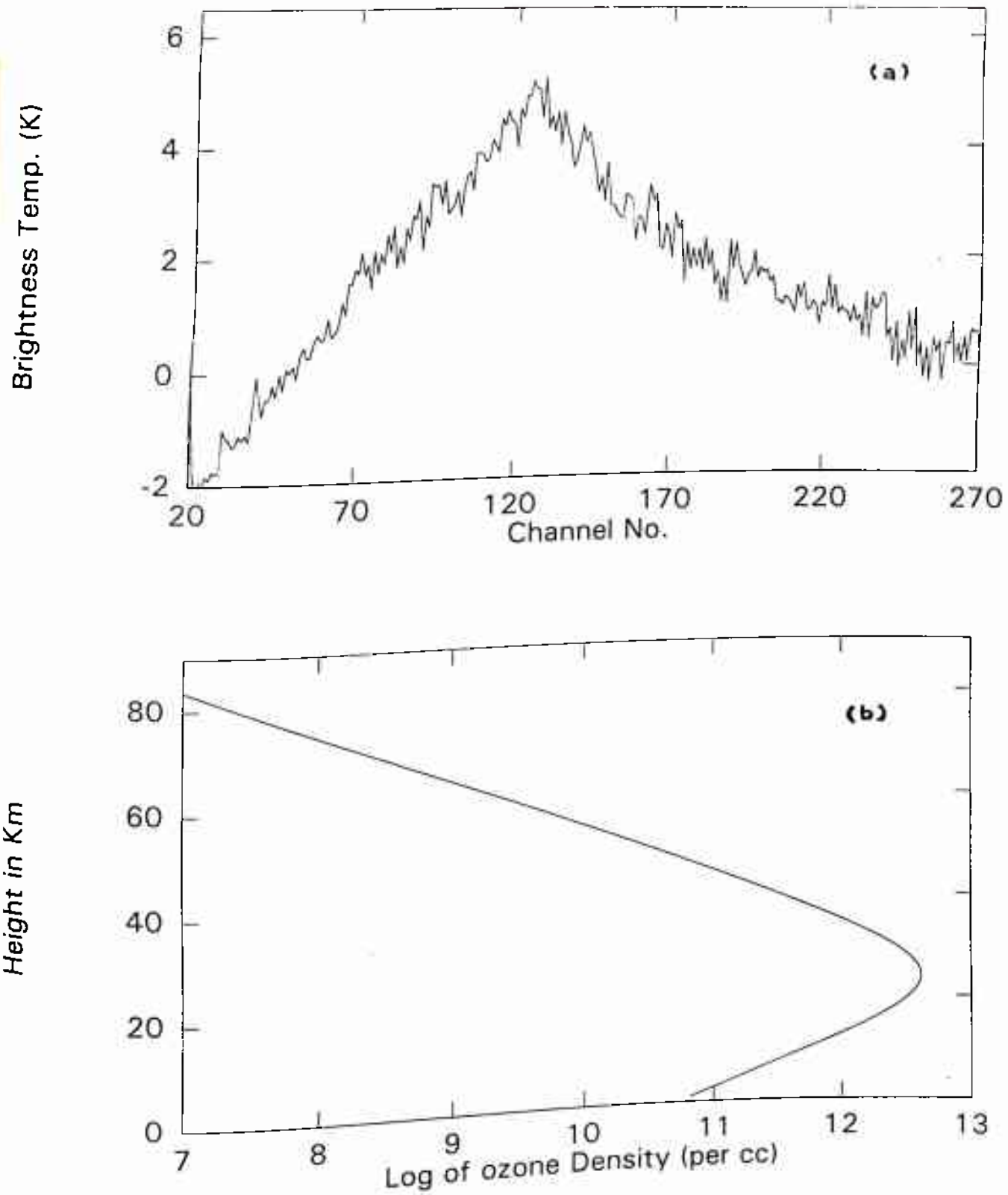

Fig. 5.11 ***(a)*** Ozone spectrum obtained on 24/1/94 at Maitri (Antarctica).

(b) Retrieved ozone profile.

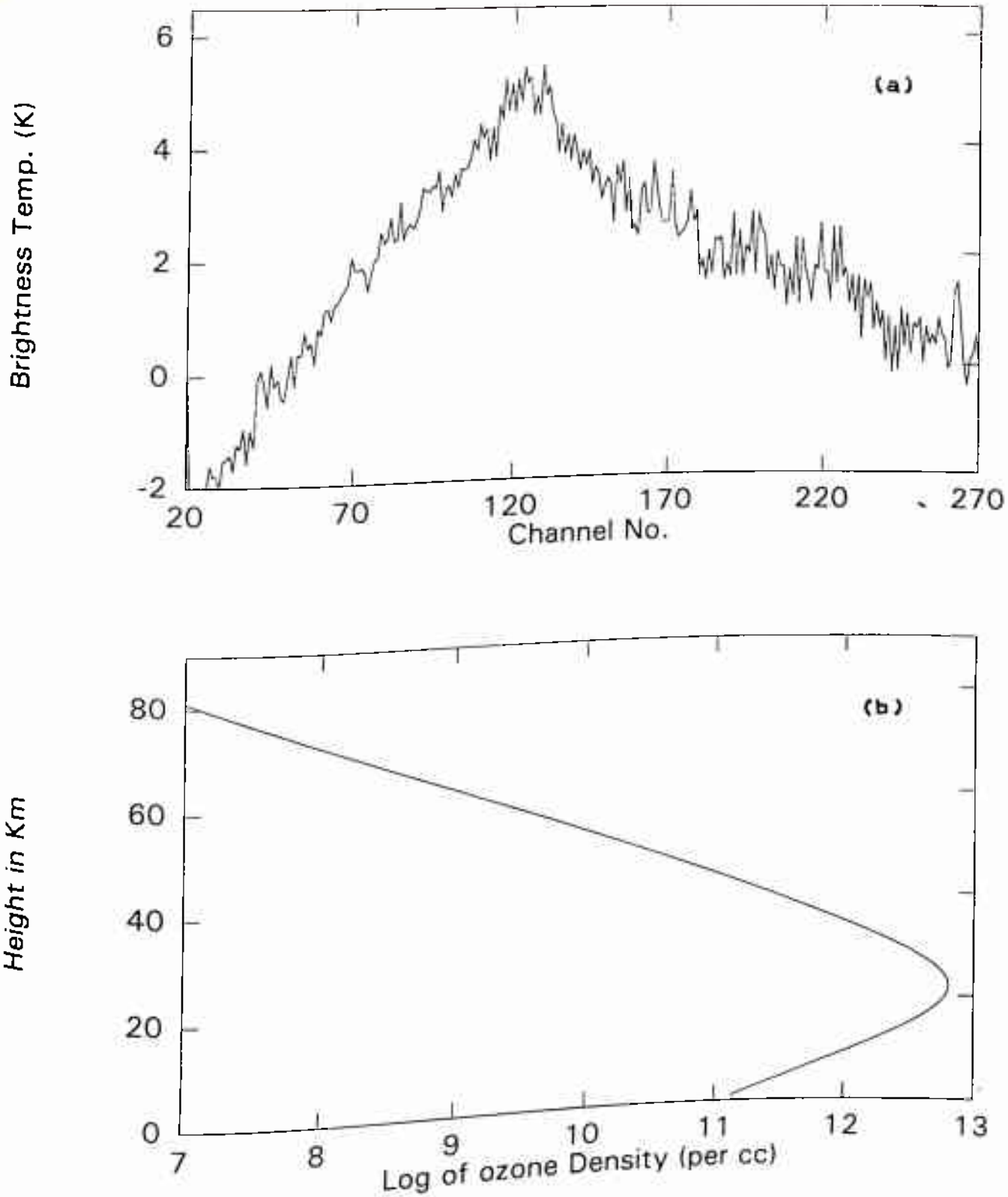

Fig. 5.12 ***(a)*** Ozone spectrum obtained on 25/1/94 at Maitri (Antarctica).

(b) Retrieved ozone profile.

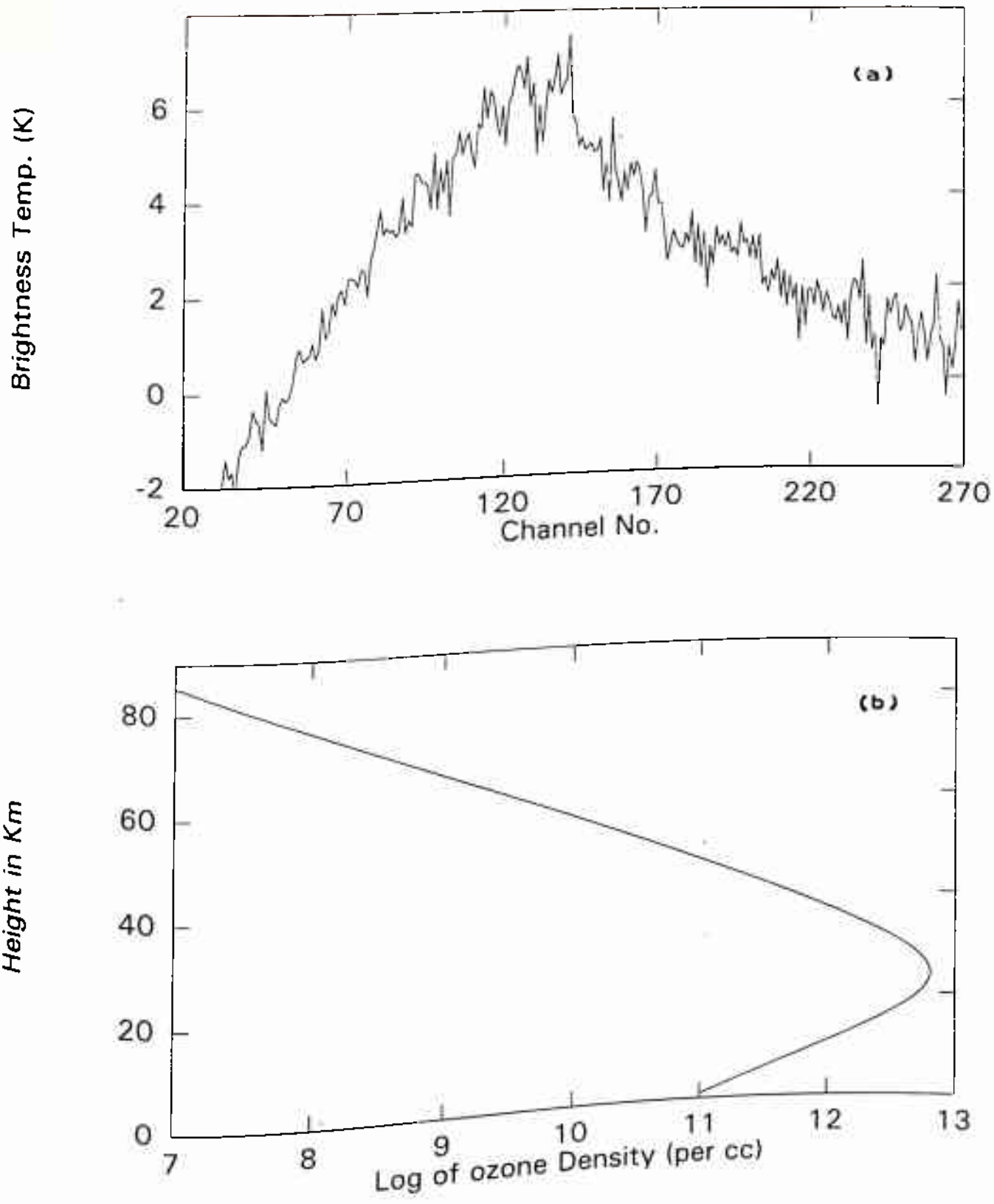

Fig. 5.13 *(a)* Ozone spectrum obtained on 28/1/94 at Maitri (Antarctica).

(b) Retrieved ozone profile.

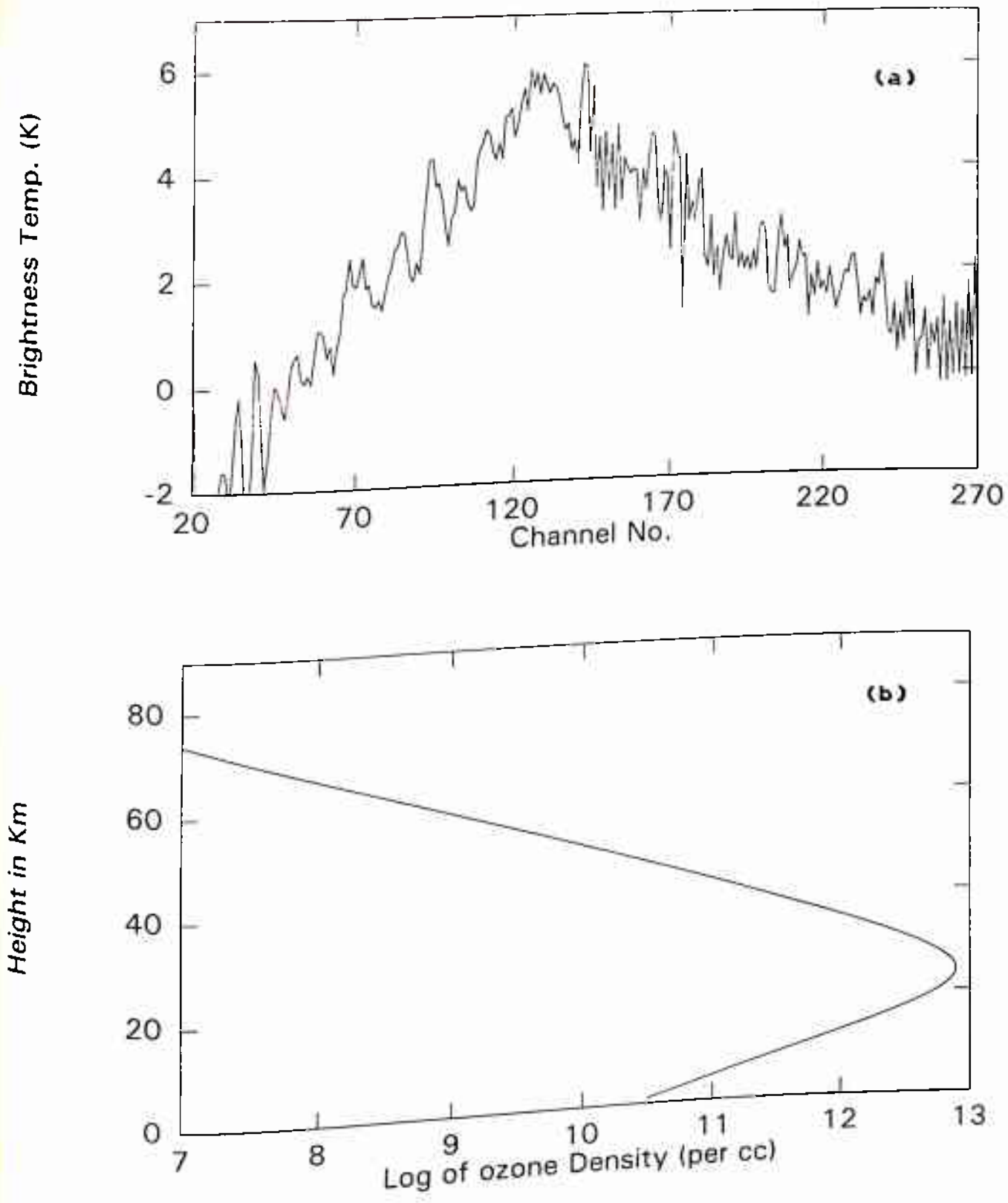

Fig. 5.14 *(a)* Ozone spectrum obtained on 29/1/94 at Maitri (Antarctica).

(b) Retrieved ozone profile.

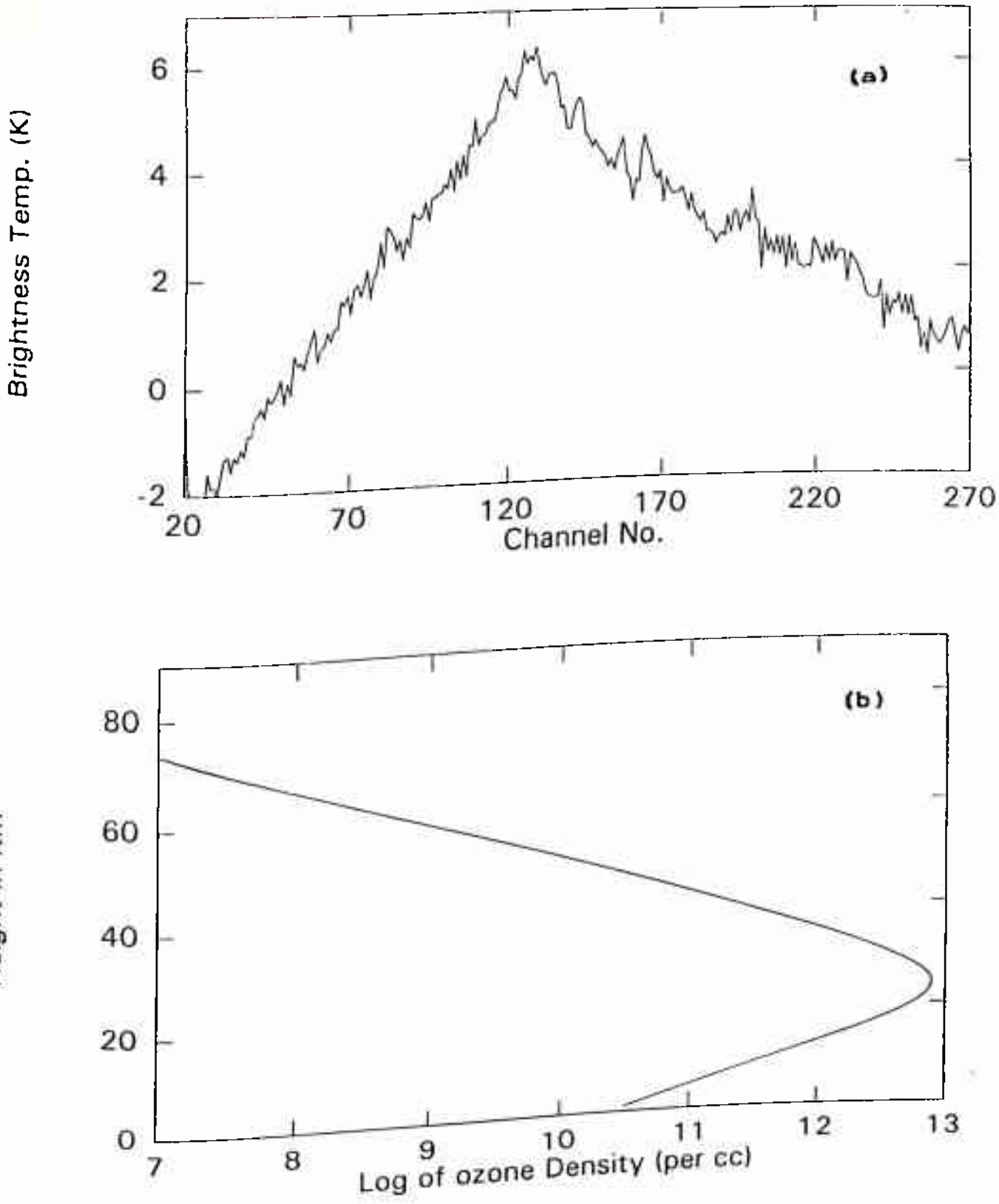

Fig. 5.15 *(a)* Ozone spectrum obtained on 30/1/94 at Maitri (Antarctica).

(b) Retrieved ozone profile.

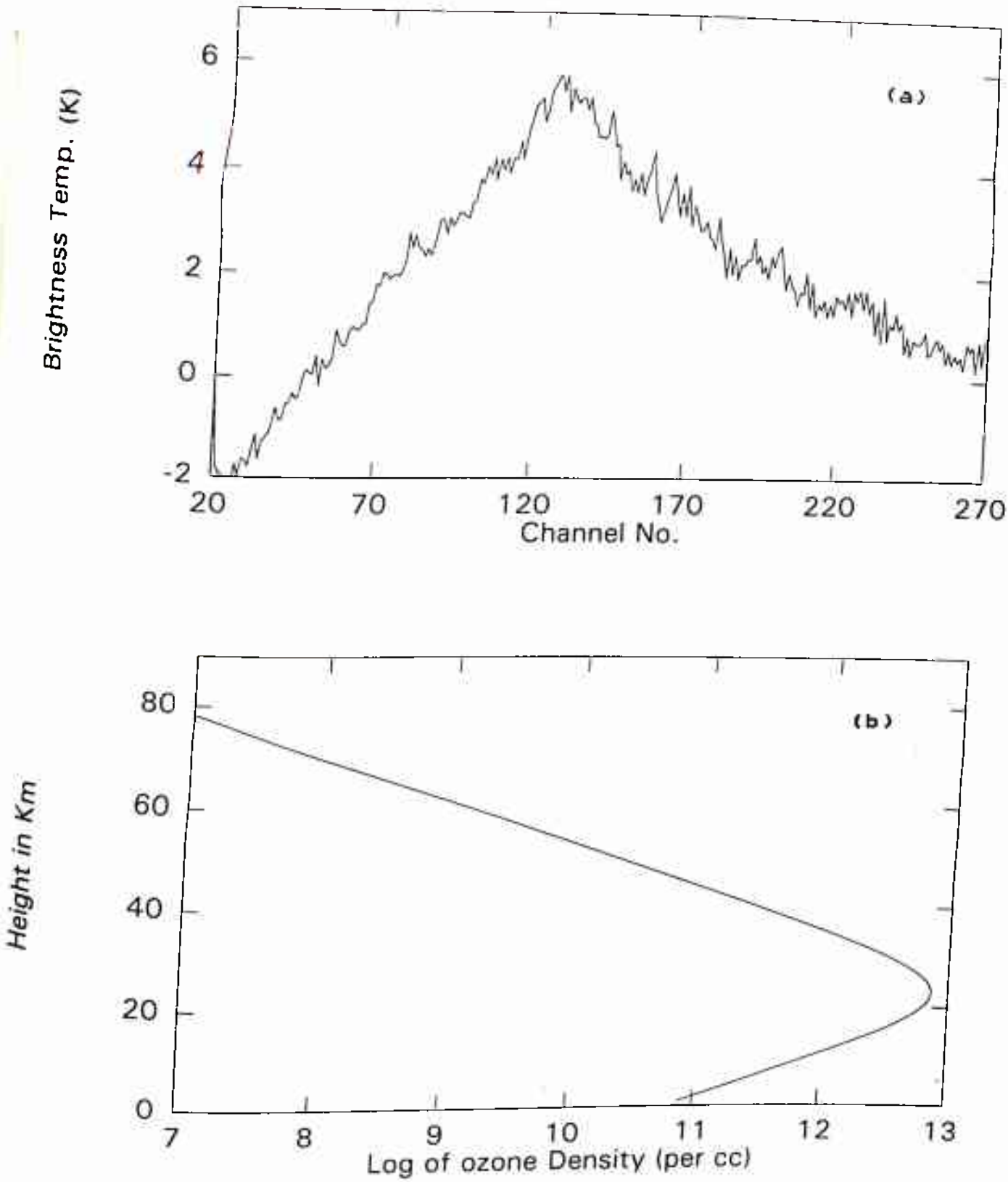

Fig. 5.16 ***(a)*** Ozone spectrum obtained on 31/1/94 at Maitri (Antarctica).

(b) Retrieved ozone profile.

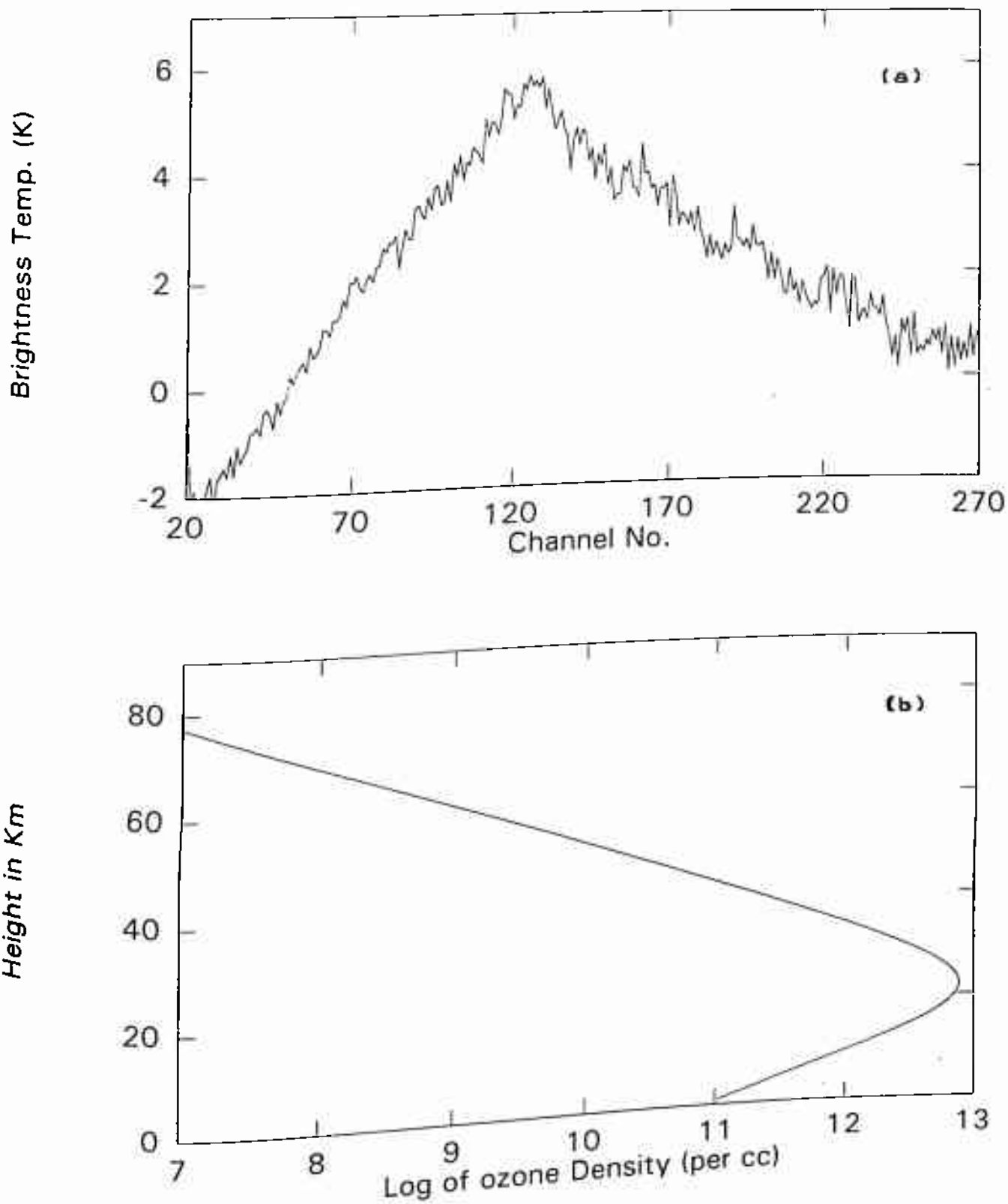

Fig. 5.17 ***(a)*** Ozone spectrum obtained on 3/2/94 at Maitri (Antarctica).

(b) Retrieved ozone profile.

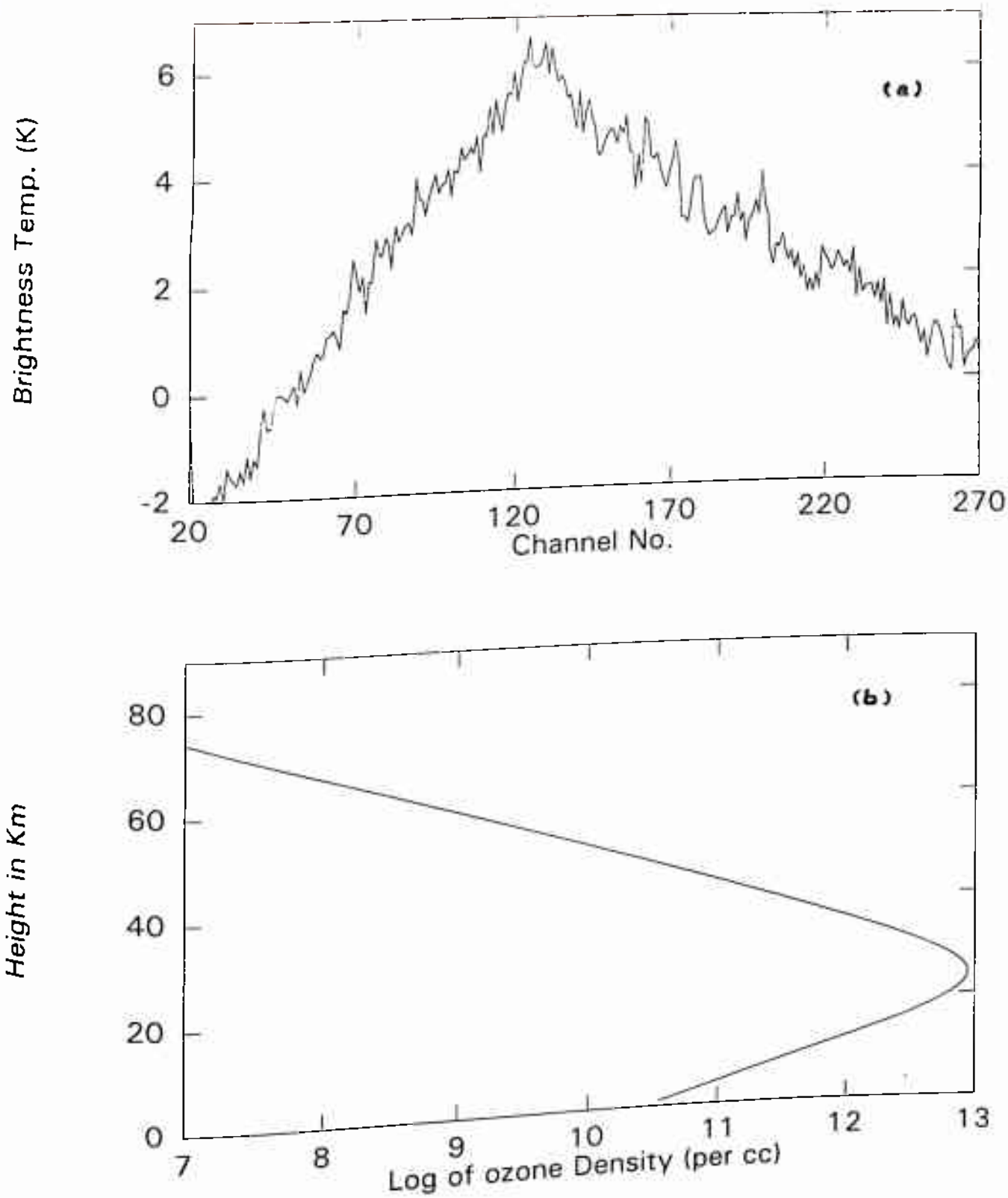

Fig. 5.18 ***(a)*** Ozone spectrum obtained on 4/2/94 at Maitri (Antarctica).

(b) Retrieved ozone profile.

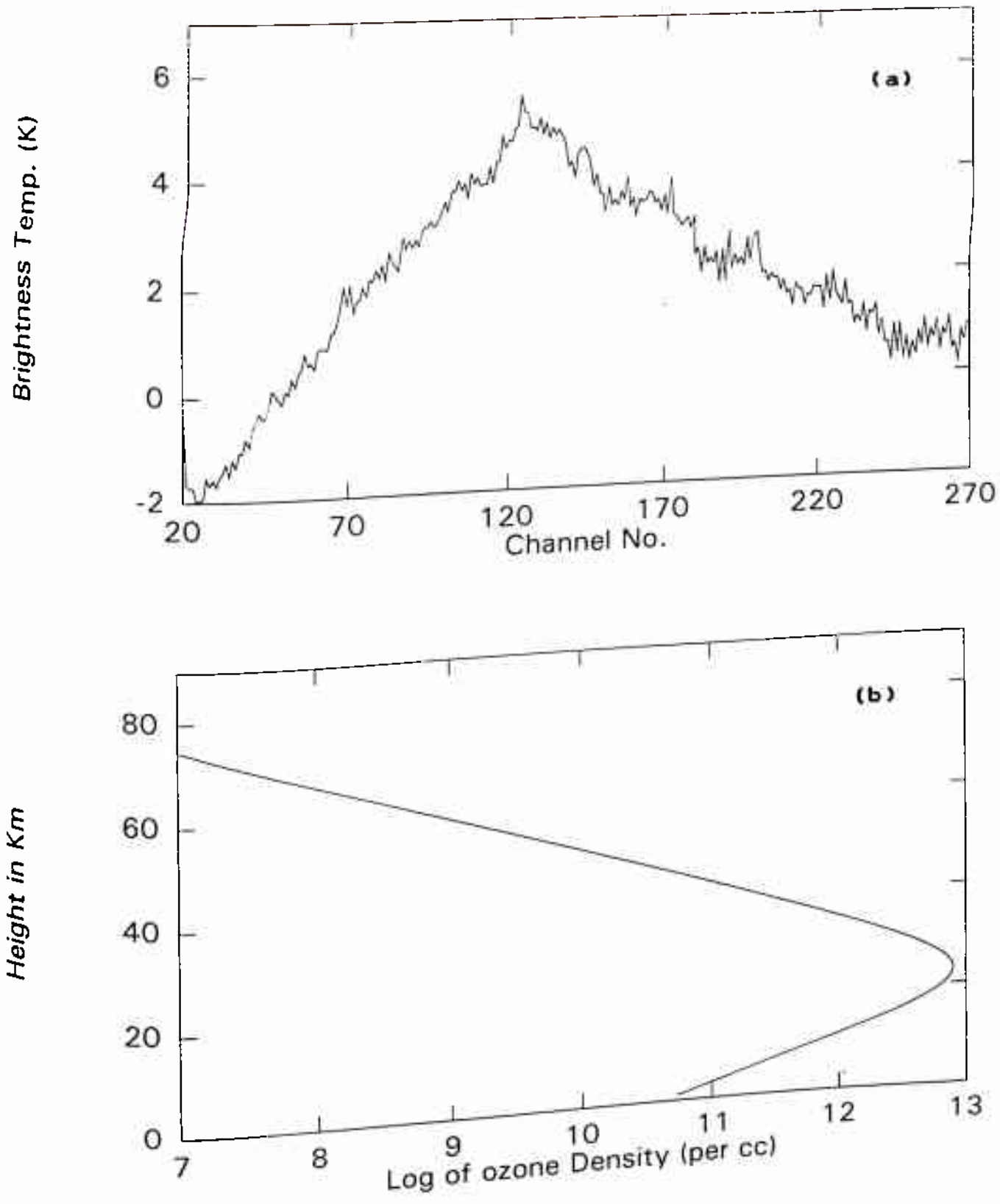

Fig. 5.19 *(a)* Ozone spectrum obtained on 5/2/94 at Maitri (Antarctica).
(b) Retrieved ozone profile.

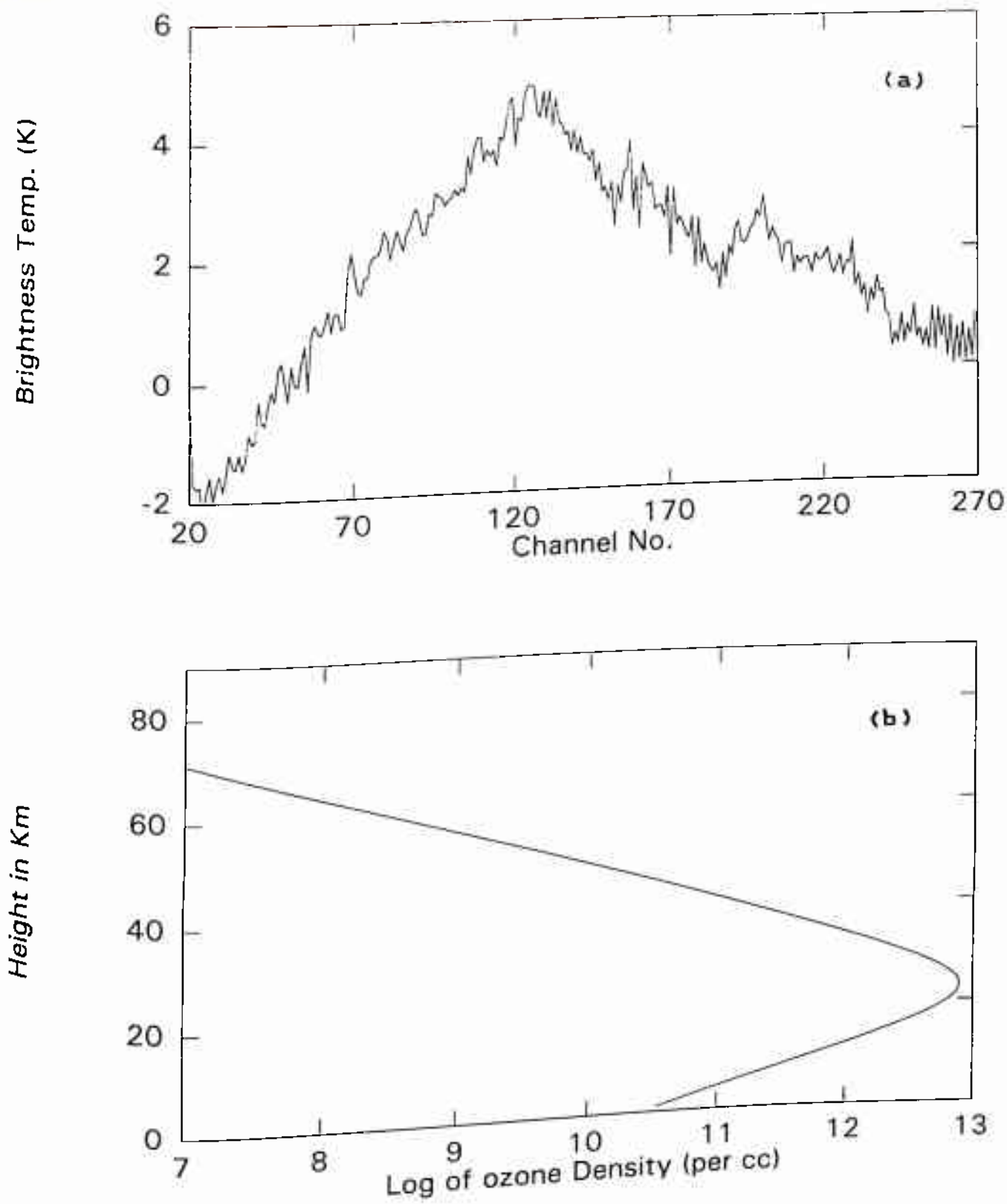

Fig. 5.20 ***(a)*** Ozone spectrum obtained on 6/2/94 at Maitri (Antarctica).

(b) Retrieved ozone profile.

Chapter 6

Results and Discussion

6.1 Discussion of Results

The ozone observations taken over Delhi (28°38' N) and over Maitri (70°45'S), Antarctica during the course of present study are presented in chapters 4 and 5 together with the retrieved ozone height profiles. The radiometer was operated for a few days in November 1993 in Delhi and from 13th January to 6th February 1994 at Maitri, Antarctica. The November data, taken at Delhi just before dismantling the instrument for Antarctica trip, provides a useful comparison for the high latitude Antarctica observations with the tropical/mid-latitude observations. Another important result obtained in the present work is the variation of ozone content over Antarctica during our observational period (mid January to early February).

Due to the frequency switched mode of operation the observed line shape is asymmetric about the center and hence could not be folded around the peak and only right wing of the line is used for the analysis of Antarctic data. Also the S/N ratio obtained in the daily spectrum is not good enough to apply the iterative inversion, and the data of a week's observation is combined in order to reduce the random noise level. The brightness temperatures are estimated by fitting Lorentzian functions in the integrated weekly spectrum which are then used for the iterative inversion scheme. This provides intercomparison of the results obtained by two different inversion techniques. For the purpose of ozone absorption coefficient calculations, US Standard Atmosphere 1966 is used. For Delhi observations the values of temperature and pressure are taken at 30°N (winter) of this document. For Antarctic observations the necessary temperature and pressure data used are 60°N (summer).

The average ozone over Delhi shows a peak value of 5.0×10^{12} at a

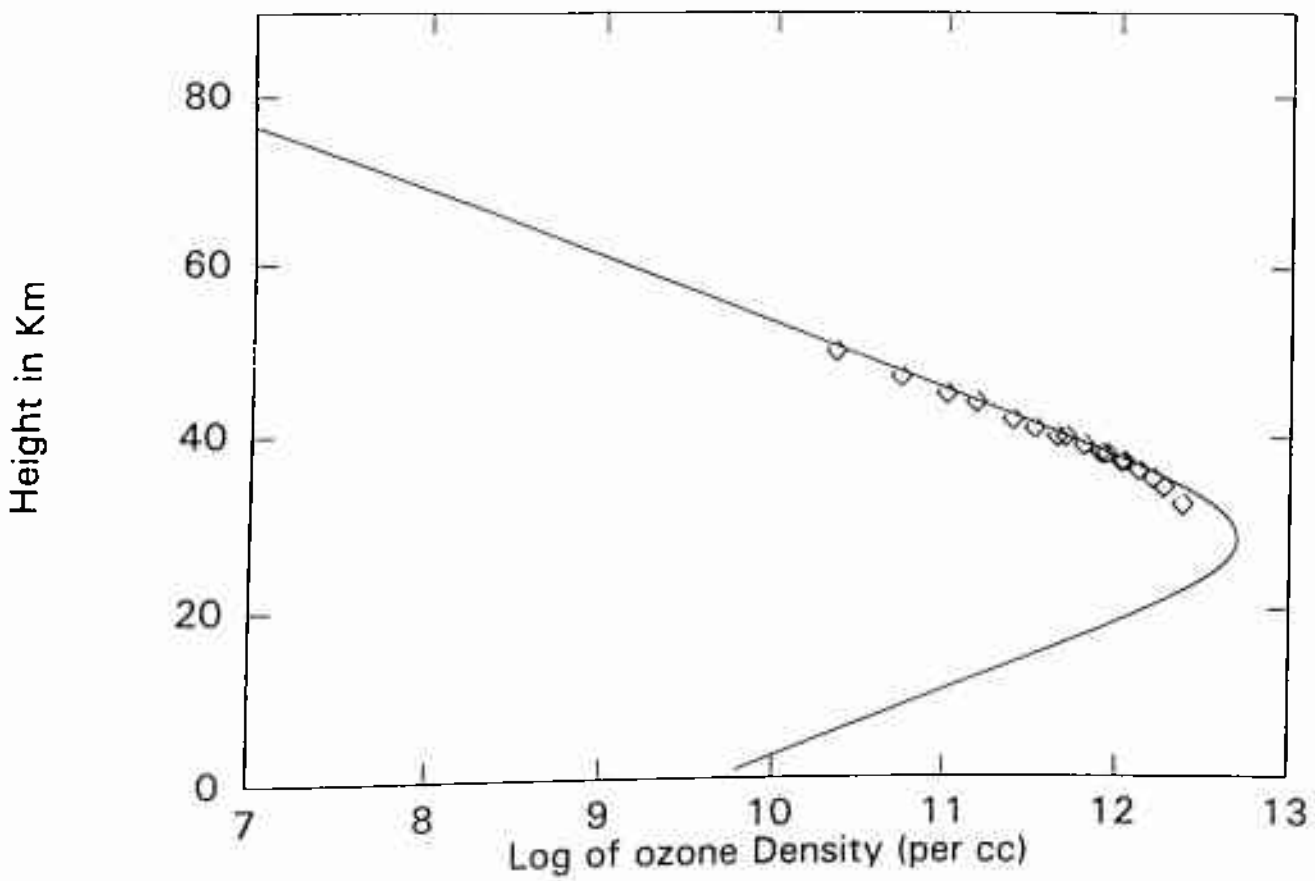

Fig. 6.1 Average November ozone profile over Delhi retrieved by spectral comparison (continuous curve) and iterative inversion (diamonds) methods.

height of 28 km. The peak density spread observed in Delhi results is less than 1.0×10^{12}. In fig 6.1 The average November profile is shown in ozone densities as obtained by the two inversion techniques viz., the spectral comparison and the iterative inversion methods. The solutions of iterative method are taken in a 30 MHz frequency range on the right wing of the line center. The mixing ratios thus obtained are converted to the ozone densities and are shown as diamonds in this figure. The continuous curve shows the ozone density obtained by spectral comparison method. It is clear from here that the results obtained by the iterative method are in good agreement with the densities found by using spectral comparison method. However, in the 30-35 km altitude region they show some divergence.

The Antarctic observations described in chapter 5 were carried out on the dates mentioned in table 5.1. The data were grouped on day to day basis and the analysis was done using the least square spectral comparison method. Again only the right wing of the observed spectrum was used for the reasons mentioned above. The ozone line spectrum obtained in Antarctica and it's corresponding retrieved height profiles are shown in fig 5.2 to 5.20. From 13th January onward the ozone has shown a rising trend in it's peak density (D_{max}). Data is further integrated by putting it into three groups each having about a week's data. These are January 13-20, 21-29 and January 30 to February 6. The total January data is also integrated to get an average January profile from 13th onward. These integrated spectra together with their retrieved height profiles are shown in figures 6.2 to 6.5. On the weekly and monthly integrated data, the iterative inversion is also applied for comparison. The conversion of ozone units is done using the table given in Annexure III.

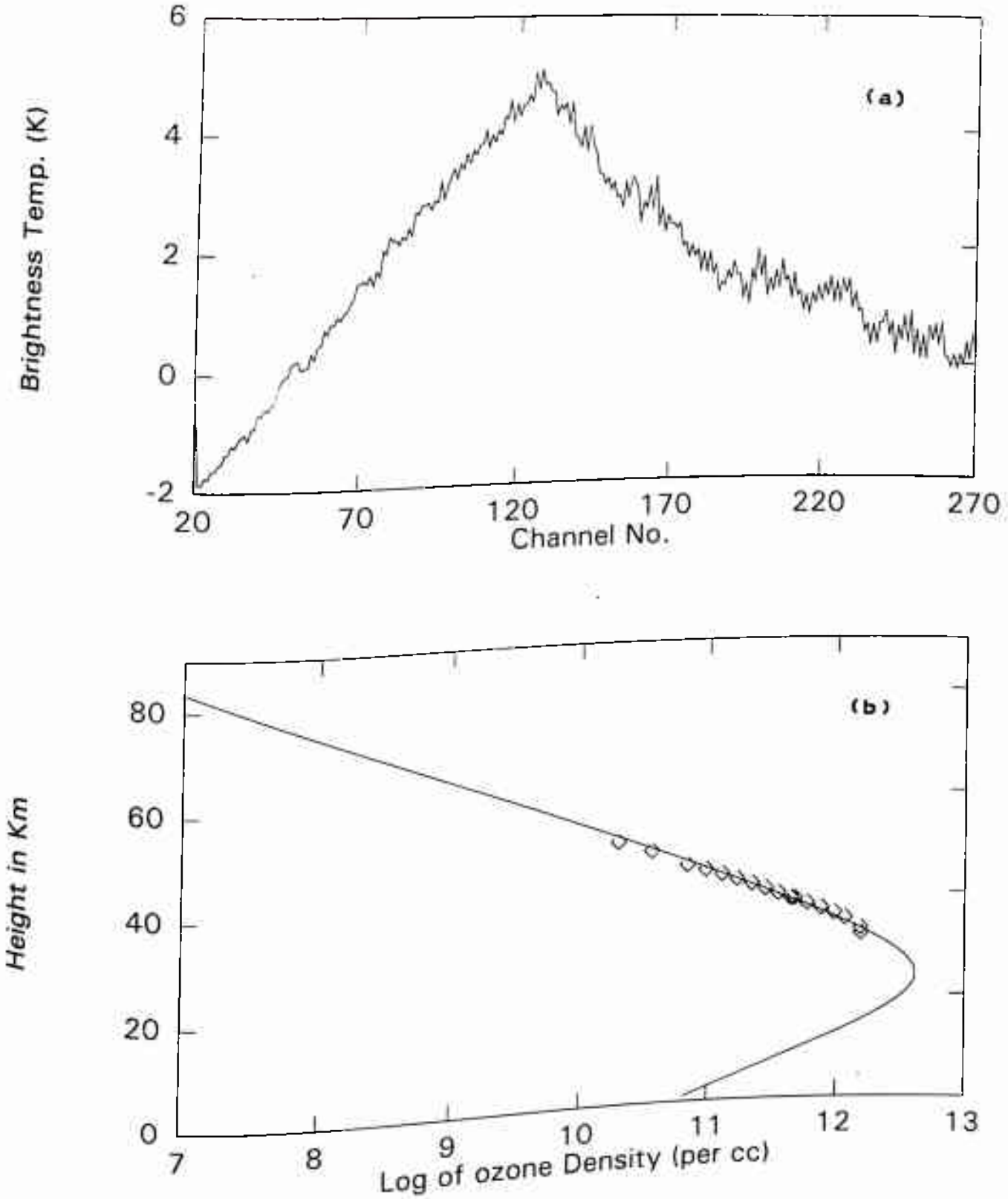

Fig 6.2 Average ozone spectrum obtained during 13-20 Jan. '94 at Maitri, (Antarctica) and the retrieved height profile. Continuous curve in graph (b) is obtained by spectral comparision method and diamonds represent ozone density values retrieved by iterative inversion.

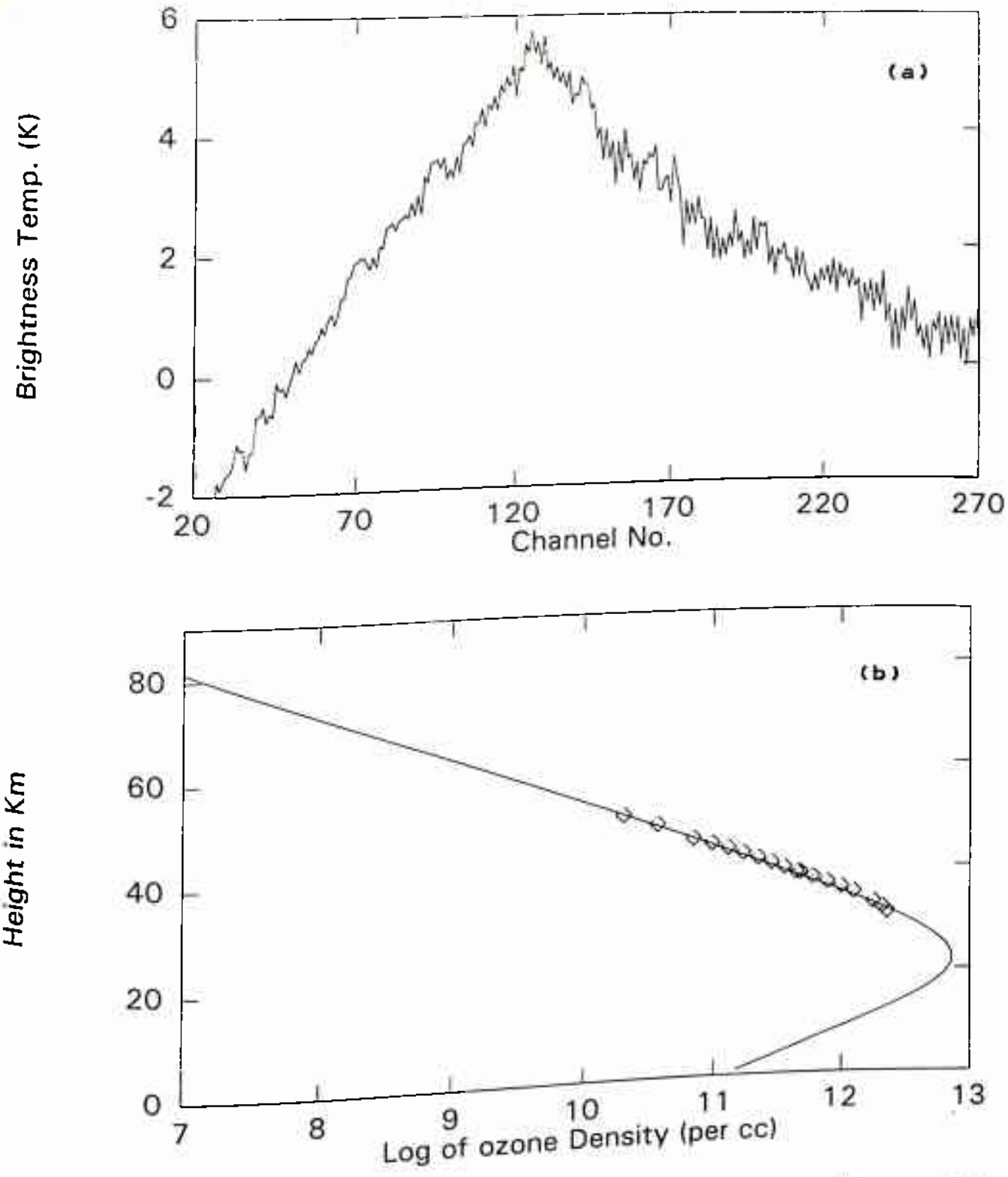

Fig.6.3 Average ozone spectrum obtained during 21-29 Jan. '94 at Maitri, (Antarctica) and the retrieved height profile. Continuous curve in graph (b) is obtained by spectral comparision method and diamonds represent ozone density values retrieved by iterative inversion.

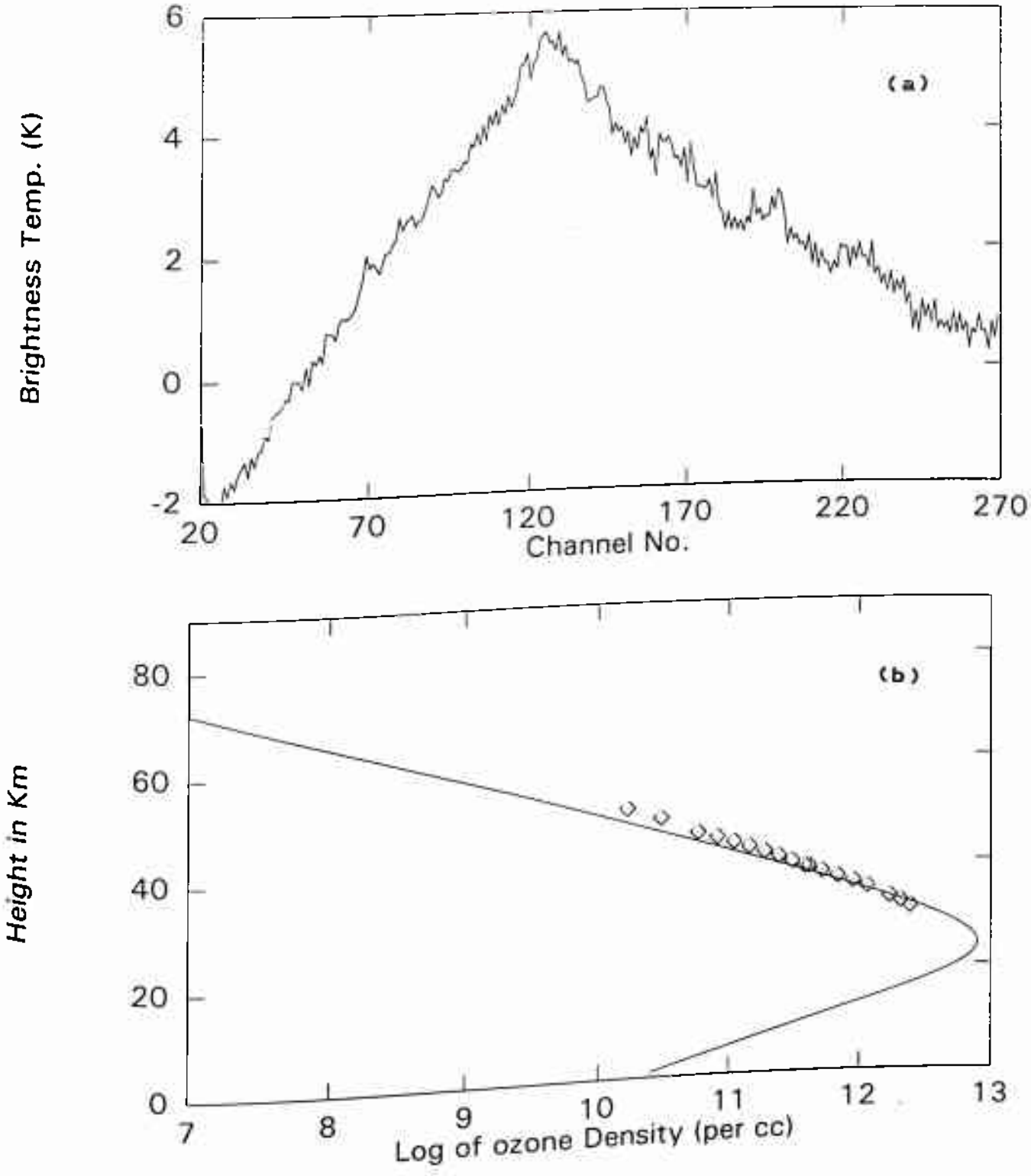

Fig. 6.4 Average ozone spectrum obtained during Jan.30-Feb.6 '94 at Maitri, (Antarctica) and the retrieved height profile. Continuous curve in graph (b) is obtained by spectral comparision method and diamonds represent ozone density values retrieved by iterative inversion.

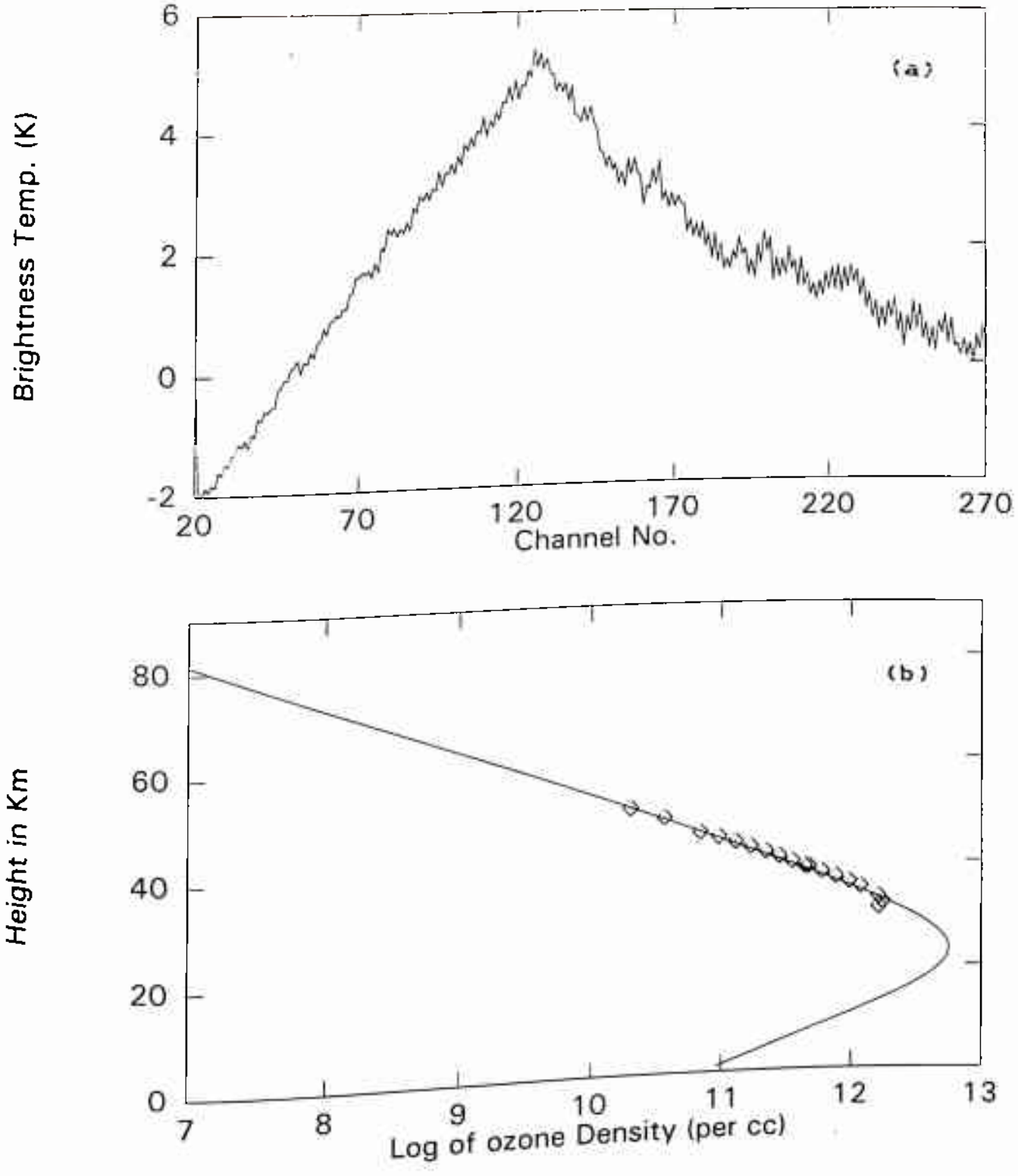

Fig. 6.5 Average ozone spectrum obtained during January (total) '94 at Maitri, (Antarctica) and the retrieved height profile. Continuous curve in graph (b) is obtained by spectral comparision method and diamonds represent ozone densitiy values retrieved by iterative inversion.

The iterative inversion algorithm starts with an arbitrary initial guess of ozone profile of 1ppm volume mixing ratio to calculate a brightness temperature spectrum. The resulting iterated profile is practically independent of the initial guess. The brightness temperature is calculated by integrating the radiative transfer in the atmosphere in 1.0 km layers from surface to 90 km. The observed brightness temperature differences at selected neighboring frequencies are then compared with the equivalent brightness temperature differences obtained from the calculated spectrum in order to correct the initial profile. The process is repeated until the difference between the calculated and observed data is smaller than the data error. The iterative algorithm modifies the profile at the iteration points using the relaxation formula derived by Chahine (1972) and interpolates the profile linearly for the integration of radiative transfer equation. In the algorithm given in annexure II, this value of number of iterations is user interactive. It was found that the solutions usually relaxed in three iterations. Our back-end spectrometer has uniformly distributed resolution bandwidth of 1 MHz. This puts an upper limit to the maximum height of observation which is about 60 km, if the iterative inversion is used. Moreover, above this altitude the pressure broadening does not remain the only dominant broadening mechanism and hence the results at heights > 60 km are not very reliable. The lower limit of retrieval is about 30 km owing to the fact that only 50 MHz frequency span on one side of the line center is used. Another important fact is the use of spectral comparison method as a complimentary scheme for calculation of baseline. This is important as in our analysis we have removed a second order baseline from the observed spectrum as described in chapter 4. This process actually removes the instrumental baseline together with some amplitude of the actual line bringing

it down to zero in the channels used for baseline calculation. Though the amplitude in the channels immediately after 50 MHz off center frequency span is not zero yet the average amplitude calculated for all the channels used for baseline removal tends to be zero. The second order baseline is calculated using the same channels in the theoretical spectrum also which is then subtracted from the theoretical spectrum before comparing it with the observed spectrum. The base line corresponding to the best least square fit is actually used for adding to the observed spectrum before using it in iterative inversion process. If the instrumental baseline function is supposed to be the first order in nature then this exercise is not needed as the iterative methods makes use of brightness temperature differences only.

6.1.1 Comparison of Delhi and Antarctica Observations

The two sets of data are presented in chapters 4 and 5 respectively. In Delhi, the observations were carried out in the month of November before dismantling the setup for Antarctica trip. The purpose of these observation was to facilitate comparison of Antarctic results with the equatorial/mid-latitude results. It is clear from here that the total ozone content over Antarctica is more compared to Delhi. The average Delhi ozone has a peak density of about 5.0×10^{12} molecules per cc in the month of November as found by our analysis. Another important result obtained from these comparisons is that the height of peak density obtained in Antarctica is comparatively lower (figure 6.6). The reason for this could be assigned to the low surface temperatures prevalent in the polar continent. The comparison based on the average results of January (Antarctica) and of November (Delhi)

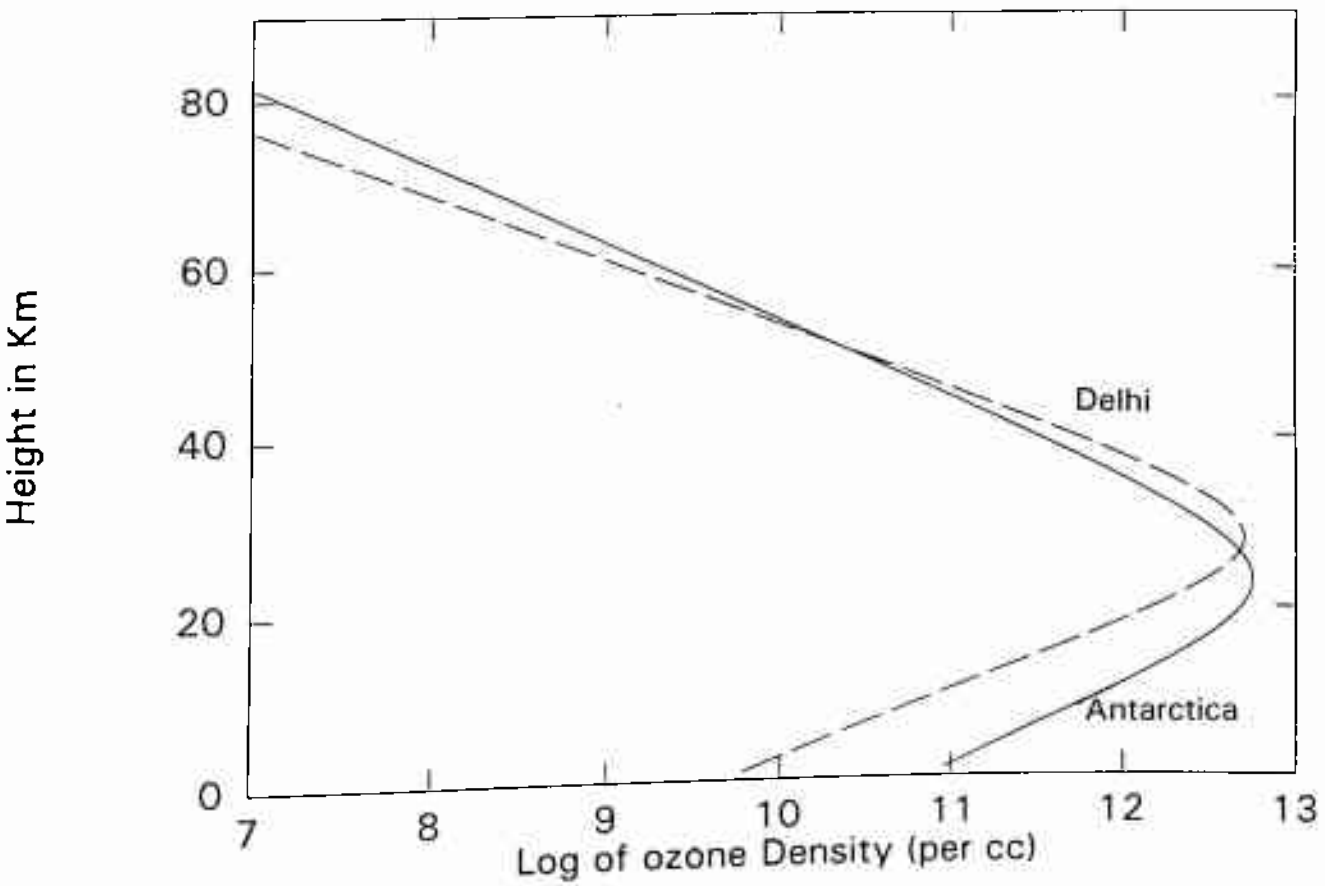

Fig. 6.6 Comparison of average ozone profiles obtained at Delhi(Nov. '93) and Antarctica (Jan. '94)

suggest a higher concentration of ozone at lower altitudes in Antarctica. The point of occurrence of the peak density is also found lower over Antarctica. The following conclusions can be drawn from this study :

(i) The total ozone content (TOC) over Antarctica (70°45'S,) is more compared to Delhi (28°37'N).

(ii) Ozone density is more in the lower heights (0-30 km range) over Antarctica compared to the lower latitude results of Delhi.

6.1.2. Antarctica Ozone Trend During January-February '94

The ozone observations over Maitri (70 45'S,11 45'E), Antarctica show a definite trend in the ozone peak density and the total ozone content observed there. The density peak value started with 4.0×10^{12} per cc on 13th and continued to rise toward the end of the month. On 29th January it shot up to as high as 7.8×10^{12}. In February it remained essentially constant around this value and hence shows no significant change from the 29th January value. This factor of increase in the ozone peak density may not be quantitatively reliable due to baseline removal limitations in our data. However, the increasing trend of total ozone variation over Maitri during our observation period can be believed. The height of the ozone density peak as measured by this experiment was between 22 to 26 km. The value of this 'h_{max}' did not show any correlation with the increasing peak density with the passing days in January. The third parameter r (scale factor), however, showed some correlation with the peak density. It's value started with 0.2 in mid January and ended up at 0.3 in early February. The increase in 'r' shows a constriction in the ozone distribution in the atmosphere. This high value of r, to some extent, compensates for the increased peak density in keeping the total ozone

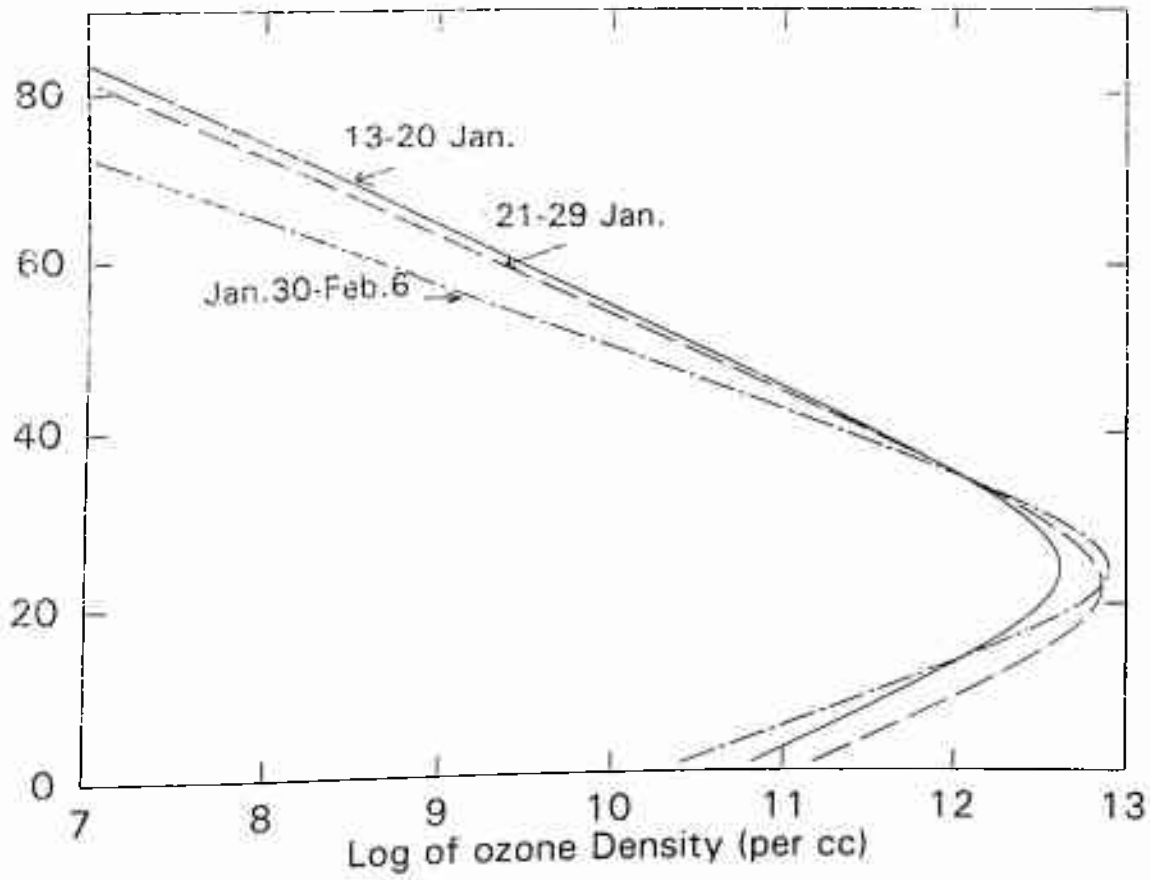

Fig. 6.7 Weekly variation of ozone over Antarctica during the observational period (mid January to early February)

variation moderate.

The weekly averaging of data revealed that the major change in ozone peak density has actually taken place during the first two weeks of observations i.e. 13-20 Jan & 21-29 Jan (figure 6.7). The change between Jan. 29 to Feb. 6 is not as much as found in the earlier two weeks. However, the trend is still positive and the maximum ozone peak density over Maitri was observed only during this week. Table 6.1 gives the D_{max}, h_{max}, r and TOC values for weekly and January (total) data. The average January value of TOC over Maitri, Antarctica is 332 Dobson Units. The peak TOC is obtained in the last week of January.

The results of Antarctic observations are compared with results of the in-situ balloon ozone sondes carried out once every week over Antarctica during our observational session. The balloon flights were limited to a maximum altitude of only 30-35 km and hence comparison could be done only in this range. The balloons were released on 11th, 21st and 27th January. Out of these only 21st Jan. flight could be directly compared with our observations. A comparison of our results with the balloon ozone observation upto 35 km is shown in figure 6.8. There seems to be a good overall agreement between the two. However, the peak density obtained from balloon ozone sonde is slightly lower than our profile. This could be an artefact of our analysis procedure which uses a mathematical model based on three parameters. This model would always produce its characteristic smooth shape irrespective of the sudden shape changes in the actual ozone distribution. But for this small discrepancy we find that the three parameter model describes Antarctic ozone with a good degree of accuracy and can be fruitfully employed for modelling of Antarctic Ozone.

Table 6.1 D_{max},h_{max}, r and Total Ozone Content (TOC) values for averaged monthly observations over Delhi (28N) and Antarctica (70S).

Place & Obs. Period	D_{max} (per cc)	h_{max} (km)	r (km^{-1})	TOC (Dobson Units)
Delhi:				
Nov. '93 (Avg.)	$5.0*10^{12}$	28.0	0.3	247.9
Antarctica:				
Jan. '94 (Avg.)	$5.6*10^{12}$	23.0	0.25	332.2
Feb. '94 (Avg.)	$7.9*10^{12}$	24.0	0.31	378.9

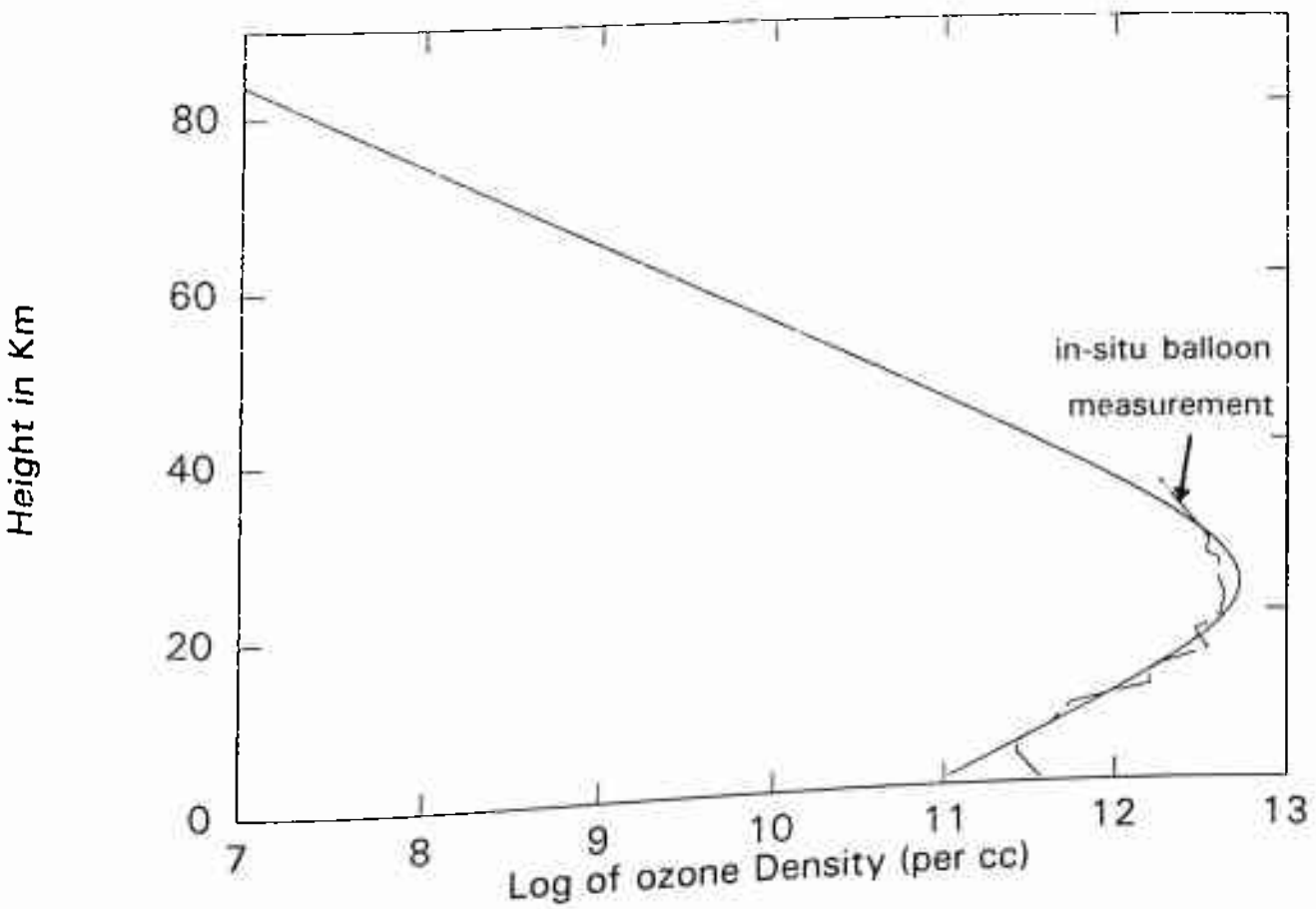

Fig. 6.8 Comparison of our results with in-situ balloon measurement of ozone density taken on 21/1/94

Chapter 7

Concluding Remarks

Consequent on the work presented in this thesis, it can be safely concluded that the ground-based millimeter-wave technique can be effectively employed for the height profiling of the stratospheric ozone. Ozone observations for Delhi and Antarctica are presented in this thesis. We have shown that this technique works even in adverse weather conditions in Antarctica. Also we used two different inversion techniques for the retrieval of ozone height profiles from the observed spectral line data. The fact that the two separate anaiysis procedures yielded similar results at least in the 30-60 km height range, enhanced confidence in the accuracy of retrieved data. Below 30 km, the ozone profile retrieved by our spectral comparison scheme compared well with that obtained from a concurrent balloon ozone sonde flight. However, a long term comparison of this new technique with other established methods of ozone height profiling (e.g. Umkehr) would be needed before a quantitative understanding of the accuracy of millimeter-wave technique could be obtained. Some suggestions for further research are given in the following paragraphs.

There is considerable scope for improvement of sensitivity of the present system and thereby improving the accuracy of measurements. A better sensitivity can be obtained by using improved millimeter-wave detectors using cooled Schottky diodes. The system noise temperature can be effectively brought down by almost an order of magnitude by using these cooled receivers. In the sensitivity equation the system temperature enters directly as first power and hence it assumes an importance which is square of the effective integration time. However, for cooling the heterodyne detector and IF amplifier down to about 20-30 K, a closed cycle helium refrigerator would be needed. This can be done only at the cost of sacrificing the

portability of the instrument somewhat.

Other design and acquisition limitations of the present system include the non-linearity of the system response for two different input powers, unavailability of large frequency switching range in the back-end spectrometer and slow data acquisition. These are collectively responsible for comparatively poor data quality and excess acquisition time. The nonlinearity problem could be solved by having an additional step in calibration. The system response for different input power levels can be obtained by introducing a calibrated noise power using a noise tube in the front-end. The responses of the individual channels can be stored in the computer which can then be used for correction of observed data. The problem of small frequency switching range can be solved by a better frequency-agile local oscillator using tunable Gunn devices. This will also reduce the time overhead for stabilization of local oscillator after each frequency change.

The problem of slow data acquisition in our instrument is a consequence of the use of a user-friendly commercial software "Asyst". Though it is relatively easy to program with Asyst, the actual acquisition turns out to be quite time consuming. A direct acquisition program using advanced software languages like turbo C is therefore suggested for more efficient data acquisition.

In this thesis, observed data have mostly been analyzed by using the so-called spectral comparison method. This method uses a model distribution of ozone defined by three parameters. This fitting procedure can be made more accurate if the values of total ozone content are also known a priori from another instrument (e.g. Dobson) operating at the same site. This will constrain the solution to a smaller range of variation for these three input

parameters. Also, the chances of getting totally unrealistic results due to various data extraction errors like improper baseline removal etc. would also be minimized.

There is considerable scope for detailed theoretical study of the inversion problem for retrieval of ozone height distribution from observed millimeter-wave spectral line data.

Annexure I

Strong Microwave Lines of Ozone Below 300 GHz

Frequency in GHz	Transition $\Delta J, \Delta K(J,K)$	Intensity factor $\phi^2 e^{-E/kT}$	Maximum absorption coefficient $\alpha(\upsilon_{lm}, T)\ cm^{-1}$	Zenith Opacity τ in Np	Zenith ΔT_B (K) of O_3
67.35624	R,P(5,1)	2.51	0.00050	1.3	0.5
96.22834	Q,R(2,0)	2.44	0.00098	.1-.5	3.2-4.1
101.73687	Q,R(4,0)	4.11	0.00185	.1-.5	5.8-7.7
103.87839	R,P(15,2)	1.13	0.00053	.2-.5	1.7-2.3
109.55933	R,P(19,3)	1.12	0.00058	.2-.5	1.8-2.5
110.83604	Q,R(6,0)	5.33	0.00248	.2-.5	7.8-12.0
118.36434	R,R(0,0)	1.00	0.00061	>10	0.0
124.08746	Q,R(8,0)	6.00	0.00402	.2-1	10-16
125.38958	R,P(7,1)	3.46	0.00236	.2-1	6-9.5
125.41319	P,R(21,3)	0.80	0.00055	.2-1	1.4-2.3
128.31385	P,R(7,1)	0.78	0.00056	.2-1	1.4-2.3
136.86024	P,R(20,3)	0.85	0.00069	.1-1	1.7-3
142.17512	Q,R(10,0)	6.13	0.00537	.1-1	12-22
144.91944	R,P(13,2)	2.05	0.00186	.1-1	4.0-7.8
148.74485	P,R(13,2)	1.11	0.00106	.1-1	2.2-4.5
154.04643	R,P(12,2)	1.11	0.00113	.1-1	2.2-4.9
164.95182	R,R(2,0)	1.98	0.00232	.1-1	3-9.7
165.78445	Q,R(12,0)	5.79	0.00686	.1-1	7.8-28
167.57271	R,P(5,1)	0.51	0.00062	.2-2	.7-2.7
175.18635	P,R(26,4)	0.45	0.00059	.2-2	.1-2.6
175.44565	P,R(19,3)	0.88	0.00117	>10	.2-4.9
184.37871	R,P(9,1)	4.34	0.00636	>10	0-26.5
184.74884	R,P(21,3)	1.04	0.00153		0-6.6

contd.

Frequency in GHz	Transition $\Delta J, \Delta K(J,K)$	Intensity factor $\phi^2 e^{-E/kT}$	Maximum absorption coefficient $\alpha(\upsilon_{lm}, T)$ cm^{-1}	Zenith Opacity τ in Np	Zenith ΔT_B (K) of O_3
193.35130	P,R(18,3)	0.92	0.00148	.5-5	.5-6.4
195.43051	Q,R(14,0)	5.12	0.00866	.5-5	3.4-34
195.72119	P,R(11,2)	1.02	0.00168	.5-5	.8-7.7
199.38477*	R,P(29,4)	0.36	0.00061	.3-3	.42.6
206.13195*	P,R(25,4)	0.49	0.00089	.2-2	.9-3.9
208.64244	R,R(4,0)	2.91	0.00545	.2-2	5.7-23
210.80380	P,R(10,2)	0.94	0.00180	.2-.8	1.9-7.7
214.95548*	R,P(15,2)	2.21	0.00440	.2-.7	10-15
226.05412*	P,R(17,3)	0.93	0.00205	.2-.6	1.8-8.7
229.57488*	P,R(24,4)	0.53	0.00120	.2-.6	1.1-5.2
231.28125*	Q,R(16,0)	4.32	0.00990	.2-.6	8.1-39
235.70964*	Q,R(16,1)		0.01430	.2-.6	9.8-53
237.14600*	Q,R(14.1)	5.9	0.01430	.2-.6	9.3-53
238.43195*	P,R(31,5)	0.2	0.00050	.2-.6	.4-2.2
239.09303*	Q,R(18,1)	5.58	0.01370	.2-.6	9.0-52
242.31860*	Q,R(12,1)	5.54	0.01390	.2-.6	9.3-53
243.45370	R,P(11,1)	5.07	0.01290	.2-.6	8.3-50
244.15804	P,R(9,2)	0.83	0.00210	.2-.6	1.5,9
247.76122	P,R(16,3)	0.94	0.00250	.2-.6	1.8-11
248.18332	Q,R(20,1)	4.97	0.01310	.2-.6	8.3-50
249.78846*	R,R(6,0)	3.78	0.01010	.2-.6	6.6-39
249.96190*	Q,R(10,1)	4.88	0.01310	.2-.6	8.3-50
258.20206*	P,R(23,4)	0.57	0.00160	.2-.6	.9-6.9
258.71610*	Q,R(8,1)	4.02	0.01150	.2-.6	6.1-45
262.85807*	R,P(23,3)	0.94	0.00280	.2-.6	1.6-12
263.69236*	Q,R(22,1)	4.16	0.01240	.2-.6	6.0-48

contd.

Frequency in GHz	Transition $\Delta J, \Delta K(J,K)$	Intensity factor $\phi^2 e^{-E/kT}$	Maximum absorption coefficient $\alpha(\nu_m, T)$ cm^{-1}	Zenith Opacity τ in Np	Zenith ΔT_B (K) of O_3
263.88606*	P,R(30,5)	0.22	0.00070	.2-.6	.4-3
264.92605*	P,R(8,2)	0.71	0.00210	.2-.6	1.1-9.0
267.26654*	Q,R(6,1)	3.05	0.00930	.2-.6	4.7-38
273.05063*	Q,R(18,0)	3.5	0.01110	.2-.6	4.8-43
274.47842*	Q,R(4,1)	2.00	0.00650	.2-.6	3.0-27
276.92378	P,R(15,3)	0.93	0.00310	.2-.6	1.3-13
279.48590	Q,R(2,1)	0.82	0.00082	.2-.6	1.0-11
279.89348	R,P(31,4)	0.28	0.00090	.2-.6	.4-3.9
282.83766	P,R(22,4)	0.61	0.00210	.3-.7	.7-9.0
286.08720	R,P(17,2)	2.30	0.00800	.3-.7	2.7-32
286.15650	Q,R(24,1)	3.31	0.01150	.3-.7	3.7-54
286.29420	Q,R(3,1)	1.38	0.00520	.3-.7	1.7-21
288.95895	R,R(8,0)	4.55	0.01620	.3-.7	4.5-60
290.97495*	P,R(29,5)	0.25	0.00090	.3-.7	.3-3.9
293.17125	Q,R(5,1)	2.27	0.00830	.3-.7	2.3-34
293.54842*	P,R(7,2)	0.56	0.00210	.3-.7	.6-9.0

(1) * represents calculated values (Gora 1959)

(2) Frequencies are from Lichtenstein et. al. 1971. The maximum absorption coefficient (α) were calculated by Gora 1959, for T=220 K, and this table includes lines with α>0.00050 cm^{-1}.

(3) A change of ΔJ or ΔK of -1,0,+1 is denoted by P,Q,R respectively, J & K values in the bracket are quantum numbers for lower state energy levels.

(4) In column 6 the ozone brightness temperatures are calculated for 2gm/cm^2 to 0 gm/cm^2 atmospheric water vapor content.

Annexure II

Data Acquisition Program

```
\ SOFTWARE "ASYST"
\ THIS PROGRAM ACQUIRES 100*100 'ON' AND 100*100 'OFF' SCANS
\ FROM A.O.S. AND STORE THEM IN THE HARD DISK OF THE COMPUTER.
\ THE FREQUENCIES SET FOR SIGNAL GENERATOR IN THE PROGRAM ARE
\ 111.05 (ON) AND 111.13 (OFF) FREQUENCIES OF SIG.GEN
\ TIME DELAY AFTER EVERY FREQUENCY CHANGE IS 1000 MILLISECONDS.
\ AFTER LOADING THIS PROGRAM, WORD "DOT5" STARTS ACQUISITION
\ AND
\ WORD "SAVE" STORES THE ON AND OFF DATA SEPARATELY ON HARD.

echo.off stack.clear
real scalar num
real scalar dum
integer dim[ 1050 ] array buffer.1    0 buffer.1 :=
real dim[ 1050 ] array dit1           0.0 dit1 :=
real dim[ 1050 ] array dit2           0.0 dit2 :=

6.0000 gpib.device sig.gen
das50
LOAD.OVERLAY ACQUIS.SOV
1 1  A/D.template c.template
1050 template.repeat
buffer.1 template.buffer

: fort
 das50.dig.trig
 das50.positive.trig
 das50.edge.trig
;
```

```
: court
c.template
EXT.TRIG
EXT.CLOCK
A/D.init
A/D.IN>ARRAY
;

: dot3
bus.init send.interface.clear
remote.enable.on  me talker sig.gen listener
" fr111.13mz" talk
;

: dot1
101 1 do
0.0 buffer.1 : =
fort  court
buffer.1 dit1  +  dit1 : =
loop
stack.clear
;

: dot4
bus.init send.interface.clear
remote.enable.on  me talker sig.gen listener
" fr111.05mz" talk
;

: dot2
101 1 do
0.0 buffer.1 : =
fort  court
buffer.1 dit2  +  dit2 : =
loop  stack.clear  ;

10 string pep
```

```
: on
" d:\on"
pep
"cat
" .dat"
"cat
;

: off
" d:\off"
pep
"cat
" .dat"
"cat
;

: save
load.overlay datafile.sov
file.template
real dim[ 1050 ] subfile
end
cr ." GIVE INPUT FILE NUMBER "
"input
pep ": =
on
defer>
file.create
dit2 10000.0 / dit2 : =
on
defer>
file.open
dit2 array>file
file.close
off
defer>
file.create
dit1 10000.0 / dit1 : =
```

```
off
defer>
file.open
dit1 array>file
file.close
;

: dot5
101 1 do
dot3
1000 msec.delay
dot1
dot4
1000 msec.delay
dot2
l.
loop
bell
;
```

Iterative Inversion Program

```
\ SOFTWARE "ASYST"
\ PROGRAM FOR RETRIEVAL OF OZONE HEIGHT PROFILE
\ USING ITERATIVE INVERSION METHOD.
\ THE PROGRAM ASSUMES THAT THE PROCESSED SPECRAL DATA IS IN
\ 'DIT1' ARRAY WITH IT'S PEAK FALLING AT 130TH CHANNEL.
\ ONLY RIGHT WING OF THE LINE IS USED FOR ANALYSIS.
\ THE RESULTANT OZONE MIXING RATIO PROFILE GOES IN 'MRP' ARRAY
\ AND IT'S CORRESPONDING HEIGHT IN THE ARRAY NAMED 'HT'.
\ THIS PROGRAM REQUIRES THE FOLLOWING INPUTS:
\ ATMOSPHERIC TEMPERATURE AND PRESSURE AS A FUNCTION OF
\ HEIGHT UPTO 90 KM.
\ A SET OF 20 FREQUENCIES TO BE USED FOR DEVELOPING WEIGHTING
\ FUNCTIONS.
```

```
stack.clear forget.all
real dim[ 1050 ] array dit1
real dim[ 50 ] array l1
real dim[ 50 ] array l2
real dim[ 364 ] array a1
real dim[ 91 ] array c1
real dim[ 19 ] array ht
real scalar dum1
real scalar dum2
real scalar dum3
real scalar dum4
real scalar dum5
real scalar dum6
real scalar dum7
real scalar dum8
real dim[ 20 , 91 ] array pbk
0.0001 pbk :=
real dim[ 91 ] array temp
real dim[ 91 ] array press
real dim[ 91 ] array pb      0.00 pb :=
real dim[ 19 ] array dbtm    1.00 dbtm :=
real dim[ 19 ] array dbtc    1.00 dbtc :=
real dim[ 19 ] array mrp
1.00 mrp :=
real dim[ 91 ] array pbi     0.00 pbi :=
real dim[ 91 ] array pbj     0.00 pbj :=
real dim[ 91 , 2 ] array f1

\ ." Give file name d:\nr\rj1.dat etc."
\ recalling

dit1 sub[ 2 , 110 , 4 ]
dit1 sub[ 4 , 110 , 4 ] +
rev[ 1 ]
dit1 sub[ 130 , 110 , 1 ] :=
dit1 sub[ 130 , 110 , 1 ] y
```

```
 dit1 sub[ 130 , 50 , 2 ] dit1 sub[ 131 , 50 , 2 ] + 2.0 / l1 :=

 : baseline
 load.overlay matfit.sov
 without.weights
 50 ramp l2 :=
l2
l1
3.0 leastsq.poly.fit
load.overlay poly.sov
l2 SWAP
poly[x]
l2 :=
l1 y l2 yd
stack.clear pckey ?drop drop
nd
;  \ baseline

load.overlay matfit.sov
: l[x]
dum3 - dup * dum2 * 1 + dum1 swap /
;
: abo
50 ramp l2 :=
5.0 dum1 :=
0.002 dum2 :=
1.0 dum3 :=
gauss-newton.fit
curve.fit[ l2 , l1 ; l[x] ; dum1 , dum2 , dum3 ]
l2 :=
l1 y l2 yd
stack.clear pckey ?drop drop
nd ;  abo

: rc
load.overlay datafile.sov
file.open  c:\asyst\p.dat
```

```
 9 subfile
 b1 file>array
 1 subfile
 c1 file>array
 file.close
 file.open c:\asyst\rr4.dat
 1 subfile
 a1 file>array
 file.close
 a1  sub[ 3 , 91 , 4 ] temp :=
 a1  sub[ 4 , 91 , 4 ] press :=
 1.00 f1 xsect[ ! , 2 ] :=
 91 ramp f1 xsect[ ! , 1 ] :=
 temp  300.0 /
 0.73 neg
 **
 press *
 2.37 *
 pb :=
 101.73683 358.00 *
 temp 48.00 /
 sqrt * db :=
 ; rc

 : salt1
 91 1 do
 pb [ I ]  2.0 **  dum2 :=
 dum2 dum1  +  dum3 :=
 dum2 dum3  /  232.00  *  pbi [ I ]  :=
 loop
 91 1 do
 pbi [ I ]  c1 [ I ]  *  1.0e-6 *  pbj [ I ] :=
 stack.clear loop ;

 : salt2
 load.overlay waveops.sov
 pbj integrate.data  pbj :=  ;
```

```
: salt3
91 1 do
pbj [ I ] neg exp dum3 : =
dum3 pbi [ I ] * temp [ I ] * 1.0e-6 * pbj [ I ] : =
stack.clear loop ;

: salt4
20 1 do
101.73683 b1 [ I ] - dum1 : =
dum1 2.0 ** 1.0e+6 * dum1 : =
salt1 salt2 salt3
pbj
pbk xsect[ I , ! ] : =
stack.clear loop ; salt4

: salt5
19 1 do
I 1 + dum1 : =
pbk xsect[ dum1 , ! ] pbi : =
pbk xsect[ I , ! ] pbj : =
pbi pbj - pbk xsect[ I , ! ] : =
0.00 pbk xsect[ I , 91 ] : =
pbk xsect[ I , ! ] []max dum2 : =
pbk xsect[ I , ! ] dum2 /
pbk xsect[ I , ! ] : =
stack.clear loop ;

: salt6
19 1 do
I 1 + dum1 : =
pbk xsect[ dum1 , ! ] pbi : =
pbk xsect[ I , ! ] pbj : =
pbi pbj - pbk xsect[ I , ! ] : =
0.00 pbk xsect[ I , 91 ] : =
stack.clear loop pbk abs pbk : = ; salt6

\ b1 rev[ 1 ] b1 : =
```

```
: salt7
20 1 do
I 1 + dum6 : =
101.737 b1 [ I ] - 1.0e3 * dum7 : =
101.737 b1 [ dum6 ] - 1.0e3 * dum8 : =
I2 [ dum7 ] I2 [ dum8 ] - dbtm [ I ] : =
stack.clear loop dbtm abs dbtm : = ; salt7

: salt8
20 1 do
pbk xsect[ I , ! ] f1 xsect[ ! , 2 ] * pbi : =
pbi []sum dbtc [ I ] : =
dbtm [ I ] dbtc [ I ] /
mrp [ I ] *
mrp [ I ] : =
stack.clear
loop mrp abs mrp : = ;

: salt11
load.overlay waveops.sov
1 set.#.optima
3 set.#.points
20 1 do
pbk xsect[ I , ! ] local.maxima drop ht [ I ] : =
stack.clear
loop ht abs ht : =
; salt11

: salt9
19 1 do
1.0 I + dum4 : =
ht [ I ] dum1 : =
ht [ dum4 ] dum3 : =
mrp [ I ] f1 [ dum1 , 2 ] : =
dum3 dum1 - 1.0 > if
mrp [ I ] mrp [ dum4 ] f1 sub[ dum1 , dum3 ; 2 ] []fill
then
```

```
 stack.clear
 loop
 ;

 : salt12
 ht [ 1 ] dum1 : =
 ht [ 18 ] dum3 : =
 dum1 1 do
 c1 [ I ] f1 [ I , 2 ] : =
 loop
 91 dum3 do
 c1 [ I ] f1 [ I , 2 ] : =
 stack.clear
 loop
 ;
 stack.clear

 : salts12
 ht [ 1 ] dum1 : =
 ht [ 18 ] dum3 : =
 0.1 mrp [ 1 ]  f1 sub[ 1 , dum1 ; 2 ] []fill
 mrp [ 18 ] 0.1 f1 sub[ dum3 , 91 ; 2 ] []fill
 stack.clear
 ;

 : salts13
 4 1 do
 salt8
 salt9
 salts12
 stack.clear loop ;
 salts13

 mrp sub[ 1 , 18 ] abs
 ht sub[ 1 , 18 ] abs
 xy.auto.plot
```

```
\ SOFTWARE "ASYST"
\ PROGRAM FOR RETRIEVAL OF OZONE HEIGHT PROFILE
\ USING SPECTRAL COMPARISION METHOD.
\ THE PROGRAM ASSUMES THAT THE PROCESSED SPECRAL DATA IS IN
\ 'DIT1' ARRAY WITH IT'S PEAK FALLING AT 130TH CHANNEL.
\ ONLY RIGHT WING OF THE LINE IS USED FOR ANALYSIS.
\ THE RESULTANT OZONE DENSITIS ARE PUT IN PBI ARRAY.
\

forget.all stack.clear
Real scalar dmax0   echo.on
Real scalar hmax0
Real scalar r0
Real scalar dmax1
Real scalar hmax1
Real scalar r1
Real scalar dum1   1.0 dum1 :=
Real scalar dum2
Real scalar dum3
Real scalar dum4   1.0 dum4 :=
Real scalar dum5   1.0 dum5 :=
Real scalar dum6   1.0e12 dum6 :=
Real dim[ 91 ] array press
real dim[ 91 ] array temp
real dim[ 91 ] array pb
real dim[ 91 ] array db
real dim[ 90 ] array pbi
real dim[ 90 ] array pbj
real dim[ 90 ] array pbl
real dim[ 90 ] array pbm   1.0 pbm :=
real dim[ 170 ] array l1
real dim[ 170 ] array l2
real dim[ 170 ] array l3
real dim[ 364 ] array a1   0.0 a1 :=
real dim[ 1050 ] array dit1
```

```
1.7e12 dmax0 : =
25.0 hmax0 : =
0.20 r0 : =
: rc
load.overlay datafile.sov
file.open c:\asyst\rr4.dat
1 subfile
a1 file > array
file.close
dit1 sub[ 130 , 170 ] l2 : =
a1 sub[ 3 , 91 , 4 ] temp : =
a1 sub[ 4 , 91 , 4 ] press : =
temp 300.0 /
0.73 neg
**
press *
2.37 *
pb : =
101.73683 358.00 *
temp 48.00 /
sqrt *
db : =
db 1.0e-6 * db : =
; rc
pb press : =
: salt0
92 55 do
1.0692 pb [ I ] *
0.8664 pb [ I ] 2.0 ** *
4.00 db [ I ] 2.0 ** * +
sqrt abs +
0.50 *
press [ I ] : =
stack.clear
loop stack.clear ; salt0
```

```
: salt1
\ pb 1.0e6 * pb : =
91 1 do
pb [ I ] dum2 : =
dum2 2.0 ** dum2 : =
dum2 dum1 + dum3 : =
pb [ I ] dum3 / pbj [ I ] : =
stack.clear
loop
pbj 1.0e-6 * pbj : = ;

: salt1.1
91 1 do
pbj [ I ] 1.7 * 1.0e-6 *
dum4 2.0 ** *
temp [ I ] 2.5 ** /
25.3 temp [ I ] /
abs
exp
/
pbj [ I ] : =
stack.clear
loop ;

: salt1.2
91 1 do
pbj [ I ] pbi [ I ] * pbl [ I ] : =
stack.clear
loop ;

: salt2
load.overlay waveops.sov
pbl integrate.data pbm : = ;

: salt3
91 1 do
pbm [ I ] neg
```

```
 exp
 dum5 : =
 dum5 pbl [ i ] * temp [ i ] *
 pbl [ i ] : =
 stack.clear
 loop  ;

 : ppp0
 91 1 do
 4.0 dmax0 *
 i hmax0 - r0 *
 exp *
 i hmax0 - r0 *
 exp
 1.0 +
 2.0
 **
 /
 pbi [ i ] : =
 stack.clear
 loop ;

 : ppp1
 91 1 do
 4.0 dmax1 *
 i hmax1 - r1 *
 exp *
 i hmax1 - r1 *
 exp
 1.0 +
 2.0
 **
 /
 pbi [ i ] : =
 stack.clear
 loop ;
```

```
: salt6
ppp0
171 1 do
\ 0.0 21.0 - I + dum1 :=
I dum1 :=
dum1 2.0 / dum1 :=
101736.87 dum1 + dum4 :=
dum1 2.0 ** dum1 :=
dum4 1000.0 / dum4 :=
salt1
salt1.1
salt1.2
salt2
salt3
salt2
pbm [ 90 ] l1 [ I ] :=
stack.clear
loop
l1 sub[ 111 , 60 ] []sum 60.0 / abs dum5 :=
l1 dum5 - l1 :=
;
: qqq
40 12 do
I ? 4.0 / dmax0 :=
dmax0 1.0e12 * dmax0 :=
35 15 do
I ? hmax0 :=
14 6 do
I ? 40 / r0 :=
    salt6
    l1 l2 - l3 :=
    l3 2.0 ** l3 :=
    l3 []sum dum5 :=
    dum5 dum6 < if
    dmax0 dmax1 :=
    hmax0 hmax1 :=
    r0 r1 :=
```

```
        dum5 dum6 :=
        then stack.clear
  loop
  loop
  loop
  ;

  qqq

  : salt61
  ppp1
  171 1  do
  I dum1 :=
  dum1 2.0 / dum1 :=
  101736.87 dum1 + dum4 :=
  dum1 2.0 ** dum1 :=
  dum4 1000.0 / dum4 :=
  salt1
  salt1.1
  salt1.2
  salt2
  salt3
  salt2
  pbm [ 90 ] l1 [ I ] :=
  stack.clear
  loop
  ;
  salt61
```

Annexure III

Conversion of Ozone units (From US Standard Atmosphere 1976)

Derived Quantity	Basic Quantity	
	Mass density $\rho(O_3)$ kg/m^3	Column density $\epsilon(O_3)$ atm-cm/km
Number Density $n(O_3)$ m^{-3}	$(N_A/M(O_3)).\rho(O_3)$ $1.25467*10^{25}.\rho(O_3)$	$10^{-5}.(N_A/V_0).\epsilon(O_3)$ $2.68684*10^{20}.\epsilon(O_3)$
Column Density $\epsilon(O_3)$ atm-cm/km	$10^5.V_0.\rho(O_3)/M(O_3)$ $4.66968*10^4.\rho(O_3)$	$\epsilon(O_3)$
Mass Density $\rho(O_3)$ kg/m^3	$\rho(O_3)$	$10^{-5}.M(O_3).\epsilon(O_3)$ $2.14148*10^{-5}.\epsilon(O_3)$
Partial Pressure $p(O_3)$ N/m^2 or Pascal mb	$R.T.\rho(O_3)/M(O_3)$ $1.73222*10^2.T.\rho(O_3)$ $1.73222.T.\rho(O_3)$	$10^{-5}.R.T.\epsilon(O^3)/V_o$ $3.70951*10^{-3}.T.\epsilon(O_3)$ $3.70951*10^{-5}.T.\epsilon(O_3)$
Mass mixing ratio $r(O_3)$ dimensionless	$\rho(O_3)/\rho_s$	$10^{-5}.$ $M(O_3).\epsilon(O_3)/(V_0.\rho_s)$ $2.1414*10^{-5}.\epsilon(O_3)/\rho_s$
Volume mixing ratio $r'(O_3)$ dimensionless	$\rho(O_3).M/(\rho_s.M(O_3))$ $6.0344*10^{-1}.\rho(O_3)/\rho_s$	$10^{-5}.M.\epsilon(O_3)/(V_o.\rho_s)$ $1.2922*10^{-5}.\epsilon(o_3)/\rho_S$

Avogadro Number (N_A) = $6.022169*10^{26}$ molecules per kmol

Gas Constant (R) = $8.31432*10^3$ J per mol

Volume of ideal gas at STP (V_0) = 22.44136 m^3/kmol

Molecular wt. of $M(O_3)$ = 47.9982 kg/kmol

Mean Molecular wt. of Air = 28.9644 kg/kmol

Mean Molecular wt. ratio $M(O_3)/M$ = 1.65714

Temperature of US Std. Atmospher at height z = T(K)

Density of US Std. Atmosphere at height z = ρ_s (kg/m^3)

1.0 Pascal = 1.0 N/m^2 = 0.01 mb

References

Allen M. et. al., 'Vertical Distribution of Ozone in the Mesosphere and Lower Thermosphere', Journal of Geophysical Research, 89, D3, 4841-4872, 1984.

Allen M. & Delitsky M. L.,'A Test of Odd Oxygen Photochemistry Using Spacelab 3 Atmospheric Trace Molecule Spectroscopy Observations', Journal of Geophysical Research, 96, D7, 12883-12891, 1991

Asyst - System Manuals 1-4, Asyst Software Technologies Inc, 100 Corporate Woods, Rochester, NY 14623, 1989

Atkinson R.J. et. al., Evidence of Mid-Latitude Impact of Antarctic Ozone Depletion, Nature, 340, 290-294, 1989.

Barcilon V., 'On Chahine's Relaxation Method for the Radiative Transfer Equation', Journal of Atmospheric Sciences, 32, 1026-1030, 1975.

Bavilacqua R.M. & Olivero J. J., 'Verticle Resolution of Middle atmospheric Measurements by Ground Based Microwave Radiometry', Journal of Geophysical Research, ***93***, D-8,pp. 9463-9475, 1988.

Bevilacqua R.M. et. al., 'An Observational Study of Water Vapour in the Mid Lattitude Mesosphere Using Ground Based Microwave Techniques', Journal of Geophysical Research, 88, C13, 8523-8534, 1983.

Ben Reuven A., 'Transition from Resonant to Nonresonant Line Shap in Microwave Absorption', Physical Review Letters, ***14,*** 10, pp 349-351, 1965.

Berret A.H. & Cheyung V.K., 'A Method for the Determination of High Altitude Water Vapour Abundance for Ground-based Microwave Observations', Journal of Geophysical Research, 67, 4259, 1962.

Brillet J., 'A Theoretical Study of Ozone Measurements Made with Ground Based Microwave Sensors', Journal of Geophysical Research ***94***, D-10,pp. 12833-12850, 1989.

Caton W.M. et. al., 'Absorption and Emission in the 8-Millimeter region by ozone in the Upper Atmosphere', Journal of Geophysical Research, 72, 24, 6137-6148, 1967.

Caton W.M. et. al., 'Radio Measurement of the Atmospheric Ozone Transion at 101.7 GHz', The Astrophysical Journal, 151, L153-L156, 1968.

Chahine M.T., 'Recent Developments In The Inversion by the Method of Relaxation', Journal of Atmospheric Sciences, ***27***, 960, 1970.

Chahine M.T., A General Relaxation Method for Inverse Solution of the full Radiative Transfer Equation', Journal of Atmospheric Sciences, ***29***, pp.741, 1972.

Chahine M.T., 'Inverse Problem in Rdiative Transfer : Determination of Atmospheric Parameters',Journal of Atmospheric Sciences, 27, 960-967, 1970.

Chandrasekhar S., 'Radiative Transfer', Dover Pubblications, New York (1960)

Connor B.J., 'Millimeter-Wave Spectrometry of Ozone in the Middle Atmosphere', Ph.D. Thesis, Harward University, Cambridge, Mass., 1985.

Connor B.J. et. al., 'Ozone over McMurdo Station, Antarctica, Austral Spring 1986 : Altitude Profiles for the Middle and Upper Stratosphere, Journal of Geophysical Research, 92, D11, 13221-13230, 1987.

Connor B.J. et. al., 'Detection of Stratospheric Ozone Trends by Ground-Based Microwave Observatios', Proceedings of SPIE conference 1491, Remote Sensing of Atmospheric Chemistry, Society of Photo-opt. Instrum. eng., Bellingham, Wash., 218-230, 1991

Conrath B.J., 'Verticle Resolution of the Temperature Profiles Obtained from Remote Radiation Measurements', Journal of Atmospheric Sciences, 29, 1262-1271, 1972.

De la Noe J. et. al., "remote and Ground-Based Measurements of Ozone Profiles During the MAP/GLOBUS 1983 Campaign, Planet. Space Science, 35, 547, 1987

Deepak A. (Ed.), Inversion Methods in Atmospheric Remote Sensing, Academic Press, 1977

Dicke R.H., 'Measurement of Thermal Radiation at Microwave Frequencies', Review of Scientific Instruments, 17, 7, 268-275, 1946.

Farman J.C., et. al., 'Large losses of Ozone in Antarctica reveal seasonal ClO_x/NO_x interaction', Nature, 315, 207-210, 1985

Gamache R.P. & Davies R.W., 'Theoretical N_2-, O_2- and Air-Broadened Halfwidths of $^{16}O_3$ Calculated by Quantum Fourier Transform Theory with Realistic Collision Dynamics', Journal of Molecular Spectroscopy, 109, 283-299, 1985.

Gloersen P. & Barath F.T., 'A scanning Multichannel Microwave Radiometer for Nimbus-G and Seasat-A, Tran. IEEE, OE-2, 2, 1977.

Gora E.K., 'Rotational Spectrum of Ozone', Journal of Molecular Spectroscopy, *3*, pp. 78-99, 1959.

Gordy W. et. al., 'Microwave Spectroscopy', John Willey & Sons, New York (1953)

Green A.E.S., 'Attenuation by Ozone and the Eath's Albedo in the Middle Ultra-Violet, Applied Optics, 3, 203, 1964.

Harsman M.S. & Poe G.A., 'Sensitivity of the Total Power Radiometer with Periodic Absolute Calibration', Tran. IEEE, MTT-29, 32-40, 1981.

Hamill P. & Toon O.B., ' Polar Stratospheric Clouds and Ozone Hole', Physics Today, 34-42, December 1991.

Hughes R.H., 'The Microwave Specrum and Structure of Ozone', Journal of Chemical Physics, 21, 959-960, 1953.

Trambarulo R. et. al., Journal of Chemical Physics, 21, 851-855, 1953.

Krueger A.J. and Minzner R.A., 'A Mid Lattitude Ozone Model for the 1976 U.S. Standard Atmosphere', Journal of Geophysical Research, 81, 24, pp. 4477-4481, 1976.

Lichtenstein M. and Gallagher J.J.,'Millimeter Spectrum of Ozone', Journal of Molecular Spectroscopy, 40, 10-26, 1971.

Levi B.G., ' Ozone Depletion at the Poles : The Hole Story Emerges' Physics Today, pp. 17-21, July 1988.

Levi B.G., 'Arctic Measurements Indicate the Chilly Prospect of Ozone Depletion' Physics Today, 17-19, July 1992

Lemonick M.D., 'The Ozone Vanishes' Time, 40-46, Feb. 17, 1992

Lobsiger E', 'Ground based Microwave Radiometry to Determine Stratospheric and Mesospheric Ozone Profiles', Journal of Atmospheric and Terrestrial Physics, ***49***, 5, pp. 493-501, 1987.

Lobsiger E. et. al., 'Comparision of Stratospheric Ozone Profiles Retrieved from Microwave-Radiometer and Dobson-Spectrometer data', Journal of Atmospheric and Terrestrial Physics, 46, 09, 799-806, 1984.

Meeks M.L.,(Ed.), 'Methods of Experimental Physics', Vol-12, Part-B, Academic Press, New York (1976)

Mouw R.B. & Silver S.,'Solar Radiation and Atmospheric Absorption for the Ozone Line at 8.3 mm', Inst. Eng. Res. 60, 277, University of California, Berkeley, June 30, 1960.

Muthu S.K., 'Statistical Theory of Errors', Journal of Metrology Society of India, 01, 01, 41-53, 1986.

Njoku E. G., 'Passive Microwave Remote Sensing of the Earth from Space, Proc. IEEE, 70, 7, 728-750, 1982

Njoku E.G. et. al., 'The Seasat Scanning Multi-Channel Radiometer (SSMR) : Instrument Description & Performance', Trans. IEEE, OE-5, 2, 1980.

Olivero J.J. & Longbothum R.L., 'Empirical Fits to the Voight line Width: A Brief Review, J. Quant. Spectrosc. Radiative Transfer, 17, 233-236, 1977

Parrish A. et.al.,'A Ground - based Technique for Millimeter-wave Spectroscopic Observations of Stratospheric Trace Constituents' Radio Science,*23*, 2, pp.106-118, 1988.

Parrish A. et. al., 'Ground-Based Microwave Monitoring of Stratospheric Ozone', Journal of Geophysical Research, 97, D2, 2541-2546, 1992.

Penfield H. et.al., 'Mesospheric Ozone Measured from Ground' based Milllimeterwave Observations, Journal of Geophysical Research, *81*, 34, pp 6115-6120, 1976.

Penzias A.A & Burrus C.A., 'Millimeter-Wavelength Radio-Astronomy Techniques', Annual Review Astron. Astrophys., 11, 51-71, 1973.

Randegger A.K., 'On Determination of the Atmospheric Ozone Profil from Ground Based Microwave Measurements', Pure and Applied Geophysics, pp. 1052-1065, Vol. 118, 1980.

Rodgers C.D., 'Retrieval of Atmospheric Temperature and Composition From Remote Measurements of Thermal Radiations', Reviews of Geophysics and Physics *14*, 4, pp. 609-624, 1976.

Rodgers C.D., 'The Verticle Resolution of Remotely Sounded Temperature Profiles With A Priori Statistics', Journal of Atmospheric Sciences, 33, 707-709, 1976.

Shimabukuro F.I. et. al., 'Estimation of the Ozone Distribution from Millimeter Wavelength Absorption Measurements', Journal of Geophysical Research, 80, 2957-2959, 1975.

Shimabukuro F.I. and Wilson W. J., 'Observation of Atmospheric Ozone at 110.836 GHz', Journal of Geophysical Research, 78, 6136, 1973

Singh A.K., 'A PC-Based Data Acquisition System', M. Tech Thesis, Univ. of Allahabad, 1991.

Smith W.L., 'Iterative Solution of the Radiative Transfer Equation for the Temperature and Absorbing Gas Profile of an Atmosphere', Applied Optics, 09, 09, 1970.

Srivastava B.N. & Zalpuri K.S. (Eds.), 'Natinal Workshop On Ozone', INSA, New Delhi, April, 1987.

Staelin D.H., 'Passive Remote Sensing at Microwave Wavelengths', Proceedings of the IEEE, 57, 04, 426-439, 1969.

Staelin D.H., 'Measurements and Interpretations of the Microwave Spectrum of the terrestrial Atmosphere Near 1-Cm. Wavelength', Journal of Geophysical Research, 71, 12, 28752881, 1966.

Sudhakar Rao G., Private communication, 1994.

Tejwani G.D.T., et. al., 'Pressure Broadened Linewidths of Ozone, Journal of Chemical Physics', *63*, 4, pp 1513- 1516 (1975)

Tomiyasu K., Remote Sensing of the Earth by Microwaves, Proc. IEEE, 62, 1 , 86-92, 1974.

Townes G.H. and Schawlow A.L., 'Microwave Spectroscoy', McGraw Hill, New York, 1955.

Trambarulo R. et. al., 'The Molecular Structure, Dipole Moment and g Factor of Ozone from it's Microwave Spectrum, Journal of Chemical Physics, 21, 959-960, 1953.

Twomey S., 'Inroduction to the Mathematicws of Inversion in remote sensing and Indirect Measurements', Elsevier Scientific Publishing company, Amsterdem (1977)

Twomey S. et. al., 'An Extention to Chahine Method of Inverting the Radiative Transfer Equation', Journal of the Atmospheric Sciences, 34, 1085-1090, 1977.

Ulaby F.T. et. al., 'Microwave Remote Sensing', Vol. I,II and III, Addison Wesley Publishing Company, 1981

Uppal G.S. et. al., 'A Direct Reading Portable 37 GHz Radiometer for Atmospheric Research and Remote Sensing Applications', Internatioal

Symposium on Optical and Radio Remote Sensing of the Atmospheric Environment', NPL, New Delhi, 24-26, Oct. 1990.

US Standard Atmosphere, 1966 & 1976, National Oceanic and Atmospheric Administration, Washington D.C.

Vivekanand M. and Arora R. S, 'Observations of atmospheric Ozone above Bangalore (13 N altitude) at 110.836 GHz', Current Science, ***57***, 20, pp. 1103-1106, Oct. 1988.

Wark D.Q. and Fleming H.E., 'Indirect Measurements of Atmospheric Temperature Profiles from Satellites', Monthly Weather Review, 94, 06, 1966.

Waters J.W., 'Ground-Based Micro-wave Specroscopic Sensing of the Stratosphere and Mesosphere, Ph.D. Thesis, Mass. Inst. Techn. 1970.

Westwater R., & Strand O.N., 'Statistical Information Content of Radiation Measurements used In Indirect Sensing', Journal of Atmospheric Sciences, ***25***, 750, 1972.

Wilson W. J. & Schwartz P. R., 'Diurnal Variation of Mesospheric Ozone Using Millimeter wave Measurements', Journal of Geophysical Research, 86, C8, 7385, 1981.

Yates H.W., 'A General Discussion of Remote Sensing of the Atmosphere', Applied Optics, 9, 1971-1975, 1970.

Zommerfelds W.C. et. al., 'Diurnal Variation of Mesospheric Ozone Obtained by Ground-Based Microwave Radiometry', Journal of Geophysical Research, 94, D10, 12819-12832, 1989.